Subchondral Bone Cysts

Filling the Void

by

Lance L. Frazer

M.S Bioengineering, University of Kansas, Lawrence, Kansas

B.S Biomedical Engineering, University of Arizona, Tucson, Arizona

Submitted to the graduate degree program in Bioengineering and the Graduate Faculty of the University of Kansas School of Engineering in partial fulfillment of the requirements for the degree of Doctor of Philosophy

Committee: _____

Chairperson: Kenneth J. Fischer, PhD

_____

Elizabeth M. Santschi, DVM

_____

Lorin P. Maletsky, PhD

_____

Suzanne M. Shontz, PhD

_____

Richard D. Hale, PhD

Date defended: _____

The Dissertation Committee for Lance L. Frazer certifies
that this is the approved version of the following dissertation:

Subchondral Bone Cysts
Filling the Void

Committee: _____

Chairperson: Kenneth J. Fischer, PhD

_____

Elizabeth M. Santschi, DVM

_____

Lorin P. Maletsky, PhD

_____

Suzanne M. Shontz, PhD

_____

Richard D. Hale, PhD

Date approved: _____

Table of Contents

Acknowledgements

Thank you, God, for giving me this opportunity. I would like to thank my advisor and primary mentor, Dr. Fischer. You have been a leader, a role model, and somebody I will always look up to. Thank you for all of the help, advice, and support in getting me to where I am today. I would also like to thank Dr. Santschi. Working with you has been incredible. Always the voice of reason and honesty (I especially appreciate your bluntness – not something engineers get a lot of). Because of you, I'm able to step outside of my math and science bubble and see the big picture – why are we doing what we're doing, and who are we helping. I would also like to thank my committee members Dr. Hale, Dr. Shontz, and Dr. Maletsky for their valuable feedback and willingness to make themselves available when needed. Dr. Hale, had I met you earlier in my life, I just may have been an aerospace engineer. Thank you to all the people at KU who've helped and supported me along the way. Namely, Nolan, Denise, Stefani, Ember, Matthew, Eileen, Alyssa, Danny, and everyone else I've had the pleasure of working with. I am forever grateful for Madison and Lila Self for their unparalleled generosity and vision for a better tomorrow. Without them, none of this would have been possible. Last but not least, I would like to thank my family. Michaela, you will always be my rock.

Table of Figures

Abstract

Subchondral bone cysts (SBCs) are voids that can occur in the bones of young horses, especially horses intended for performance. Believed to be caused by trauma or osteochondrosis, these defects most often occur in the medial femoral condyle (MFC). Current treatments for equine SBCs have poor outcomes and have not improved over the last several decades. The gold standard for surgical treatment consists of cyst debridement and grafting. However, radiographic healing is not often reported, and when it is, only 20% of horses exhibit full radiographic healing. A novel treatment strategy has been recently introduced that places a lag screw across the SBC and has demonstrated high rates of radiographic healing. However, the mechanics of how a transcondylar lag screw could enhance SBC healing are unknown.

The goals of this study were to determine a plausible mechanism of SBC initiation and growth, as well as understand the mechanics of the transcondylar lag screw. A finite element modeling approach has been taken to examine the mechanics associated with SBCs. Using CT scans from young Thoroughbred horses, several finite element models have been developed for this study. The results of this study show that high-impact loading from gallop can cause stresses high enough to initiate bone damage in a healthy equine stifle joint. Additionally, once a small defect has manifested, stresses rise even higher and further damage is likely. Medial meniscus stress also increases with a MFC SBC, which suggests that secondary injury to the medial meniscus may be due to a disrupted load path through the MFC. Furthermore, it was determined that the transcondylar screw is able to heal SBCs by providing enough mechanical stimulus to the adjacent bone to promote bone formation. Not only is the stimulus for growth present, but the screw also aligns third principal stresses transverse to trabecular orientation across the cyst. This encourages bone to form across the void, as opposed to trabecular thickening, which results in

the sclerosis typically seen in MFC SBCs. Lastly, it was determined that larger cysts respond best to the transcondylar screw. Full penetration of the screw into the cystic cavity provides the highest bone-forming stimulus, and also best aligns stresses across the void.

This work demonstrates that trauma can initiate SBCs and that the transcondylar screw provides a unique mechanism to enhance healing. Since humans are susceptible to a wide range of bone defects that exhibit similar characteristic of an equine SBC, it is believed that there is huge potential for translational applications.

Motivation

Radiographic abnormalities (RAs) develop in the stifle joint in 40% of young racehorses. These abnormalities typically occur in the medial femoral condyle and may affect performance or cause lameness. Most commonly, clinicians observe femoral bone, flattening of the femoral condyles, and/or a subchondral bone cyst (SBC).

While some believe osteochondrosis is the primary cause of SBC initiation and development, histologic examination of an SBC reveals evidence of trauma, such as degenerated bone and cartilage, woven bone, fibroplasia, disorganized granulation tissue, and capillary proliferation. When an SBC has been identified, clinicians aim to reduce inflammation and promote bone regeneration. Common conservative treatments, such as reduced exercise or corticosteroid shots, have low reported efficacy. More invasive treatments involve debridement of the SBC and subsequent filling of the void with cancellous bone or a combination of biological substances. The arthroscopic debridement treatment was developed over 40 years ago, and because most clinicians believe this treatment to be the obvious solution, the development of treatment strategies has been stagnant. Unfortunately, complete radiographic recovery is reported to be less than 20% with convalescent periods reaching as long as 24 months.

While these poor outcome metrics might lead clinicians to alter their strategies, the lack of information on stifle joint mechanics with and without a SBC makes it difficult to assess new options. However, obtaining experimental mechanics data of the stifle is impractical. The major obstacles are the expenses of both conventional acquisition equipment and maintenance of live specimens. Most of all, it is impossible to make direct empirical observations of these metrics without joint access, which would require the removal of critical structures and therefore compromise the health of the horse.

As an alternative to experimentally collecting data, we have developed a robust 3-D finite element model of the equine stifle joint to date. To our knowledge, our model is the most accurate and comprehensive equine stifle model available.

Understanding the mechanics of an SBC far exceed the immediate impact in equine populations. SBCs are also prevalent among human populations and pose similar health issues, such as pain or the inability to load the affected leg. Knee osteoarthritis (OA) is the most common form of OA and will develop in 50% of people by the age of 85. More often found in women, SCLs are reported in over 30% of all knee OA cases. Adolescents also develop SBCs usually as a result of sport-related trauma. As such, the need for safe and effective treatment is imperative. And, as in equine populations, not much is known about human SBCs, especially their mechanical consequences on surrounding bone and soft tissues. With the anatomical similarities to human knees and the spontaneous occurrence of SBCs, the equine stifle is an advantageous animal model for the study of human SBCs.

Recently, a novel treatment has been developed in horses that places a lag screw across the MFC and has demonstrated an improved convalescent period (4 months) and consistent post-treatment SBC healing (80%). The effectiveness of the screw may be due to its mechanical influence on the adjacent bone, which suggests that MFC biomechanics are critical in understanding SBC development. Besides our own preliminary work, very little research has been done on MFC biomechanics in the equine stifle, and a woeful lack of understanding has played a significant role in stagnant therapy success. Therefore, studying MFC biomechanics, as well as how they are perturbed by a SCL, will provide clinicians with the resources to better understand stifle joint injury and may provide compelling evidence for the use of a transcondylar screw.

Extending upon our previous work, the primary objectives of this study are to provide both a detailed exploration of equine stifle joint mechanics with and without SBCs and a thorough evaluation of the lag screw treatment. This information will provide clinicians with a way to visualize healthy and unhealthy contact mechanics, identify possible equine stifle joint pathologies, and understand how the lag screw may enhance the healing of an SBC. Additionally, another primary objective of the study is to identify what sizes and shapes best respond to the lag screw treatment strategy. This would provide clinicians with a predictive measure of success before surgery.

Specific Aim 1

To determine MFC mechanics in an extended (155^{o}) equine stifle joint with and without an SBC. The current goal was to investigate stresses, strains, and contact pressures in the MFC without an SBC, assess SBC initiation potential, and further examine stresses and strains once an SBC has manifested. Additionally, stresses, strains, and contact pressures from the tibial cartilage and medial meniscus were of interest to determine how their mechanics are perturbed with an SBC.

Research question

Can overload and trauma explain SBC initiation? How are the mechanics in the joint affected once an SBC has manifested? How do the soft tissue mechanics in the stifle joint change with an SBC?

Hypothesis

At the gallop, stresses in the MFC are high enough to suggest damage if bone remodeling is unable to sustain the high-impact loading. When an SBC is present, stress concentrations will occur around the cystic boundary, which may cause further damage and subsequent SBC growth.

Since load cannot pass through a void, the medial meniscus and tibial cartilage will experience local stress concentrations, which may lead to secondary injury.

Stress, strain, and contact pressure data at extension will provide new knowledge on stifle joint mechanics during impact loading and how these mechanics are perturbed with an SBC defect in the MFC. This information will provide clinicians with the understanding of SBC mechanics, which may lead to improved treatment strategies and preventative measures for SBCs.

Specific Aim 2

To evaluate the effect of a transcondylar lag screw on the bone remodeling stimulus in bone surrounding an SBC in the equine MFC. The current goal was to use a developed theory of bone remodeling to assess the mechanical stimulus a transcondylar lag screw imposes on the bone surrounding an SBC.

Research Question

How does a transcondylar lag screw enhance the healing of an SBC in an equine MFC? How do different factors of the treatment strategy, such as amount of screw compression, angle of entry, and allowable joint load, affect bone remodeling?

Hypothesis

A transcondylar lag screw will provide necessary mechanical stimulus to the bone surrounding an SBC to promote bone formation. The stimulus will increase with increasing screw compression and allowable joint load. The angle of entry should allow the screw to fully penetrate the SBC, if possible.

Currently, the transcondylar screw's mechanism of healing is unknown. Understanding how the screw works and validating the model's predictions against known clinical outcomes will allow for other screw configurations to be tested, and much more can be learned on how to best implement this treatment strategy. This information will also serve to provide evidence for (or against) the use of the transcondylar screw. There is no consensus in the field as to the best treatment for SBCs, even though the transcondylar screw appears to be the most effective treatment to date. With more surgeons adopting the screw treatment strategy, the <20% radiographic healing statistic may finally be replaced with the much more promising 80% radiographic healing statistic.

Specific Aim 3

To evaluate the impact of cyst size and shape on the bone remodeling stimulus provided by a transcondylar lag screw. The current goal was to use a 3^k factorial analysis to assess how the height, width, and depth of an SBC affects the bone remodeling stimulus from a transcondylar lag screw. It was of importance to understand which sizes and shapes of SBCs are worth operating on and to hypothesize ways in which non-responsive SBCs can be treated.

Research question

Which spatial characteristic of the SBC has the most influence on the transcondylar screw's efficacy? Can smaller cysts be treated in the same way as larger cysts?

Hypothesis

Height will have the most influence on the efficacy of the transcondylar screw's ability to promote bone formation. The screw should be able to penetrate fully into the cyst, and the height

will determine if this is possible. Smaller cysts will not respond sufficiently to the current transcondylar lag screw treatment.

The CT scan used in aims 1-2 is of a healthy joint. In order to investigate SBCs in the MFC, the sclerosis and cyst have been artificially implemented using assumed densities and simple spherical geometries. Spherical geometries are not common in small and medium-sized cysts. One of the major criticisms of our past work has been that these artificial characteristics of the model do not represent what is seen clinically, and the results obtained may not reflect reality. Moreover, a single cyst size and shape will be tested in aim 2, whereas cysts come in many different sizes and shapes. Not surprisingly, it is of clinicians' interest to understand the types of cyst that will respond positively to the screw treatment strategy. By using a cystic CT scan, and varying the cyst dimensions following the observations of Walker et al. [27], the model will overcome these shortcomings and provide relevant and useful information to the medical field. Additionally, a regression analysis of the 3^k factorial study will provide early insight into which dimension(s) contribute most to the variability in bone healing stimulus surrounding the SCL.

1. Introduction

1.1 Equine Subchondral Bone Cysts

In the last 25 years, young racehorses, particularly Thoroughbreds, have been under much radiographic scrutiny. The reason - radiographic abnormalities are quite common in young racehorses with reports citing occurrence as high as 42%.[1] Horse breeders and trainers are becoming more aware of the high incidence, and therefore, radiographs are becoming more common throughout the young horse's early years. By the time of a horse sale for a 2-year-old Thoroughbred, 4 scans would likely have occurred. The reason for this well-intentioned radiographic scrutiny? Detect these abnormalities early and begin to treat them.

One such abnormality, and arguably the most insidious, is a subchondral bone cyst (SBC). SBCs are often referred to as a subchondral lucency because these defects are diagnosed through radiographs that show a non-dense lucency where dense bone would normally reside (Figure 1.1, left). Subchondral bone cysts are the cause of significant pain and lameness in a horse. In high-performance horses, either sport or work related, these cysts can result in a complete loss of intended function causing both financial and emotional turmoil for the owner, as well as quality of life for the horse. Furthermore, untreated, or improperly treated, SBCs can lead to a complete degradation of the stifle joint causing irreversible damage. As such, prevention, early detection, and treatment for subchondral bone cysts is of utmost importance to the horse trainer.

Equine subchondral bone cysts were first described in the fetlock of the horse in a 1968 study by Pettersson et al.[2] Early detection mechanisms were limited, and the true extent of subchondral bone cysts were not fully understood. Over the next decade, advancements in

radiographic technology made it possible to survey other joints. By the 1980's, sufficiently powerful portable radiographic machines were available, and clinicians began to examine other joints in the horse, which allowed for a more in-depth examination of causes of lameness. In particular, subchondral bone cysts were found most commonly in the medial femoral condyle (MFC), although have been described in all diarthrodial joints.[3,4] Histologic examination of SBCs shows just how severe the defect can be (Figure 1.1, right). Examiners have found fibroplasia, capillary proliferation, fibrous tissue, as well as crushed bone, woven bone, and disorganized areas of granulation tissue within the cystic cavity.[5,6] These examinations reveal clues of trauma, which has given researchers an early insight into the etiology of these bone cysts.

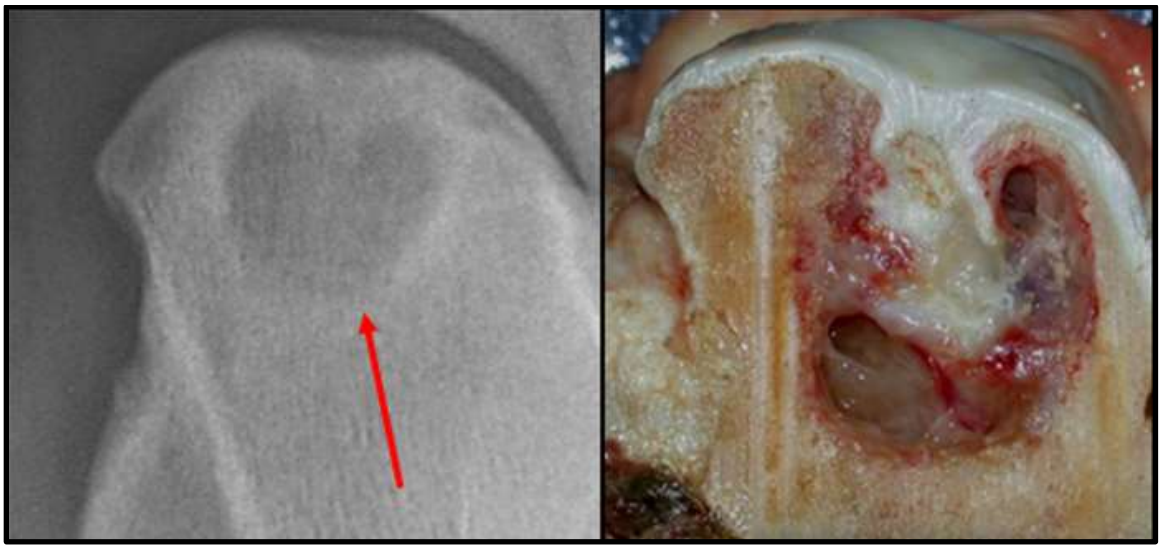

Figure 1.1. Medial femoral condyle subchondral bone cyst. Left) Radiograph of a subchondral bone cyst present in the medial femoral condyle of a young Thoroughbred. Right) Histological examination of a subchondral bone cyst in the medial femoral condyle.

Coming in all different sizes and shapes, early research efforts found it difficult to discern their etiology and what exactly constituted a "bad" or "mild" SBC. Initially, attributed to White

et al., cysts were defined as being in either 1 of 2 categories: Type 1) a dome shaped cyst that was most commonly coupled with a flattened femur, and Type 2) a circular cyst with a narrow stem-like opening that communicated with the tibial cartilage surface.[5] Fortunately, imaging technology continued to improve, and clearer radiographs from different angles provided more data for cystic classification. At last, clinicians were able to characterize SBCs in a more consistent and meaningful manner. In 2014, Santschi et al. devised a grading scheme that classifies SBCs into 1 of 6 categories, or grades, ranging from a flattening of the MFC to large cysts in both the femur and tibia with cartilage degeneration (Figure 1.2).[7]

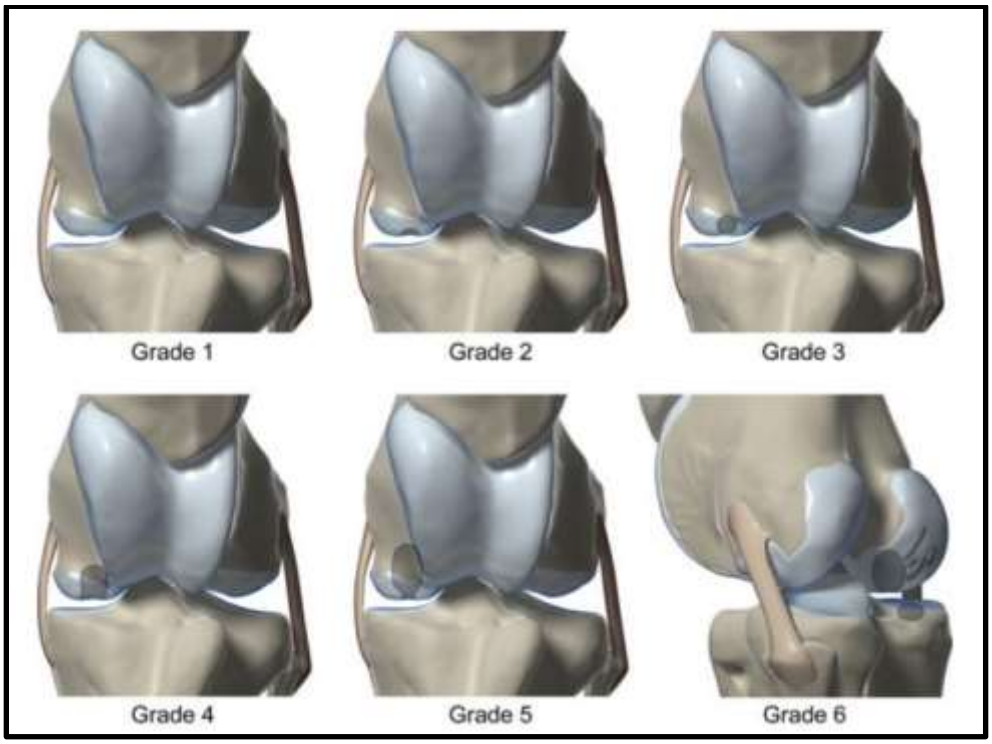

Figure 1.2. Classification of subchondral cystic lesions of the medial femoral condyle as described by Santschi et al. Grade 1 = flattening or a small defect in the subchondral bone of the central MFC, Grade 2 = a <10 mm height dome-shaped lucency, Grade 3 = a condylar lucency with no evidence of a cloaca in the subchondral bone, Grade 4 > 10 mm large dome shape extending to the articular defect, Grade 5 > 10 mm lucency with a narrow cloaca at the articular surface, Grade 6 = a combination of Grade 4 or Grade 5 SCL and other lucencies in the caudal MFC or proximal medial tibial plateau. Reprinted from *The American College of Veterinary Surgeons*, 2014; 44:281-288 with permission.

What makes subchondral bone cysts all the more egregious is their relatively high prevalence rate. In a 2017 study that examined radiographs from 1962 Thoroughbred yearlings from 2005-2013, subchondral lesions were identified in 23% of the horses.[8] Quarter horses are even more prone to developing subchondral bone cysts, but limited data is available for a

prevalence estimation.[9] Even in the 2017 study, the authors state that the 23% incidence rate is a conservative estimate for the true incidence of SBCs occurring in Thoroughbreds. With such a high population of horses affected, SBCs are a high-priority research topic in the veterinary community. Yet, little elucidation has been made into their etiology, and treatment options have stagnated over the past few decades. The stagnation in treatment options recently inspired the development of a novel surgical technique that has shown promising early results.[7] This study, which became the foundation of this body of work, may prove to revolutionize SBC treatments in both animals and humans alike. Discussed later (see Novel Treatment), the first step in determining the best surgical technique is to better understand SBC etiology, which could provide clues as to how they should be managed and treated.

1.2 Equine Subchondral Bone Cyst Initiation

The etiology of equine SBCs is still debated, even though they've been medically described since the 1960s.[2] There are several theories that explain the initiation of equine SBCs, but two theories in particular have received the most attention: 1) developmental failure of ossification (osteochondrosis) and 2) mechanical trauma. These two theories will be discussed further and a hypothesis made by the author of the primary cause.

1.2.1 Osteochondrosis

Osteochondrosis describes a focal interruption in the process of endochondral ossification.[10-12] In a healthy, developing bone, specialized growth cartilage located at the growth plate or at the end of appendicular long bones divides, grows, matures, and eventually ossifies into primary bone. When the blood supply that nourishes the growth cartilage is perturbed, the cartilage cannot properly ossify (Figure 1.3), strength is compromised, and the poorly developed bone becomes susceptible to injury.[13,14] As a consequence, these osteochondrotic areas can

fracture and may cause a free-floating fragment, known as osteochondrosis dissecans (OD) (Figure 1.4). Laboratory results have demonstrated this phenomenon. Cell necrosis occurring with a perturbed blood supply that shows similarities to spontaneous osteochondrosis has been reproduced experimentally.[15-17] However, characteristics of OD are not particularly evident in traditional cases of SBC (compare Figures 1.3 and 1.4 with 1.1). Nonetheless, bilateral SBC cases and SBCs having the proclivity to manifest in younger horses does suggest that developmental issues may be at fault.

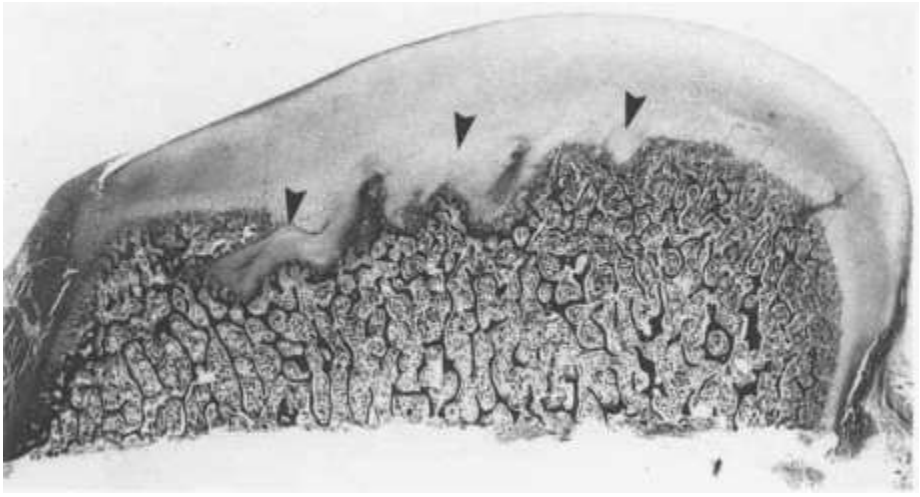

Figure 1.3. Medial femoral condyle from 50 kg pig with multiple areas of necrotic cartilage (arrowheads) associated with delayed endochondral ossification. Taken from *Journal of Orthopaedic Research*, 1991; 9:317-329 with permission.

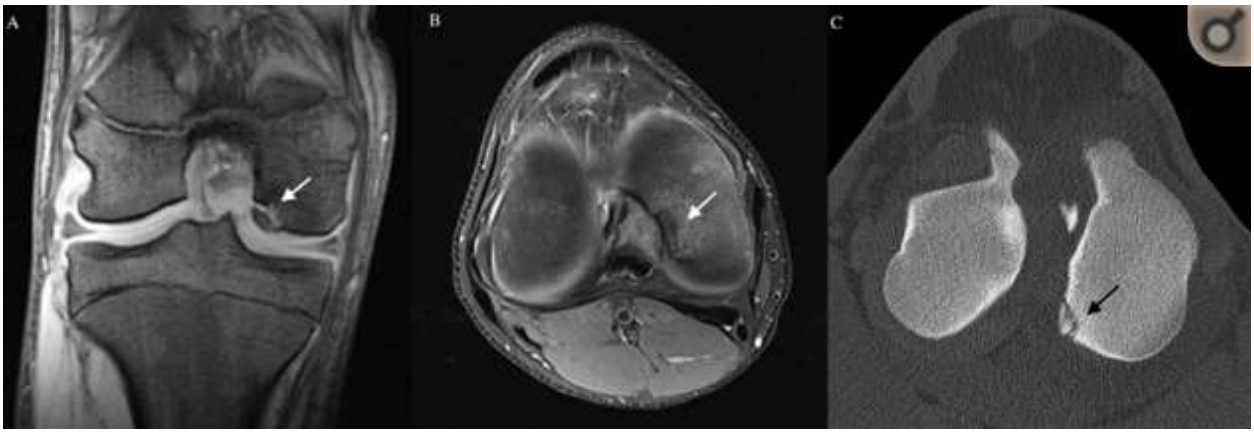

Figure 1.4. Osteochondrosis dissecan in the equine medial femoral condyle. Discernible flaps, or broken off pieces of bone, are staple findings for osteochondritis dissecans. A) MR imaging findings in the coronal plane. B) MR imaging findings in the transverse plane. C) CT image in the transverse plane. Note the visual difference in these images compared to Figure 1.1. Adapted from *Osteoarthritis Cartilage*, 2013; 21(11):1638-1647 with permission.

Osteochondrosis dissecans occur in developing horses and have been observed clinically for a number of years. The question is not whether they occur, but rather if they are the *cause* of subchondral bone cysts? There is strong evidence that would suggest osteochondrosis dissecans are not the primary cause of SBCs. The first piece of evidence comes from the growing recognition that older horses may develop subchondral bone cysts. Since older horses are well beyond development, there cannot be a disturbance in the blood supply to growth cartilage because growth cartilage is no longer present. Equine osteochondrosis dissecans also tend to occur in the trochlear ridge (Figure 1.5) and not in the primary weight-bearing portions of bones, such as the medial femoral condyle. Furthermore, histological analysis of SBCs reveals crushed trabecular bone, and rarely is a single broken section of the condyle found in the void.

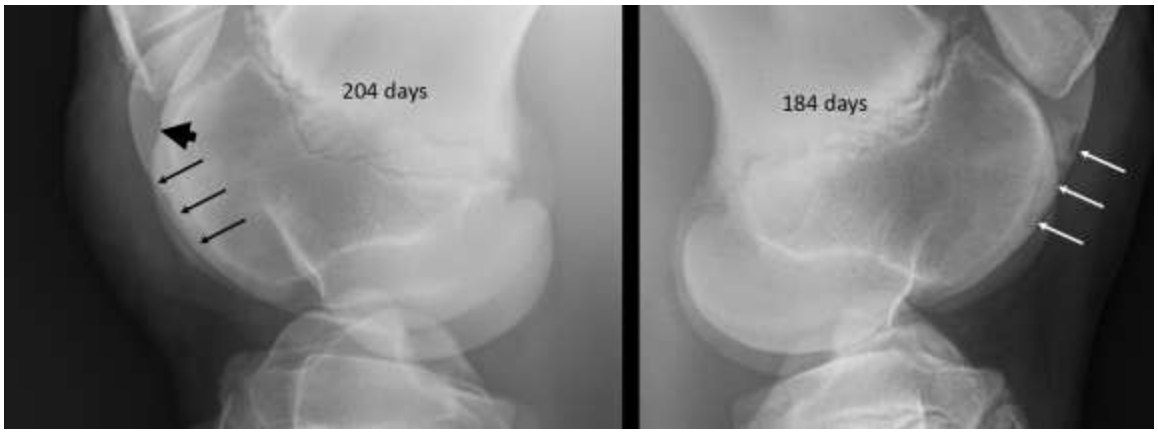

Figure 1.5. Medial-lateral radiographs of two different equine stifle joints with osteochondritis dissecans in the trochlear ridge (arrows). Images courtesy of Dr. Elizabeth Santschi.

1.2.2 Mechanical Trauma

As an alternative to osteochondrosis being the primary cause of equine SBC initiation, mechanical trauma and overload has been suggested. A key, almost obvious, piece of evidence to support this arises from the observation that SBCs are most common in high weight-bearing sites, such as the equine MFC. Additionally, those that are most prone to develop SBCs are those that participate in high-impact loading. Young horses intended for racing or work, and as will be described later, human adolescent athletes, older populations with osteoarthritis, and young military recruits tend to be the most affected population.[4,10,18-23]

Equine researchers first addressed mechanical trauma in the 1980s, shortly after osteochondrosis was proposed. In a 1983 study by Jeffcott and Kold, subchondral bone cysts in the medial femoral condyle were examined for clues as to their pathogenesis. One of the most important findings from that study was that the cartilage in and around the defect did not have significant degeneration commonly observed in osteochondrosis dissecans of the lateral trochlear ridge.[6] If SBCs in the MFC are caused by osteochondrosis, which leads to osteochondrosis

dissecans, one would expect appreciable cartilage degeneration consistent with improper blood supply. Other important findings included the presence of trabecular microfractures in the subchondral bone plate, flattening on the MFC prior to cystic development, as well as sclerosis in the MFC (Figure 1.6). These findings suggest forceful impacts are ultimately responsible for SBC development. The authors then hypothesized that continued loading would cause collapse of the bone, thus initiating a subchondral lesion.

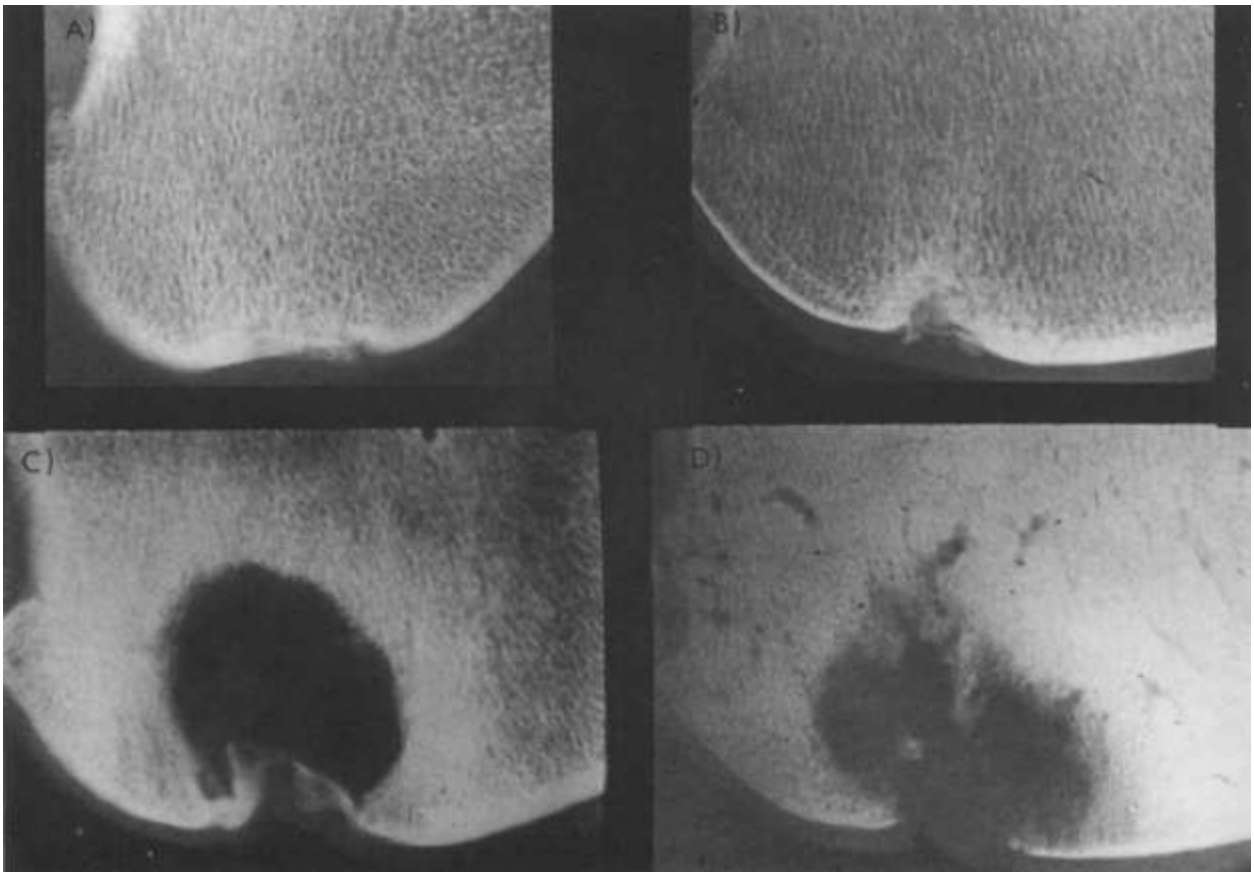

Figure 1.6. Likely progression of a subchondral bone cyst. A) condylar flattening with sclerosis suggesting mechanical trauma. B) Small defect with a sclerotic rim. C) Large subchondral bone cyst surrounded by sclerosis with collapse of the articular cartilage, a clearly defined cloaca, and a smooth lining. D) Degenerated bone, undefined cloaca, and often with concurrent cartilage degeneration. Adapted from *Equine Veterinary Journal*, 1983; 15(4):304-311 with permission.

Kold et al. continued to investigate the trauma hypothesis, and in 1986, they were able to experimentally create SBCs by creating a linear cartilaginous defect in the weight-bearing portion of the medial femoral condyle.[24] Yovich and Stashak's study in 1989 corroborated the mechanical trauma hypothesis by demonstrating that SBCs could form from an intra-articular defect in the equine elbow.[25] Additionally, McIlwraith showed that a subchondral defect could lead to the development of subchondral bone cysts.[11] With the mounting evidence implicating trauma, the author believes mechanical damage is the primary cause of SBC initiation.

In addition to the work done by the veterinary community, studies in humans have corroborated the mechanical trauma theory.[26-28] Predating the equine research, Ondrouch proposed trauma as the cause for osteoarthritic SBCs in 1963.[29] Durr et al. convincingly demonstrated that altered mechanics due to osteoarthritis causes significant stress increases in the subchondral bone. These increased stresses may cause stress-induced bone damage and subsequent resorption.[30] However, as with equine research, SBC development from a healthy joint has not been exclusively researched.

1.2.3 Summary

Perhaps, a happy medium exists in which both mechanical trauma and a developmental failure in the ossification process contribute to SBC initiation.[31] Mechanical trauma could contribute further deformation and damage to the thickened cartilage that failed to fully ossify in the endochondral ossification process. While this theory is certainly plausible, it is difficult to explicitly test for this phenomenon and little work has been done to lend additional support. However, this theory along with osteochondrosis alone, does not account for older horses developing SBCs.

Both osteochondrosis and mechanical trauma have been shown to induce bone cysts. As such, it remains hotly debated as to which pathology best explains the larger occurrence of SBCs. Mechanical trauma best explains the affected populations; however, little work had been done to show how a healthy bone could develop such a defect. Most of the work has been done using a cartilage defected model, or with direct lesions to the subchondral bone. Research into the development of a cyst from a healthy joint may provide the missing piece of evidence to affirm mechanical trauma's role in SBC initiation. Accordingly, one of the primary objectives of this research was to determine if a subchondral defect could form in a healthy joint given a horse's typical daily loading. Chapter 2 delves into this research question.

1.3 Subchondral Bone Cyst Growth and Progression

1.3.1 Hydraulic Theory

Not only is there disagreement about how SBCs start, but also about what causes subsequent SBC growth and development. Once an initial defect has manifested, two theories have been proposed to explain their continual progression. In the first theory, known as the hydraulic theory, synovial fluid pushed into the cavity is responsible for cyst enlargement.[24,32] First proposed by Freund in 1940 investigating human SBCs, it was initially believed that forceful intrusion of synovial fluid caused further damage to the surrounding bone.[33] Many years later, in a 2011 study by Cox et al., it was demonstrated that fluid pressure could actually cause stress-shielding and that bone may resorb away due to a lack of mechanical stimulus.[34] Thus, the intrusion of fluid was implicated as the culprit of growth. Two major problems arise with this hydraulic theory of cyst progression. One, it does not explain cyst growth in SBCs without an opening to the joint. If there is no joint communication, it would be difficult for synovial fluid to intrude into the void. Secondly, it does not explain the sclerosis observed in all stages of SBC

development (Figure 1.7). Sclerosis, or densification of focal bone, would be a functional adaptation response to increased stress.[35] If synovial fluid is causing stress-shielding in the bone surrounding the cyst, one would not expect this bone to be sclerotic. Instead, the bone would be of lower density until completely resorbed away or damaged. Nonetheless, the presence of fluid in subchondral bone cysts has been repeatedly observed, and researchers are hesitant to ignore its role in SBC progression.

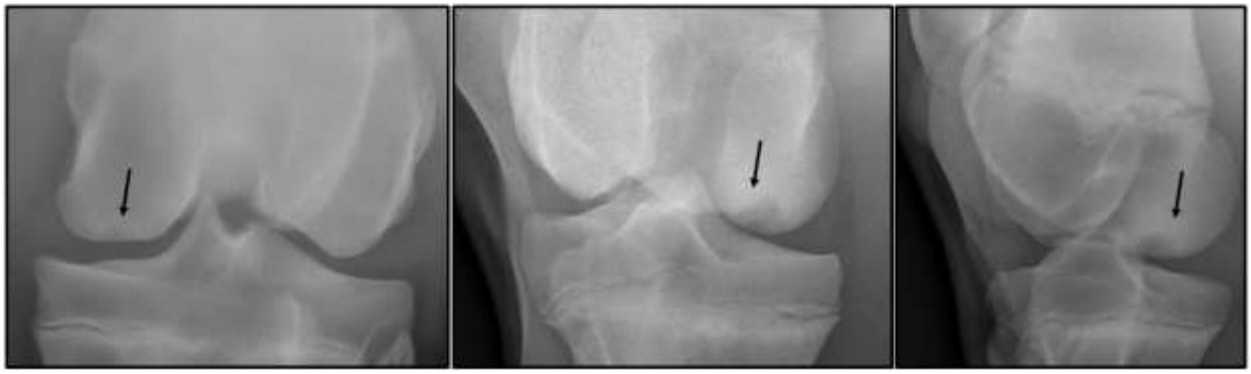

Figure 1.7. Radiographs of three different subchondral bone cysts illustrating the ubiquitous presence of sclerosis (black arrows) in developing SBCs. Sclerosis is a functional adaptation to increased loading. Therefore, sclerosis suggests increases in stress in the surrounding bone. Images courtesy of Dr. Elizabeth Santschi.

1.3.2 Mechanical Trauma

Trauma and overload with initial cyst development have been implicated as the primary reason cysts continue to develop. This mechanism is supported by the work of McErlain et al and Frazer et al.[26,36] Stress concentrations occur on the cystic boundary and would explain the sclerosis, as well as further damage if the stresses are high, or the bone remodeling cannot keep up with the compounding microfractures. Since the horse is not lame at the initial onset of the cystic lesion, the horse continues regular, high-impact loading on the joint. As such, the already

compromised bone is highly susceptible to further damage. This theory is further supported by the understanding that conservative treatment of rest tends to halt cyst progression. If stress-shielded bone resorption accounted for the expansion of the cyst, then rest would further unload the bone and one would expect the hole to continue to grow. However, if mechanical trauma grows the void, then reducing the mechanical forces on the compromised bone would halt cyst progression, as observed clinically.

1.3.3 Inflammation

In both theories of initiation and continued growth, the detrimental effects of inflammation factors are recognized. Factors such as interleukin-6 and prostaglandin E3 have been reported in SBCs and are known to increase bone resorption, as well slow healing.[37,38] Interestingly, recent research has uncovered some of the beneficial effects of inflammation in bone healing, especially in trabecular bone. Bernhardsson found evidence that supports monocytes' role in osteogenesis in cancellous bone after injury.[39] Sandberg also demonstrated that depleting macrophages hamper cancellous bone healing.[40] Certainly more research is needed in the role of the immune system in healing cancellous bone injuries.

1.3.4 Summary

Again, as is the case with SBC initiation, more research is needed to better understand SBC progression. If we can better understand SBC initiation and progression, rational treatment and preventative strategies can be implemented. Accordingly, similar to the previously stated research objective of cyst initiation, Chapter 2 addresses the possibility of subsequent cyst development from trauma given an existing defect in the subchondral bone.

1.4 Traditional Treatments

Treatment strategies for SBCs fall into one of two categories: conservative and non-conservative treatment. Depending on the severity of the defect, age of the horse, and the owner's preference, the veterinary surgeon will elect which categorical option to take. The general distinction between the two options is that conservative treatments do not require surgery, whereas non-conservative treatment strategies require some form of surgical intervention. Since conservative treatment is easier, it is often recommended that a horse undergo conservative treatment first and then elect for a surgical option if the results are not satisfactory.[41]

With conservative treatment, the main focus is directed towards anti-inflammation and/or rest. The two most common conservative treatments are strict rest and arthroscopic injection of corticosteroids. In an early study by Jeffcott and Kold, 25 horses with SBCs were given strict field rest. Success, determined as return to soundness, was observed in 14 of 25 (56%) and on average, had a 6-month convalescence period.[18] Unsatisfied with these results, surgeons developed anti-inflammation techniques to aid in recovery and have experienced much improved outcomes. In 2008, Wallis et al. developed a technique that injects corticosteroids into the cystic lining, ensuring that the substrate is not lost into the void cavity. In their study, they reported success, determined as return to their athletic function without lameness, in 35 out of 52 horses (67%).[42] This study, inspired by a 1999 study with a similar technique,[43] demonstrated that conservative treatment strategies are not only viable, but can be quite successful relative to the more invasive, non-conservative treatments.

Non-conservative, or surgical, treatment strategies have become the most common method for addressing SBCs. Surgical treatment strategies, intuitively, make the most sense.

SBCs are voids filled with evidence of trauma, such as crushed bone, inflammation, etc. It is then reasonable, almost obvious, to develop treatment strategies that clean out (debride) the cyst and/or fill it with some sort of graft or biological stimulus to replace bone and/or improve healing (Figure 1.8). As such, in the 1980s, clinicians began arthroscopic debridement surgeries and elected to fill the void with cancellous bone grafts.[5,24] Over time, cancellous bone grafts fell out of favor, and more complex biological stimuli grafting became the gold standard treatment, such as autologous chondrocytes and IGF-1 grafts.[44] Though these surgeries are intended to heal an SBC, success rates have not improved notably over the past several decades. In fact, conservative treatment involving the corticosteroid injection into the cyst lining produces similar success rates. Though the success rates may be similar, 67% is still not as high as surgeons would like, and the next answer/treatment strategy remained elusive for several more years.

Figure 1.8. Surgical debridement and bone graft procedure. Reprinted from the *Equine Veterinary Journal*, 2012; 44:606-613 with permission.

1.5 Novel Treatment

Dr. Elizabeth Santschi introduced a novel surgical strategy in 2015 that did not involve any form of debridement or grafting.[7] Instead, Dr. Santschi placed a transcondylar lag screw across the void in a proximodistal oblique fashion (Figure 1.9). Astonishingly, the lag screw treatment resulted in a >80% success rate with some of the healed horses not having responded to the corticosteroid injection treatment. Additionally, convalescence time averaged just 4 months. Lag screwing is less expensive, more successful, and an easier surgery to perform compared to the gold standard of SBC debridement and grafting. So why, several years later, are clinicians still not convinced of its efficacy, and why is the best treatment strategy still hotly debated?

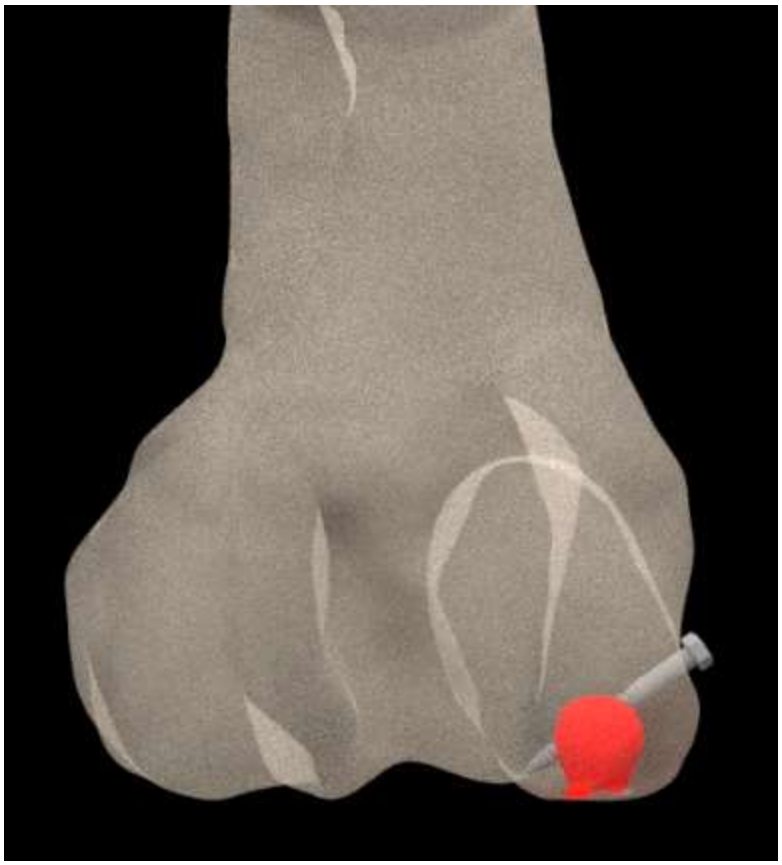

Figure 1.9. Illustration depicting the transcondylar screw surgery developed by Dr. Elizabeth Santschi. A lag screw is inserted across (proximoblique) the defect with compression applied across the void (shown in red).

It should be noted that many have, in fact, adopted the surgery and enjoyed high success. However, two possible reasons may explain the overall community's reluctance to adopt the transcondylar screw treatment. One, there is a lack of understanding as to why lag screwing would heal a bone cyst. Historically, bone screws are used to fix broken bones or to attach an implant to a bone. A SBC is neither a broken bone nor does it appear to warrant any form of implant. So, understandably, clinicians ask, why a lag screw across the cyst? The second reason that may promote reluctance is that anecdotal cases of low success and horses not responding at

all to the treatment have been noted. Though Dr. Santschi has demonstrated an 80+% success rate, many believed she was simply lucky.

The use of a transcondylar lag screw to treat SBCs is new enough that, to the author's knowledge, peer-reviewed research into its mechanisms do not exist. Therefore, a healthy view of skepticism into its capability and place in the surgical community is justified. The lack of research should compel us to dig deeper into the transcondylar lag screw. With the highest recorded success rates and the pronounced radiographic healing, that we work to understand why the treatment works and explore how to improve it. Accordingly, one of the primary objectives of this research was to determine how a TCS could elicit radiographic healing. In the later chapters of this dissertation, most notably chapter 3, the transcondylar lag screw is tested under much scrutiny. Its mechanism of healing is hypothesized, tested, and validated against existing clinical data.

To address the second concern of irreproducibility and lackluster results from others, the clear mechanism of TCS healing must be identified. If the mechanism is understood, then variations of the lag screw technique can be tested to see if improved healing is predicted. It must be remembered that there is no established standard as to how exactly the lag screw treatment should be administered. What sized/shaped cysts respond to it? What material should the screw be? At what angle should the screw insert into the cavity? How much compression should be applied across the screw? Various combinations of the above may result in wildly different results. Perhaps lackluster results are due to a combination of such factors that do not promote healing. Therefore, another primary objective of this research is to assess controllable surgery variables, as well as certain non-controllable variables such as cyst size and shape, to determine the most effective lag screw technique. In the later chapters of this dissertation, most notably

chapters 3 and 4, variables, both controllable and non-controllable, will be tested and compared for effectiveness.

It is clear that more information is needed before one can have confidence in the transcondylar lag screw to treat SBCs. Additionally, there is no question that more information is needed regarding SBC etiology. Therefore, this body of work focuses on addressing these two concerns: why do SBCs develop, and how can a transcondylar lag screw treat them?

1.6 Finite Element Analysis

Both major objectives (SBC etiology and treatment) of this research could be caused by mechanics as the primary driver. SBC initiation and subsequent development are hypothesized to occur due to mechanical trauma and lag screwing's efficacy is hypothesized to be due in part to its mechanical interaction with the bone. Thus, intra-osseous stresses are of utmost concern. Unfortunately, intra-osseous stresses and strains are difficult, if not impossible, to obtain through experimental means. Lack of instrumentation, difficult access to the joint space of a live equine stifle joint (knee), and limitations with existing technologies (i.e. using strain gauges for highly curved surfaces) all inhibit experimental analysis of SBCs. Finite element analysis (FEA) is a computational technique that can be used to investigate intra-osseous mechanics and overcome existing challenges of experimentation.

Finite element analysis was first developed by Courant,[45] a mathematician. The finite element method is a class of numerical techniques to approximate solutions to boundary value partial differential equations (PDEs). Demonstrating high accuracy compared to closed-solution problems, the finite element method quickly found a place in engineering practice as a tool to approximate non-closed solutions. By the 1950's, both civil and aerospace engineers had recognized its utility in structural mechanics and were utilizing FEA to solve complex

engineering problems. Today, an overwhelming number of researchers use FEA across a wide breadth of industries and academic disciplines. With computational power exponentially increasing over the past several decades, FEA has become one of the most ubiquitous tools in an engineer's kit to solve some of today's greatest challenges.

Developing a finite element model typically consists of four distinct steps: 1) geometry, or domain, development, 2) discretization of the domain into a finite number of elements, 3) assigning material properties to each element, and 4) applying boundary conditions. These steps will be further outlined below.

1.6.1 Domain

Geometry, or domain, development is incredibly important in developing a robust solution to an engineering problem. A working knowledge of continuum mechanics demonstrates that the geometry of a structural problem has profound influence on the response of the system. The slightest changes in size and shape can result in substantial changes in the calculated output. The magnitude of this effect has recently been quantified. Recent work has begun to quantify response changes due to geometrical differences highlighting the importance of geometric consideration.[46,47] In summary, the geometry that one develops for finite element analysis is especially important, and careful considerations should be taken when developing a finite element model.

In the biomechanics discipline of engineering, the domain one wishes to develop is most often an anatomical structure, such as an articular joint. In order to achieve high geometric fidelity, medical image data is often used as opposed to creating idealized structures. Magnetic Resonance (MR) imaging and Computed Tomography (CT) are the two most common medical imaging technologies that aid finite element model development for use in biomechanics. By

using medical image data, one can identify, and segment, each anatomical structure directly from the image data. However, the two imaging technologies do not yield the same image data, and one may be more suitable than the other to answer a specific question. With MR imaging, soft tissue boundaries are more readily identifiable because MR imaging measures the response from water molecules undergoing an energy transition. Since soft tissues are saturated with water, these structures are more readily observed than less hydrated tissues, such as bone. In contrast, CT imaging reveals denser structures, such as bone, more readily than soft tissues. In a recent study, it was found that CT imaging is far superior in bone fidelity compared to MR imaging.[48] In fact, MR imaging can greatly underestimate the volume of bone. SBCs are defects that affect bones, and thus, high bone fidelity is especially important. As such, this study utilizes CT image data as the medical imaging technology of choice to ensure high bone fidelity and provide a robust foundation for calculating bone stresses and strains.

1.6.2 Discretization

In the second step of developing a finite element model, the geometry, or domain of the problem, is discretized into a finite number of elements – hence the name finite element method. For an ideal PDE, an analytical solution can be achieved that provides the response for any time and space in the problem domain. This is a continuous solution. However, real-world physical problems rarely have such an analytical solution, which is where the finite element method can be of use. In the finite element approximation, instead of a continuous response (displacement or temperature, for example) being calculated, the response is approximated at specific points, or nodes. It is then this step in the finite element model development process where these nodes are specified in the domain.

Two key considerations should be assessed when discretizing a domain. How should the nodes be connected (which element type), and how many total nodes are needed? For 3-D structural mechanics problems, especially biomechanics problems, two types of elements are most common to establish node connectivity: tetrahedra and hexahedra (Figure 1.10). Hexahedral elements were considered to be the superior element choice for several decades due to their numerical stability compared to tetrahedral elements. The finite element method was developed before the boom of computing capabilities. With very little memory and low clock speed, finite element problems had to be set-up with the most efficiency possible. Linear (first-order) elements were therefore more attractive, and furthermore, hexahedral elements could achieve the same, if not better, accuracy compared to tetrahedral elements with a fraction of the number of elements used. This legacy stuck, and many researchers still believe that hexahedral elements are vastly superior.[49] However, with the enormous growth in computing power, tetrahedral elements have become the default option for many biomechanics related problems. Quadratic element can have similar accuracy as linear hexahedral elements, even for surface contact problems.[50]

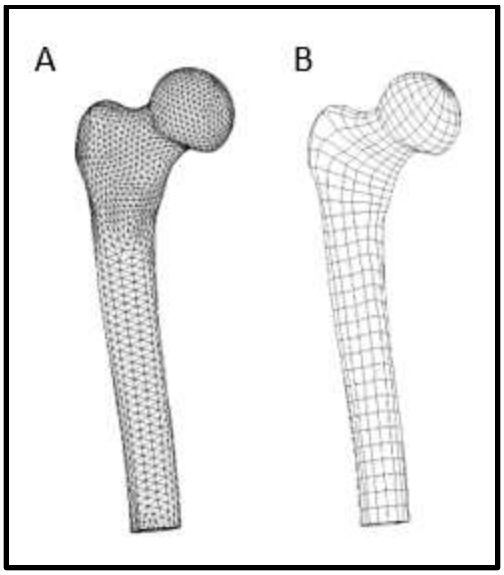

Figure 1.10. A) Femur mesh using tetrahedral elements. B) femur mesh using hexahedral elements. Generally, less hexahedral elements are required to achieve a similar level of accuracy to a solution as a high-density tetrahedral mesh. However, it should be noted that more nodes equate to higher geometric fidelity. Adapted from *Medical Engineering & Physics*, 2006; 28(9)916-924 with permission.

Tetrahedral elements have a distinct advantage over hexahedral elements: their capability of conforming to any geometry. Automatic meshing algorithms today have not quite mastered the ability to mesh a geometry with hex elements but can easily do so with tetrahedra. As discussed earlier, the geometry of the problem is critical to accuracy. Therefore, the ability to generate a mesh that is true to the native geometry is paramount. Only tetrahedral elements can do this automatically and reliably. Moreover, the shortcomings of tetrahedral elements have been overcome with the advent of higher computing power.[50-52] Higher-order elements, finer meshes, and special element formulations have allowed researchers to use tetrahedral elements in problems that would have previously yielded less accurate results. Even still, caution should be taken when using tetrahedral elements, especially for bending dominated problems. But in

typical biomechanical simulations, tetrahedral elements are most commonly used mainly due to their geometry conforming capabilities.

Once the element type has been identified, likely tetrahedral elements, the question of mesh refinement arises. How many nodes, and consequently elements, are needed? Theoretically, an infinite number of nodes would yield the most accurate results, as the solution begins to look like a continuous solution generated from analytical analysis. Computationally, this is obviously inefficient. A trade-off arises then between accuracy and efficiency. To find the balance, engineers can perform what is known as a convergence analysis. The more nodes added, the more the solution can be accurately represented. However, if enough nodes are in the model, adding more nodes produces a negligible improvement in the accuracy in the solution. Finding the point in which adding more nodes yields a negligible change in the solution is what researchers try to achieve with mesh convergence. To do this, a mesh is generated, a finite element problem established, and the output is calculated. The mesh is further refined (typically reducing element size by 50%), and the output is again calculated. The process is repeated until the output changes less than a present criterion, typically 5%. Of course, relatively large changes in element size should occur, as a small change in element edge length may not change the solution more than 5%, even though the mesh may be far from converged. In summary, tetrahedral elements are most common and in order to overcome their numerical hurdles, a large number of elements should be used, or quadratic (second-order) tetrahedral elements should be used, and element size should be determined by mesh convergence.

1.6.3 Material Properties

In the third step of finite element analysis, material properties are assigned to each element in the model. Material properties are assigned according to the structure the elements are representing. For example, bone elements would be assigned bone properties, whereas cartilage properties would be assigned much softer, cartilage-like properties. In a subject-specific model, material properties would ideally be obtained by characterizing the very tissue from the subject using mechanical testing procedures. However, this is not possible for in vivo studies and is often not feasible for ex vivo studies due to the time required, resources, equipment, specimen availability, tissue preparation, and even limitations in the mechanical testing itself. As such, material properties are often obtained from the literature as a best-estimate for the model. A few precautions can be taken that ensure more confidence in the final output.

Since physiology is unique person-to-person, or animal-to-animal, a single material property cannot possibly be guaranteed to represent the physical response in question. Either a mean value can be used, most often reported in the literature from material testing studies, or one can perform a sensitivity analysis. A sensitivity analysis is highly recommended even if a mean value is taken from literature. In a sensitivity analysis, a material property is set at a low value of the reported spectrum for that certain material, a medium value, and a high value. However much the output changes determines how sensitive the model is to that material property. It is then up to the researcher to decide how best to handle the sensitivity for their specific purpose of the model. Either a range can reported for the output, or more testing (in-house) of the material properties may be necessary. In comparative studies, material sensitivity is less important if the goal of the model is to simply qualitatively report how a different parameter changes the output.

The appendix of this work shows various sensitivity analyses performed for one of the models used.

A newer branch of mechanics has recently arisen that combines statistics with finite element analysis. Known as probabilistic finite element analysis, uncertainties, especially in material properties, can be handled in a statistical way that gives a probability of a certain outcome occurring.[53] For example, given all the uncertainty in what types of weather a bridge may encounter, a probability of failure can be computed. In this approach, the uncertainty is correctly accounted for, and engineers would not have to make the most conservative designs by accounting for the worst-case scenario. If the worst-case scenario is impossibly unlikely, much time and resource may be wasted trying to design for such. Probabilistic finite element analysis is a rising star in handling issues of material uncertainty, as well as boundary condition uncertainty, in mechanics problems.

1.6.4 Boundary Conditions

In the final step of creating a finite element model, boundary conditions are established. Boundary conditions include the loading, zero-displacement nodes, zero-rotation elements, etc. Typically, in biomechanics problems, these boundary conditions are chosen using kinematic and kinetic data found experimentally. Boundary conditions are also useful for "tying down" a model and prevent rigid body motion in the model.

For example, if one wishes to model the knee joint during running to predict intra-osseous stresses of the femur, it would be important to have motion data of the joint and a good-estimate of the joint reaction forces throughout the gait cycle. For other problems where kinematic and kinetic data does not exist, sensitivity analyses are useful as noted earlier. Also, posing the problem as comparative reduces the influenced of boundary conditions and material

properties. Keeping all parameters equal except the parameter being tested, the quantitative changes in the output data are meaningful. Knowing the comparative response of a system is often useful before resources are expended to determine and apply detailed and complex dynamic boundary conditions.

Other considerations for creating a well-posed finite element problem are boundary conditions for contact between separate bodies in the system. In addition, discrete structures, like springs, may be used to model continuum structures, and may be needed in the model to assure stability between bodies.

1.6.5 Summary

In this study, several finite element models have been utilized and details of their development can be found in the later chapters of this dissertation. Developing a finite element model to investigate subchondral bone cyst initiation and development in and of itself will provide novel data for researchers developing ways to prevent SBC growth. Technologies and preventative measures that reduce the likelihood of SBC formation could prove to be the greatest mitigation to the problem. Until that time, rationale for effective treatment strategies needs to be established for equine surgeons. The proposed development of a finite element model to investigate the transcondylar screw surgery could be the definitive step in establishing (supporting) such a rational surgery. However, the benefits do not stop with equine surgeons. There is much reason to be encouraged and optimistic that equine SBC treatment techniques could be translated into an even bigger problem: human bone lesions. The horse stifle joint is anatomically similar to the human knee and humans suffer a wide range of subchondral lesions. There is no consensus for optimal treatments, and the need for improved options is pressing.

1.7 Human Subchondral Bone Lesions

In horses, subchondral bone cyst is the common lexicon, as most bone lesions demonstrate similar symptoms and presentations. In humans, the characterization is less transparent, and more labels have been developed in attempt to separate the different "types" that clinicians treat. Some of these bone lesions are strikingly similar to equine SBCs, whereas others appear to be more unique to the human species. A prominent theme will arise as these defects are discussed - a consensus for optimal treatments has not been reached. In each of these described bone defects, there is much room for improving treatment.

1.7.1 Unicameral Bone Cysts

Unicameral bone cysts (UBCs) are benign, fluid-filled cavities most often occurring in long bones (i.e. humerus, femur) believed to be caused by trauma or circulatory obstruction and fluid accumulation.[54] These cysts primarily affect children as most cases are reported in adolescents between the ages of 3 and 14 years old.[55-57] Males are twice as likely to develop a UBC compared to females.[57] While considered benign on their own, UBCs can lead to catastrophic failure of the bone. A UBC can expand over time and weaken the local bone. As the local bone weakens, fracture risk escalates, and the asymptomatic child may experience severe traumatic fracture (Figure 1.11).

Figure 1.11. Frontal radiograph of a humeral fracture as a consequence of a large unicameral bone cyst. Adapted from *Clinical Orthopaedics and Related Research*, 2009; 467(11)2949-2954 with permission.

Currently, there is no consensus on the best treatment for unicameral bone cysts. Many techniques exist but success rates are often low, success is not standardized for each surgeon/technique, and treatment options must be balanced against fracture risk. Injection techniques appear to be the least successful, although early reports misleadingly showed high success rates. First described by Scaglietti, methylprednisolone injections were administered to young patients with UBCs and a 90% rate was reported as "favorable".[58] However, "favorable" cysts included those that did not exhibit radiographic healing. Moreover, these results have not been repeated by others and high recurrence rates have been reported.[59,60] Other injection

mediums were developed such as autologous bone marrow and demineralized bone marrow, but these techniques failed to produce promising results.[61-65]

With poor results coming from injection techniques, surgeons began developing more invasive techniques. Once considered the gold standard of treatment, curettage and bone grafting does not show much more benefit than injection techniques (50% even with a repeat surgery).[66,67] Calcium sulfate pellets for grafting slightly improved the healing rate to 66% but did not address the high recurrence rate of 25%.[68] Recognition of the fluid's presence in the cyst increased, and surgeries began to develop to address UBCs from a different perspective – draining the fluid. Using needles, curettes, or intramedullary nails, fluid can be drained, and native marrow contents can then fill into the cavity. Healing rates improved to 80% when this technique was combined with biological injection agents.[69] However, these success rates reflect partial healing and not complete healing. Convalescent times are high, recurrence rates are high, and multiple surgeries are often required.

Unicameral bone cysts will spontaneously heal as the child reaches skeletal maturity. Therefore, clinicians must carefully assess fracture risk and determine whether or not surgical intervention is necessary. When the surgeon deems invasive intervention necessary, failure rates between 10-30% leave many children still at serious risk of catastrophic fracture. The induced cost, wasted time and opportunity, and risk of secondary infection exacerbate the problem of high failure rates. Surgeries should promote bone growth to refill the localized void caused from the UBC. Clearly, more reliable treatment options are needed.

1.7.2 Aneurysmal Bone Cysts

Aneurysmal bone cysts (ABCs) are less common than UBCs, but still primarily affect younger populations.[70,71] Similar in radiographic appearance and location, ABCs are benign, osteolytic lesions that are most common in long bones such as the femur and tibia.[72] These bone cysts are more aggressive in their expansion and are often associated with pain – making them more readily detected as children become symptomatic. Microscopic examination of these cysts reveals more than just fluid cavities observed in UBCs. Blood filled membranes separated by septa, and immature trabecular bone interwoven throughout the septa comprise the typical findings of an ABC.[73] The primary concern of ABCs are osteolysis and their aggressive growth, which can quickly expand into the cortical bone creating a high risk of fracture.

Treatment options are more limited for ABCs, and none guarantee a cure. Failure rates are reported between 15-30% with multiple procedures usually administered. In a less invasive treatment, sclerotherapy, absolute alcohol is injected into the cyst.[74] Surgical options include curettage, grafting, and at the most extreme case, wide resection.[75,76] With each treatment option available, except for wide resection, recurrence rates remain high, although cryotherapy can help reduce the risk.

For both UBCs and ABCs, some form of drainage or curettage makes sense considering the volume of material inside the cysts that inhibit proper bone formation. Once the cysts have been drained or cleaned, a surgical technique that encourages bone growth would return the bone back to its healthy state and significantly reduce the rate of recurrence. Therefore, these bone cysts are logical candidates for a compressive screw treatment that has been shown to promote bone growth.

1.7.3 Osteochondritis Dissecans

Osteochondritis dissecans (OD) is a painful condition that most commonly affects the medial femoral condyle, the patella, and the lateral femoral condyle in children. Researchers have estimated it to be a relatively common occurrence affecting 15-30 children per 100,000 with males twice as prone.[77] Children may first experience pain and swelling in their knee and clinical radiographs reveal subchondral lesions. Human studies have implicated poor blood supply to developing cartilage, as well as trauma as primary causes for OD. It should be noted that for humans, subchondral bone cysts are described distinctly separate from OD, and this separation is evident from the presentation alone.

Early detection of OD is paramount for a positive prognosis. As the condition progresses, subchondral bone can detach from the bone (Figure 1.12), become unstable, and eventually lead to degeneration of the entire joint. With early detection, conservative treatment has been found to be successful. Patients are directed to avoid excess weight-bearing on the affected joint. However, as the condition progresses, either by a lack of detection or by a poor response to conservative treatment, prognosis worsens. Surgical options thus aim to maintain joint congruity, establish stable fixation of unstable fragments, repair osteochondral defects, and provide complete healing and pain relief.[78,79]

Figure 1.12. frontal radiograph revealing an unstable OD lesion in the lateral aspect of the medial femoral condyle. Adapted from *Journal of the American Academy of Orthopaedic Surgeons, 2006; 14(2):90-100 with permission.*

With stable lesions, those that have not separated from the joint, most surgeons are confident in a positive outcome of complete healing. By drilling vascular channels arthroscopically, blood can access the damage region and provide much needed vascularity to promote healing.[79,80] Kocher et al. reported an excellent healing outcome by transarticular drilling in 29 out of 30 treated lesions (97.5%).[81] Another similar study performed by Hayan et al. reported success rates in 95% of their patients.[82] In a much larger study, Edmonds et al. reported 98% of their 59 patients had radiographic healing at 36 months by treating epiphyseal OD with articular drilling.[83] As such, articular drilling is the treatment of choice, and little is needed in the advancement of treating stable OD lesions.

However, there is less consensus for the best treatment of unstable OD lesions – lesions that have broken off from the subchondral plate with a loss of integrity of the overlaying cartilage. Accordingly, there is much more room for improvement with currently available treatments. Currently proposed treatments for unstable lesions primarily focus on fixation and/or bone grafting techniques. The most common choices include countersunk screws, Herbert (headless) screws, bioabsorable screws, and pins.[79] The limited studies that have looked at these techniques do not report the same high successes as those seen in stable lesions.

Several studies have reported relatively high success rates, although complications with these treatments make surgeons slightly weary of their current utility. Kocher et al. reported an 85% healing rate using various methods of fixation and concluded one wasn't any better than the others.[84] Adachi et al. reported the most encouraging study with healing rates of 97% using bioabsorbable screws combined with multiple nonthreaded pins – although a large number of these lesions occurred in the lateral femoral condyle. Also, the OD lesions in this study were of "sufficient quality to enable fixation".[85] In a less successful study, Webb et al. reported overall healing rates at 75% in a study of 20 patients requiring internal fixation.[86]

Even with the relatively high reported rates of healing, the necessity for quality bone make them narrowly effective, and the complications incurred make them less attractive for establishing a consensus of treatment. For example, these surgeries typically require a secondary surgery to remove the implanted hardware, which has resulted in harmful wire migration, damage to the adjacent cartilage, and implant fracture. Bioresorbable screws could absolve the requirement of a second surgery.[87] In ODs that have poorer quality lesions, bone grafting has been suggested but this technique has resulted in a progressively deteriorating outcome with longer follow-ups.[88]

Surgeons have become acutely aware that fixation only provides the means to an end – stimulating healthy subchondral bone repair via compression. In order to achieve this compression, the broken lesion is fixed congruent to the subchondral bone, and compressive screws are inserted proximally into the bone to avoid further damage to cartilage. An interesting solution could be to capitalize on the knowledge of compression aiding subchondral bone repair. If the contents of the lesion have to be excised, then perhaps a low success rate bone graft is not necessary if proper compression could be applied to the adjacent bone to stimulate native growth. Since the patient would be in pain and swelling may persist, regular joint loading would be difficult. But a compressive treatment could provide a solution because that would stimulate bone formation without external joint loading. Or, a bone graft could be combined with a transverse compressive screw. The relatively high rate of occurrence of OD and lack of high-quality treatment options make this defect a high-priority candidate for the transcondylar screw treatment to "trick" the bone into formation to handle the screw-induced stresses, and thus healing.

1.7.4 Subchondral Bone Cysts

The actual distinction for a "subchondral bone cyst" in humans is typically reserved for lesions that occur secondary to osteoarthritis (although, children are still affected as discussed later). These lesions are so common, in fact, SBCs are considered to be a symptom of osteoarthritis with occurrence rates reported as high as 57%[89] with more conservative estimates of 30%.[21] An estimated 1 in 2 people over the age of 65 will develop some form of osteoarthritis.[90] Shockingly, there is very little done to address subchondral bone cysts in patients with OA. This is especially shocking because SBCs are associated with increased knee pain,[91] joint disability,[92] and increased cartilage degradation – ultimately increasing the risk for joint

replacement.[93] In 2010, an estimated 4.7 million individuals were living with a knee replacement and 2.5 million individuals with a hip replacement.[94] Using historical data from 1969 to 2010, researchers concluded that the incidence of total joint replacement is rising, and younger patients are receiving them.[94] Total joint replacements generally last 15-20 years, and it's alarming that younger individuals are requiring these surgeries. With so much money poured into joint replacements, and SBCs increasing the risk for joint replacement, why has so little been done to address SBCs independent of total joint replacement?

Even in children, SBCs pose a problem, especially amongst young athletes and young military recruits. A 2011 study demonstrated the higher propensity of active individuals to develop osteoarthritis at a young age making these individuals more susceptible to SBCs.[95] Idiopathic lesions can also occur in young individuals, especially in the ankle (Figure 1.13).[96] For younger individuals, more attention is given to treating these cysts and several surgical options exist. Debridement, bone marrow stimulation, retrograde drilling, internal fixation, cancellous bone grafting, osteochondral autograft transfer, autologous chondrocyte implantation, and allograft transplantation are all treatments that have been attempted.[96] These treatments have varying levels of success with most reports showing an average of 80% success rate.[96] Even so, these success rates include radiographic findings 3-4 years later of edema-like signals in the bone – suggesting an incomplete healing and an elevated risk for recurrence.[97] Subchondral bone cysts in humans present a major opportunity for translatable research using the equine stifle joint. The hundreds of billions of dollars spent on osteoarthritis, the lack of available treatment options, and poor long-term healing rates in younger patients all point to the need for more effective treatments.

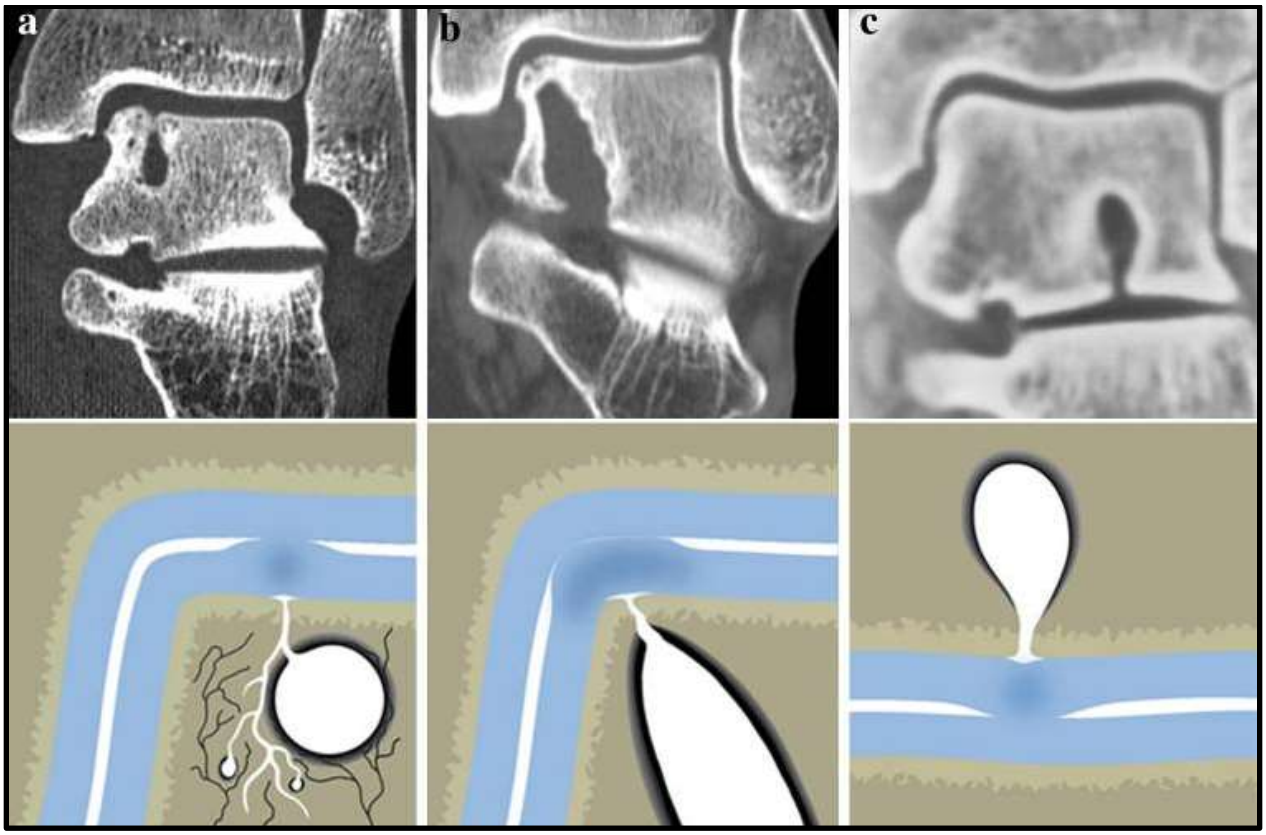

Figure 1.13. Coronal CT scans (upper row) with corresponding schematic diagrams (lower row) showing the ankles of three young patients (26-37 years). a) Cystic lesion in the talar body with a small opening in the subchondral bone plate. Black lines illustrate the nerve endings in the subchondral bone – may explain severe pain associated with these cysts. b) The subchondral bone cyst has extended to the subtalar joint. c) Similar cyst to (a), but sclerosis around the cyst is visible emphasizing the functional adaptation that has occurred. Adapted from *Knee Surg Sports Traumatol Arthrosc*, 2010; 18:570. Copyright C.N. van Dijk et al.

1.7.5 Other Bone Defects

Not only are the aforementioned bone defects candidates for a novel surgery, but many other bone defects exist that require better, more reliable treatment options.[98] These defects include, but are not limited to:

Brodie abscesses (Figure 1.14) – a variant of subacute osteomyelitis seen as radiographic lucencies surrounded by a sclerotic margin. Treatments include curettage, bone grafting, and antibiotics. Brodie abscesses are especially problematic in developing countries, and simple, effective treatments are necessary where access to high-grade medical equipment is limited.[99]

Figure 1.14. Brodie abscess in the distal femur from an AP radiograph. Taken from *Current Problems in Diagnostic Radiology*, 2007; 36(3)124-141 with permission.

Intraosseous ganglion cysts (Figure 1.15) – cystic lesions that contain gelatinous material that typically affect populations in their middle-ages.[100] Treatment of choice includes curettage coupled with bone grafting.

Figure 1.15. Intraosseous ganglion cyst revealed using a lateral radiograph of the upper fibula. Taken from *Current Problems in Diagnostic Radiology*, 2007; 36(3)124-141 with permission.

Fibrous dysplasia (Figure 1.16) – benign fibro-osseous lesions that can result in fracture. Treatments are limited to changes in diet, exercise, and therapeutic medications, such as bisphosphonates.[101]

Figure 1.16. Fibrous dysplasia shown using an anteroposterior radiograph of the right femur. Taken from *Current Problems in Diagnostic Radiology*, 2007; 36(3)124-141 with permission.

1.8 Summary

In this body of work, a finite element model of the equine stifle joint will be further developed from Frazer et al.'s previous work.[36] This model will be leveraged to study equine subchondral bone cyst initiation and development, as well as determine transcondylar screw mechanics to assess whether or not there is a mechanical basis for the treatment being more beneficial than other existing treatments. Humans and animals alike stand to gain immensely from a better understanding of SBCs and their treatment options. In Chapter 2, subchondral bone cyst initiation and development will be studied with the hypothesis that trauma and mechanical forces are the primary etiology. In Chapters 3 and 4, the transcondylar screw surgery will be examined with the hypothesis that its mechanism of healing is in part due to the bone stimulating stress it exerts on the adjacent bone. Chapter 5 will conclude with the optimistic outlook that we now have a more thorough grasp of subchondral bone cyst etiology and perhaps more importantly, we now have a candidate treatment option to consider for human and equine bone defects alike – the trans-cyst lag screw.

1.9 References

1. Santschi EM: Formation and prevalence of radiographic abnormalities of the medial femoral condyle in Thoroughbred horses from 6 to 20 months of age, Proceedings, American Association of Equine Practitioners, 2016.
2. Pettersson H, Sevelius F: Subchondral Bone Cysts in the Horse: a Clinical Study. Equine Veterinary Journal 1:75-82, 1968.
3. Bramlage L: Osteochondrosis-related bone cysts. Proc Am Ass Equine Practnrs 39:83-85, 1993.
4. Baxter GM: Subchondral cystic lesions in horses, in Joint disease in the horse, Vol. Philadelphia, WB Saunders, 1996, pp 384-397.
5. White NA, McIlwraith CW, Allen D: Curettage of subchondral bone cysts in medial femoral condyles of the horse. Equine Veterinary Journal 20:120-124, 1988.
6. Jeffcott LB, Kold SE, Melsen F: Aspects of the pathology of stifle bone cysts in the horse. Equine Vet J 15:304-311, 1983.
7. Santschi EM, Williams JM, Morgan JW, Johnson CR, Bertone AL, Juzwiak JS: Preliminary investigation of the treatment of equine medial femoral condylar subchondral cystic lesions with a transcondylar screw. Vet Surg 44:281-288, 2015.
8. Russell J, Matika O, Russell T, Reardon RJM: Heritability and prevalence of selected osteochondrosis lesions in yearling Thoroughbred horses. Equine veterinary journal 49:282-287, 2017.
9. Contino EK, Park RD, McIlwraith CW: Prevalence of radiographic changes in yearling and 2-year-old Quarter Horses intended for cutting. Equine Vet J 44:185-195, 2012.

10. McIlwraith CW: Subchondral Cystic Lesions (Osteochondrosis) in the Horse, in Compend Contin Educ Pract Vet, Vol 4, 1982, pp 282-294.
11. McIlwraith CW: What Is Developmental Orthopedic Disease, Osteochondrosis, Osteochondritis, Metabolic Bone Disease?, Proceedings, Am Assoc Equine Pract, 1993.
12. Olstad K, Ostevik L, Carlson CS, Ekman S: Osteochondrosis Can Lead to Formation of Pseudocysts and True Cysts in the Subchondral Bone of Horses. Vet Pathol 52:862-872, 2015.
13. Rejno S, Stromberg B: Osteochondrosis in the horse. II. Pathology. Acta Radiol Suppl 358:153-178, 1978.
14. Ytrehus B, Carlson CS, Ekman S: Etiology and pathogenesis of osteochondrosis. Vet Pathol 44:429-448, 2007.
15. Carlson CS, Meuten DJ, Richardson DC: Ischemic necrosis of cartilage in spontaneous and experimental lesions of osteochondrosis. J Orthop Res 9:317-329, 1991.
16. Ytrehus B, Andreas Haga H, Mellum CN, et al: Experimental ischemia of porcine growth cartilage produces lesions of osteochondrosis. J Orthop Res 22:1201-1209, 2004.
17. Olstad K, Hendrickson EH, Carlson CS, Ekman S, Dolvik NI: Transection of vessels in epiphyseal cartilage canals leads to osteochondrosis and osteochondrosis dissecans in the femoro-patellar joint of foals; a potential model of juvenile osteochondritis dissecans. Osteoarthritis Cartilage 21:730-738, 2013.
18. Jeffcott LB, Kold SE: Clinical and radiological aspects of stifle bone cysts in the horse. Equine Veterinary Journal 14:40-46, 1982.
19. Stewart B, Reid CF: Osseous cyst-like lesions of the medial femoral condyle in the horse. J Am Vet Med Assoc 180:254-257, 1982.

20. Ghahremani S, Griggs R, Hall T, Motamedi K, Boechat MI: Osteochondral lesions in pediatric and adolescent patients. Semin Musculoskelet Radiol 18:505-512, 2014.
21. Audrey HX, Abd Razak HR, Andrew TH: The truth behind subchondral cysts in osteoarthritis of the knee. Open Orthop J 8:7-10, 2014.
22. Edmonds EW, Polousky J: A review of knowledge in osteochondritis dissecans: 123 years of minimal evolution from Konig to the ROCK study group. Clin Orthop Relat Res 471:1118-1126, 2013.
23. Pouders C, De Maeseneer M, Van Roy P, Gielen J, Goossens A, Shahabpour M: Prevalence and MRI-anatomic correlation of bone cysts in osteoarthritic knees. AJR Am J Roentgenol 190:17-21, 2008.
24. Kold SE, Hickman J, Melsen F: An experimental study of the healing process of equine chondral and osteochondral defects. Equine Vet J 18:18-24, 1986.
25. Yovich JV, Stashak TS: Subchondral osseous cyst formation after an intra-articular fracture in a filly. Equine Veterinary Journal 21:72-74, 1989.
26. McErlain DD, Milner JS, Ivanov TG, Jencikova-Celerin L, Pollmann SI, Holdsworth DW: Subchondral cysts create increased intra-osseous stress in early knee OA: A finite element analysis using simulated lesions. Bone 48:639-646, 2011.
27. van Dijk CN, Reilingh ML, Zengerink M, van Bergen CJ: The natural history of osteochondral lesions in the ankle. Instr Course Lect 59:375-386, 2010.
28. Cahill BR: Osteochondritis Dissecans of the Knee: Treatment of Juvenile and Adult Forms. J Am Acad Orthop Surg 3:237-247, 1995.
29. Ondrouch A: Cyst formation in osteoarthritis. J Bone Joint Surg Br 45:755-760, 1963.

30. Dürr H, Martin H, Pellengahr C, Schlemmer M, Maier M, Jansson V: The cause of subchondral bone cysts in osteoarthrosisA finite element analysis. Acta Orthopaedica Scandinavica 75:554-558, 2004.
31. McIlwraith CW: Subchondral bone cysts in the horse: aetiology, diagnosis and treatment options. Equine Veterinary Education 10:313-317, 1998.
32. Santschi EM: Equine Subchondral Bone Cysts. Proc Am Col of Vet Surg, 2011.
33. Freund E: The Pathological Significance of Intra-Articular Pressure. Edinburgh medical journal 47:192-203, 1940.
34. Cox LG, Lagemaat MW, van Donkelaar CC, et al: The role of pressurized fluid in subchondral bone cyst growth. Bone 49:762-768, 2011.
35. Ruff C, Holt B, Trinkaus E: Who's afraid of the big bad Wolff?: "Wolff's law" and bone functional adaptation. American Journal of Physical Anthropology 129:484-498, 2006.
36. Frazer LL, Santschi EM, Fischer KJ: The impact of subchondral bone cysts on local bone stresses in the medial femoral condyle of the equine stifle joint. Med Eng Phys, 2017.
37. von Rechenberg B, Leutenegger C, Zlinsky K, McIlwraith CW, Akens MK, Auer JA: Upregulation of mRNA of interleukin-1 and -6 in subchondral cystic lesions of four horses. Equine Veterinary Journal 33:143-149, 2001.
38. von Rechenberg B, Guenther H, McIlwraith CW, et al: Fibrous tissue of subchondral cystic lesions in horses produce local mediators and neutral metalloproteinases and cause bone resorption in vitro. Vet Surg 29:420-429, 2000.
39. Bernhardsson M, Aspenberg P: Osteoblast precursors and inflammatory cells arrive simultaneously to sites of a trabecular-bone injury. Acta orthopaedica 89:457-461, 2018.

40. Sandberg OH, Tatting L, Bernhardsson ME, Aspenberg P: Temporal role of macrophages in cancellous bone healing. Bone 101:129-133, 2017.
41. O'Brien EJO: What is the best treatment for medial femoral condylar subchondral bone cysts? Equine Veterinary Education, 2019.
42. Wallis TW, Goodrich LR, McIlwraith CW, et al: Arthroscopic injection of corticosteroids into the fibrous tissue of subchondral cystic lesions of the medial femoral condyle in horses: a retrospective study of 52 cases (2001-2006). Equine Vet J 40:461-467, 2008.
43. Vandekeybus L, Desbrosse F, Perrin R: Intralesional longacting corticosteroids as a treatment for subchondral cystic lesions in horses. A retrospective study of 22 cases. in Proceedings 8th Annual Scientific Meeting of the European College of Veterinary Surgery 33-35, 1999.
44. Ortved KF, Nixon AJ, Mohammed HO, Fortier LA: Treatment of subchondral cystic lesions of the medial femoral condyle of mature horses with growth factor enhanced chondrocyte grafts: a retrospective study of 49 cases. Equine Vet J 44:606-613, 2012.
45. Courant R: Variational methods for the solution of problems of equilibrium and vibrations.1-23, 1943.
46. Bredbenner TL, Mason RL, Havill LM, Orwoll ES, Nicolella DP: Fracture risk predictions based on statistical shape and density modeling of the proximal femur. J Bone Miner Res 29:2090-2100, 2014.
47. Francis WL, Eliason TD, Thacker BH, Paskoff GR, Shender BS, Nicolella DP: Implementation and validation of probabilistic models of the anterior longitudinal ligament and posterior longitudinal ligament of the cervical spine. Comput Methods Biomech Biomed Engin 17:905-916, 2014.

48. Campanelli V, Howell S, Hull M: Morphological errors in 3D bone models of the distal femur and proximal tibia generated from magnetic resonance imaging and computed tomography determined using two registration methods, 2019.
49. Wang E, Nelson T, Rauch R: Back to Elements - Tetrahedra vs. Hexahedra, 2004.
50. Maas SA, Ellis BJ, Rawlins DS, Weiss JA: Finite element simulation of articular contact mechanics with quadratic tetrahedral elements. Journal of Biomechanics 49:659-667, 2016.
51. Ramos A, Simões JA: Tetrahedral versus hexahedral finite elements in numerical modelling of the proximal femur. Medical Engineering & Physics 28:916-924, 2006.
52. C Tadepalli S, Erdemir A, R Cavanagh P: Comparison of hexahedral and tetrahedral elements in finite element analysis of the foot and footwear, 2011.
53. Thacker BH: Why do probabilistic finite element analysis?, NAFEMS, 2008.
54. Pretell-Mazzini J, Murphy RF, Kushare I, Dormans JP: Unicameral bone cysts: general characteristics and management controversies. J Am Acad Orthop Surg 22:295-303, 2014.
55. Wilkins RM: Unicameral bone cysts. J Am Acad Orthop Surg 8:217-224, 2000.
56. Biermann JS: Common benign lesions of bone in children and adolescents. J Pediatr Orthop 22:268-273, 2002.
57. Boseker EH, Bickel WH, Dahlin DC: A clinicopathologic study of simple unicameral bone cysts. Surg Gynecol Obstet 127:550-560, 1968.
58. Scaglietti O: L'azione osteogenetica dell acetate di metilprednisolone. Biull Sci Med (Bologna):15-17, 1974.

59. Oppenheim WL, Galleno H: Operative treatment versus steroid injection in the management of unicameral bone cysts. J Pediatr Orthop 4:1-7, 1984.

60. Scaglietti O, Marchetti PG, Bartolozzi P: Final results obtained in the treatment of bone cysts with methylprednisolone acetate (depo-medrol) and a discussion of results achieved in other bone lesions. Clin Orthop Relat Res:33-42, 1982.

61. Wright JG, Yandow S, Donaldson S, Marley L: A randomized clinical trial comparing intralesional bone marrow and steroid injections for simple bone cysts. J Bone Joint Surg Am 90:722-730, 2008.

62. Cho HS, Seo SH, Park SH, Park JH, Shin DS, Park IH: Minimal invasive surgery for unicameral bone cyst using demineralized bone matrix: a case series. BMC Musculoskelet Disord 13:134, 2012.

63. Chang CH, Stanton RP, Glutting J: Unicameral bone cysts treated by injection of bone marrow or methylprednisolone. J Bone Joint Surg Br 84:407-412, 2002.

64. Rougraff BT, Kling TJ: Treatment of active unicameral bone cysts with percutaneous injection of demineralized bone matrix and autogenous bone marrow. J Bone Joint Surg Am 84-a:921-929, 2002.

65. Di Bella C, Dozza B, Frisoni T, Cevolani L, Donati D: Injection of demineralized bone matrix with bone marrow concentrate improves healing in unicameral bone cyst. Clin Orthop Relat Res 468:3047-3055, 2010.

66. Brecelj J, Suhodolcan L: Continuous decompression of unicameral bone cyst with cannulated screws: a comparative study. J Pediatr Orthop B 16:367-372, 2007.

67. Sung AD, Anderson ME, Zurakowski D, Hornicek FJ, Gebhardt MC: Unicameral bone cyst: a retrospective study of three surgical treatments. Clin Orthop Relat Res 466:2519-2526, 2008.

68. Hou HY, Wu K, Wang CT, Chang SM, Lin WH, Yang RS: Treatment of unicameral bone cyst: a comparative study of selected techniques. J Bone Joint Surg Am 92:855-862, 2010.

69. Mik G, Arkader A, Manteghi A, Dormans JP: Results of a minimally invasive technique for treatment of unicameral bone cysts. Clin Orthop Relat Res 467:2949-2954, 2009.

70. Zehetgruber H, Bittner B, Gruber D, et al: Prevalence of aneurysmal and solitary bone cysts in young patients. Clin Orthop Relat Res 439:136-143, 2005.

71. Leithner A, Windhager R, Lang S, Haas OA, Kainberger F, Kotz R: Aneurysmal bone cyst. A population based epidemiologic study and literature review. Clin Orthop Relat Res:176-179, 1999.

72. Rapp TB, Ward JP, Alaia MJ: Aneurysmal Bone Cyst. JAAOS - Journal of the American Academy of Orthopaedic Surgeons 20:233-241, 2012.

73. Lichtenstein L: Aneurysmal bone cyst. A pathological entity commonly mistaken for giant-cell tumor and occasionally for hemangioma and osteogenic sarcoma. Cancer 3:279-289, 1950.

74. Lambot-Juhan K, Pannier S, Grevent D, et al: Primary aneurysmal bone cysts in children: percutaneous sclerotherapy with absolute alcohol and proposal of a vascular classification. Pediatr Radiol 42:599-605, 2012.

75. Cottalorda J, Bourelle S: [Aneurysmal bone cyst in 2006]. Rev Chir Orthop Reparatrice Appar Mot 93:5-16, 2007.

76. Varshney MK, Rastogi S, Khan SA, Trikha V: Is sclerotherapy better than intralesional excision for treating aneurysmal bone cysts? Clin Orthop Relat Res 468:1649-1659, 2010.

77. Linden B: The incidence of osteochondritis dissecans in the condyles of the femur. Acta Orthop Scand 47:664-667, 1976.

78. Bray CC, Watson ST: Current review of juvenile osteochondritis dissecans of the knee. Current Orthopaedic Practice 26:466-474, 2015.

79. Schulz JF, Chambers HG: Juvenile osteochondritis dissecans of the knee: current concepts in diagnosis and management. Instr Course Lect 62:455-467, 2013.

80. Smillie IS: Treatment of osteochondritis dissecans. J Bone Joint Surg Br 39-b:248-260, 1957.

81. Kocher MS, Micheli LJ, Yaniv M, Zurakowski D, Ames A, Adrignolo AA: Functional and radiographic outcome of juvenile osteochondritis dissecans of the knee treated with transarticular arthroscopic drilling. Am J Sports Med 29:562-566, 2001.

82. Hayan R, Phillipe G, Ludovic S, Claude K, Jean-Michel C: Juvenile osteochondritis of femoral condyles: treatment with transchondral drilling. Analysis of 40 cases. J Child Orthop 4:39-44, 2010.

83. Edmonds EW, Albright J, Bastrom T, Chambers HG: Outcomes of extra-articular, intra-epiphyseal drilling for osteochondritis dissecans of the knee. J Pediatr Orthop 30:870-878, 2010.

84. Kocher MS, Czarnecki JJ, Andersen JS, Micheli LJ: Internal fixation of juvenile osteochondritis dissecans lesions of the knee. Am J Sports Med 35:712-718, 2007.

85. Adachi N, Deie M, Nakamae A, Okuhara A, Kamei G, Ochi M: Functional and radiographic outcomes of unstable juvenile osteochondritis dissecans of the knee treated with lesion fixation using bioabsorbable pins. J Pediatr Orthop 35:82-88, 2015.

86. Webb JE, Lewallen LW, Christophersen C, Krych AJ, McIntosh AL: Clinical outcome of internal fixation of unstable juvenile osteochondritis dissecans lesions of the knee. Orthopedics 36:e1444-1449, 2013.

87. Dervin GF, Keene GC, Chissell HR: Biodegradable rods in adult osteochondritis dissecans of the knee. Clin Orthop Relat Res:213-221, 1998.

88. Gudas R, Simonaityte R, Cekanauskas E, Tamosiunas R: A prospective, randomized clinical study of osteochondral autologous transplantation versus microfracture for the treatment of osteochondritis dissecans in the knee joint in children. J Pediatr Orthop 29:741-748, 2009.

89. Raynauld JP, Martel-Pelletier J, Berthiaume MJ, et al: Correlation between bone lesion changes and cartilage volume loss in patients with osteoarthritis of the knee as assessed by quantitative magnetic resonance imaging over a 24-month period. Ann Rheum Dis 67:683-688, 2008.

90. Barbour K, Helmick C, Boring M, Brady T: Vital Signs: Prevalence of Doctor-Diagnosed Arthritis and Arthritis-Atrributable Activity Limitation - United States, 2013-2015, in MMWR Morb Mortal Wkly Rep, Vol, 2017, pp 246-253.

91. Kornaat PR, Bloem JL, Ceulemans RY, et al: Osteoarthritis of the knee: association between clinical features and MR imaging findings. Radiology 239:811-817, 2006.

92. Kumar D, Wyatt CR, Lee S, et al: Association of cartilage defects, and other MRI findings with pain and function in individuals with mild-moderate radiographic hip osteoarthritis and controls. Osteoarthritis Cartilage 21:1685-1692, 2013.

93. Tanamas SK, Wluka AE, Pelletier J-P, et al: The association between subchondral bone cysts and tibial cartilage volume and risk of joint replacement in people with knee osteoarthritis: a longitudinal study. Arthritis Research & Therapy 12:R58-R58, 2010.

94. Maradit Kremers H, Larson DR, Crowson CS, et al: Prevalence of Total Hip and Knee Replacement in the United States. J Bone Joint Surg Am 97:1386-1397, 2015.

95. Cameron KL, Hsiao MS, Owens BD, Burks R, Svoboda SJ: Incidence of physician-diagnosed osteoarthritis among active duty United States military service members. Arthritis Rheum 63:2974-2982, 2011.

96. Reilingh M, van Bergen C, van Dijk C: Diagnosis and treatment of osteochondral defects of the ankle. SA Orthopaedic Journal 8:44-50, 2009.

97. Giannini S, Buda R, Faldini C, et al: Surgical treatment of osteochondral lesions of the talus in young active patients. J Bone Joint Surg Am 87 Suppl 2:28-41, 2005.

98. Gould CF, Ly JQ, Lattin GE, Beall DP, Sutcliffe JB: Bone Tumor Mimics: Avoiding Misdiagnosis. Current Problems in Diagnostic Radiology 36:124-141, 2007.

99. Olasinde AA, Oluwadiya KS, Adegbehingbe OO: Treatment of Brodie's abscess: excellent results from curettage, bone grafting and antibiotics. Singapore Med J 52:436-439, 2011.

100. Sakamoto A, Oda Y, Iwamoto Y: Intraosseous Ganglia: A Series of 17 Treated Cases. BioMed Research International 2013:4, 2013.

101. Riddle ND, Bui MM: Fibrous dysplasia. Arch Pathol Lab Med 137:134-138, 2013.

2. Mechanics Associated with an Equine Subchondral Bone Cyst

Manuscript submitted to Veterinary Surgery

Published December 2018

Running head

Bone stress and contact pressure in an equine stifle model

Title

Impact of a void in the equine medial femoral condyle on bone stresses and peak contact pressures in a finite element model

Lance L. Frazer[A], MS

Elizabeth M. Santschi[B], DVM, Diplomate ACVS

Kenneth J. Fischer[A], PhD

[A]University of Kansas, Lawrence, KS

[B]Kansas State University, Manhattan KS

This research is supported by the Madison and Lila Self Graduate Fellowship, University of Kansas

The corresponding author is Dr. Santschi:

Kansas State University

College of Veterinary Medicine

1800 Denison Ave

Manhattan KS 66506

Santschi@ksu.edu

2.1 Abstract

Objectives: To predict bone and medial meniscal stresses and contact pressures in an equine stifle with a medial femoral condyle (MFC) intact or with a 2 cm^3 subchondral bone void, under varying degrees of internal femoral rotation.

Study design: Finite element model (FEM) of a cadaveric equine stifle loaded to 8000N.

Methods: The FEM was made from a CT of the right, extended stifle of a yearling. The CT was segmented into relevant anatomic structures and meshed into 4-node tetrahedrons. Bone material properties were assigned based on Hounsfield units, soft tissue properties were estimated from published data, and the model was loaded to 8000 N in 155° extension.

Results: The main stresses found in the intact MFC were in compression, with very small areas of shear and tension. Adding a 2 cm^3 MFC void increased peak compression stress 25%, shear 50% and tension 200%. A MFC void also increased tension and shear placed on the medial meniscus by 30%. Under load, internal femoral rotation (IFR) of 2.5° and 5° increased MFC peak stresses 8-21%.

Conclusions: A 2 cm^3 MFC void in an equine stifle FEM increased stress in the bone and meniscus. Internal femoral rotation slightly increased predicted bone stress.

Clinical significance: Increases in bone and meniscal stress predicted in a MFC with a void provide evidence to understand the persistence of voids and mechanism of damage to the medial meniscus.

2.2 Introduction

Subchondral bone cysts (SBC) of the medial femoral condyle (MFC) of the horse cause stifle lameness. There are multiple treatment methods, resulting in confusion about the ideal therapeutic strategy.[1] Recently, a novel treatment using a transcondylar screw has been reported that results in faster and more complete healing of subchondral bone in the MFC.[2] However, the procedure was developed using clinical observations without experimental data. The goal of the transcondylar screw is to alter the mechanical environment of the MFC to support bone formation, but normal bone stresses and those around a MFC SBC are not known. As direct measurements of bone stress in the equine stifle is impossible, a finite element model (FEM) was constructed to provide a better understanding of the mechanics of the equine MFC when intact and with a SBC and provide possible improvements in treatment.

Currently, there is very little data on normal equine stifle kinematics and mechanics due to the technical difficulties of instrumenting and imaging the *in vivo* stifle. Published studies regarding some aspects of stifle mechanics are limited to cadaveric specimens describing tibial pressure maps,[3,4] bone density,[5] ligament strain,[6] and articular surface contact.[7] Cadaveric studies are useful, but are limited by a lack of muscle activity, the removal of some structures to apply instrumentation, inherent technology limitations (pressure sensors and strain gauges), and the difficulty in safely applying *in vivo* loads.

A FEM is a computational method used to investigate joint mechanics and local stresses. Finite element modeling constructs an *in silico* model based on digital anatomic information from computed tomography or magnetic resonance imaging.[8-10] When the structure consists of several components (bone, cartilage, ligaments, menisci, etc.) like the stifle joint, discrete anatomic structures are segmented from the digital anatomic information using visible

boundaries, tissue density (Hounsfield units) and known anatomical relationships. The segmentation volumes are discretized into finite elements and material properties are assigned to structures based on either measured values or published data. Additionally, boundary conditions are limits put on the model for displacement/rotation or applied forces. Finite element modeling has been used in a small number of equine mechanics studies, largely of the distal limb and teeth.[11-14] An initial project from our group is the only publication of a finite element model of the proximal equine limb[15], and this study aims to refine that model and enhance our understanding of the equine stifle joint.

However, because little is known about the kinematics of the loaded equine stifle, the in vivo kinematics must be estimated for computational studies. The normal human femoro-tibial joint can be very useful to help understand equine stifle kinematics, however there are substantial anatomic and biomechanical differences between species, probably due to the high load on the equine stifle, and a bipedal versus quadrupedal stance. Due to a lack of good kinematic data for the loaded equine stifle, many of these factors must be estimated. After the model geometry is developed, loads can be applied to estimate internal stresses within structures. Validity of the outputs relies on the accuracy of the model relative to the mechanical behavior of biologic structures and the appropriateness of the external loading conditions relative to physiologic loading conditions.

Our first finite element model of the stifle was constructed from CT data from a yearling Thoroughbred and was developed to estimate changes in bone stress associated with the development of an SBC.[15] The model was loaded to 3000 N, in 155º extension, and allowed translation but not internal femoral rotation (IFR). The present model was tested in 3 varying degrees of rotation because IFR occurs during flexion in the human knee[16], dog stifle[17], and has

been described in stripped, unloaded equine cadaver stifles, although described as tibial external rotation.[7]

The initial objectives of this study were to enhance the previous model by allowing IFR and to increase the load to 8000 N to approximate ground reaction force loads measured during gallop.[18,19] Our specific goals were to predict the impact of a 2 cm^3 MFC void on bone and medial meniscus stresses and on tibial contact pressures.

2.3 Methods

2.3.1 Segmentation and Discretization

A three-dimensional computed tomography (CT) scan (kVp-140; filter-body; 0.625 slice thickness; X-ray tube current 170 mAs; exposure 1320 s) was obtained of a stifle joint from a yearling Thoroughbred without stifle disease euthanized for reasons unrelated to this study (Figure 2.1A). The limb was removed at the coxofemoral joint and positioned in 155° of joint extension; the entire limb was scanned, cranial surface up with soft padding to stabilize the limb. No effort at other positioning was performed. The CT scan was segmented using ScanIP (Simpleware, United Kingdom) under supervision from a veterinary surgeon to include the femur, tibia, patella, femoral/tibial/patellar cartilage, three distal patellar ligaments, and the lateral and medial menisci (Figure 2.1B).[15] In summary, the bones were segmented by using an automatic HU threshold filter. The bones were completely filled once the filter identified bone boundaries. It was assumed that cartilages were 2 mm thick. As such, the bones were copied and subsequently dilated by 2 mm to create a uniform cartilage. The cartilage on the axial portions of the medial femoral condyle were thickened to 2.5-3 mm, as observed clinically. The menisci and patellar ligaments were manually segmented using a soft-tissue window to identify tissue boundaries. The posterior cruciate ligament (PCL), medial collateral ligament (MCL), lateral collateral ligament (LCL), and the anterior cruciate ligament (ACL) have been added to the model using one-dimensional nonlinear springs.

Two versions of the model were tested: an intact MFC and an MFC with a 2 cm^3 void. The bone void is the primary anatomic characteristic of a MFC SBC and the volume is the average volume of 6 clinical MFC SBC measured from CT images.[5] A 10 cm^3 spherical region

of interest (ROI) was created in the MFC where all stress measures were extracted. The three-dimensional segmentation (Figure 1C-D) was discretized into 4-node tetrahedral elements (C3D4) and imported into ABAQUS 6.14-2 (SIMULIA, Providence, RI). Mesh convergence was achieved for all outputs by iteratively reducing element size resulting in ~1,800,000 elements with an average edge length of 1 mm for soft tissues, 0.75 mm in the ROI, and 1-5 mm for other bone elements, with larger elements in areas distant from the ROI and contact zones (Figure 2.2).

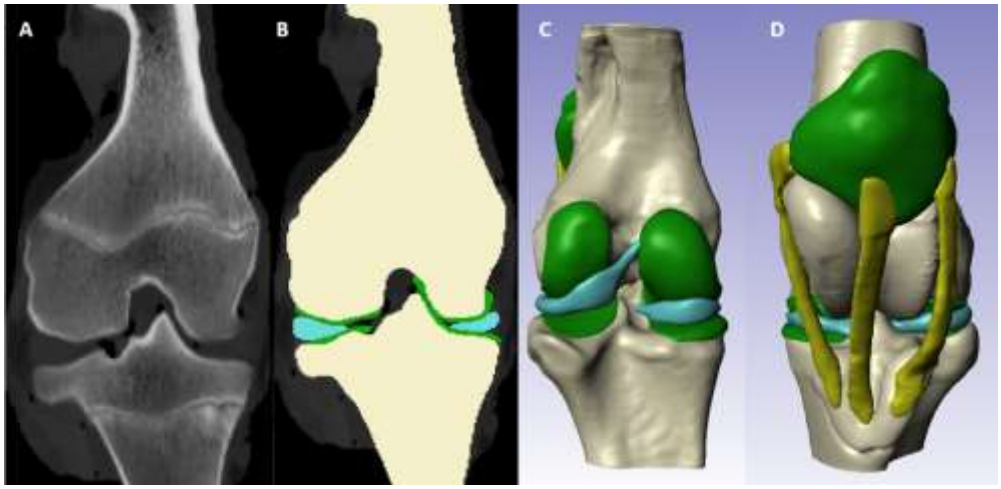

Figure 2.1. A) Unsegmented frontal plane slice from the CT scan. B) Segmentation of image A with the femur and tibia shown in tan, cartilages shown in green, and the menisci shown in blue. C) Caudal to cranial view of the 3-D, non-discretized stifle joint geometry. D) Cranial to caudal view of the 3-D, non-discretized stifle joint geometry showing the patella and surrounding cartilage in green and the patellar ligaments in yellow.

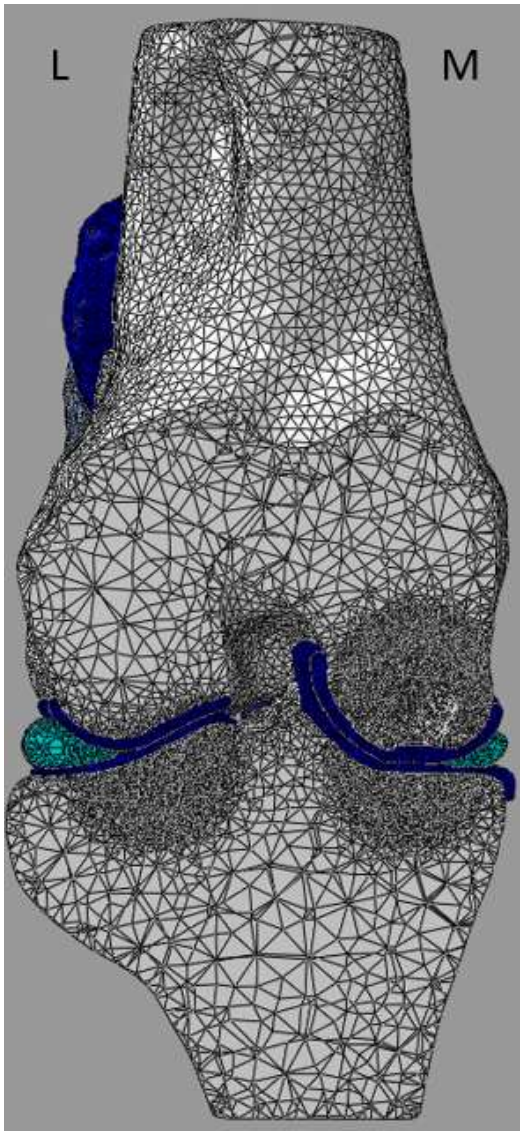

Figure 2.2 Frontal plane caudal to cranial view of the stifle joint revealing the element sizes determined by mesh convergence. Elements in the ROI, soft tissues, and contact zones are most refined.

2.3.2 Material Properties

Linear, elastic constitutive relationships were used to define bone, cartilage, and patellar ligament tissue properties. Such properties were appropriately used since the purpose of this study was to examine instantaneous material responses during compressive loading; therefore, more complex, time-dependent material definitions were not necessary.[20-22] Bone was modeled as a heterogeneous structure using a conversion from Hounsfield units to local Young's Modulus with 20 unique moduli levels resulting in a modulus range of 50 MPa to 21,000 MPa.[15] Bone moduli in the MFC ranged between 300-750 MPa consistent with moduli in the human MFC, as these values have been reported to be around 400 MPa.[22,23] With overall bone density being slightly higher in an equine MFC,[24] a higher modulus would be expected with the highest values at the subchondral bone plate. The patellar ligaments were the only ligaments modeled with 3D elements, to allow for ligament-bone contact and wrapping, as well as providing a naturally occurring cranial constraint. Patellar ligaments were assigned a modulus of 300 MPa.[25]

The PCL, ACL, MCL, and LCL insertions were located as detailed by Aldrich et al.[26] and were modeled as non-linear springs using Equation 1.

$$f = \begin{cases} \frac{1}{4}k\epsilon^2/\epsilon_i, & 0 \leq \epsilon \leq 2\epsilon_i, \\ k(\epsilon - \epsilon_i), & \epsilon > 2\epsilon_i, \\ 0, & \epsilon < 0, \end{cases} \quad (1)$$

In this piecewise function, k is the ligament stiffness parameter and ε_i is a ligament stiffness transition parameter assumed to be 0.03.[23,27] The force-displacement relationship is quadratic up until the value of $2\varepsilon_i$ at which point the relationship becomes linear. This force-displacement

equation produces values consistent with those reported by Rich et al.[28] Each meniscus was tied to their anatomical insertion points (menisco-tibial ligaments), and the outer edge of each meniscus was partially constrained to the tibial plateau using springs to simulate the natural constraint from the joint capsule, since there was no joint capsule in the model.[29] Meniscal properties were adopted from Donahue et al,[23] and cartilage properties were adapted from Malekipour et al.[30] A summary of the material properties used in this study can be found in Table 2.1. The void was not given any material properties and was modeled as a 2 cm^3 oblong void with a narrow opening in the distal MFC (Figure 2.3; black arrow).[5]

Table 2.1. Summary of the 3-D material properties used in this study.

Structure	**Type**	**Young's Modulus (MPa)**	**Poisson's Ratio**
Bone	Isotropic	50-21,000	0.3
Menisci	Anisotropic	Radial and Axial = 20 Circumferential = 120	Radial and Axial = 0.3 Circumferential = 0.45
Cartilage	Isotropic	50	0.45
Patellar Ligaments	Isotropic	300	0.3

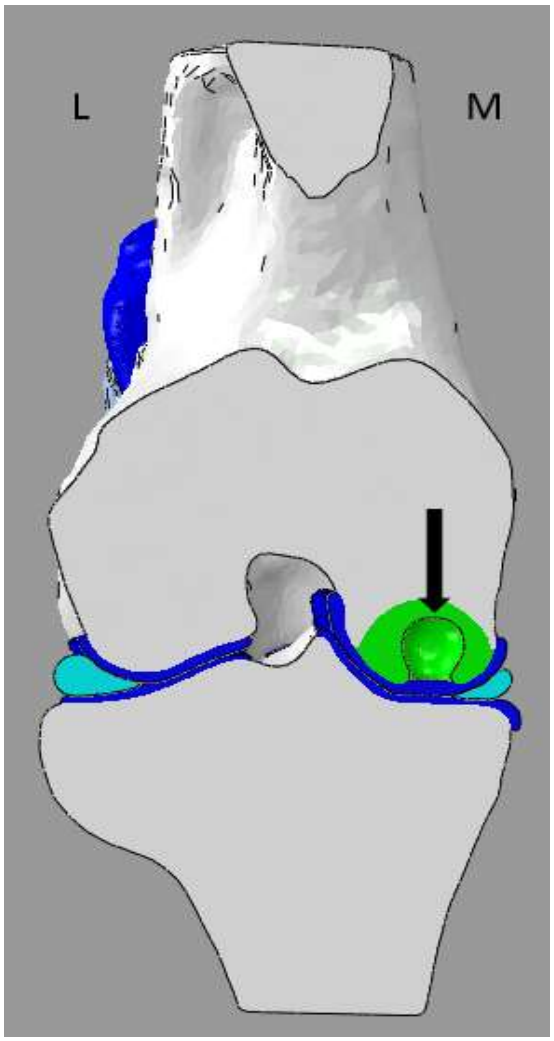

Figure 2.3. Frontal plane caudal to cranial view of the stifle joint revealing the 2 cm^3 void in the distal MFC. Articular cartilage is dark blue, menisci are light blue, and the ROI is green. M=medial, L=lateral.

2.3.3 Loading Conditions and Analysis

Rotation in the sagittal plane (flexion angle) was constrained to 155° (extension). Preliminary investigations of unconstrained frontal plane rotation resulted in valgus angulation and a significant increase in lateral tibial peak pressures. This is not consistent with the known

human knee kinematics[31,32] or equine clinical experience, as equine lateral femorotibial injury is uncommon.[33] As a result, frontal plane rotation was constrained in the present model.

For each simulation, a compressive force of 8000 N was uniformly distributed on the proximal femur that acted normal to a transverse section of the femur, and a uniformly distributed tensile force of 1000 N was placed on the patella parallel to the femoral long axis to simulate quadriceps contraction. There is no available data for these forces in the horse at the gallop. We chose 8000 N for the femoral load because it is similar to the ground reaction force measured in the forelimb of galloping horses.[18,19] The patellar tension load was chosen because at 8000 N load without patellar tension, the joint dislocated due to cranial translation of the femur. Providing 1000 N of proximal patellar tension limited cranial femoral translation. When load was applied with patellar tension, the femur was allowed to translate in all three anatomical directions, and the distal aspect of the tibia was fully constrained. Frictionless, surface-to-surface contact was defined between each articulating surface, and the contact gap was closed using a penalty function with a default penalty stiffness assigned by ABAQUS. See the visual representation of the boundary conditions on the finite element mesh in Figure 2.4.

The amount of rotation of the tibia (external relative to the femur) and femur (internal relative to the tibia) in the horse is not known,[17] but there is evidence it exists.[7] This study tested 3 levels of IFR (0°, 2.5° and 5°), each with and without a subchondral bone cyst. In each of the three variations, stifle joint varus/valgus angulation and joint flexion were constrained. In the first setup, IFR was fully constrained. In the second setup, IFR was partially constrained to 2.5° by using a 630 N-m/rad rotational spring on the proximal femur. In the third and final setup, the femur was fully free to internally rotate under the 8000 N load.

For each simulation, the stress distribution and peak stresses (compression, tension, shear) were extracted from the ROI and medial meniscus. Compression was defined as the third principal stress, as long as the value was negative. If the value was positive, it was not recorded. Tension was defined as the first principal stress, as long as the value was positive. If the value was negative, it was not recorded. Shear was defined as tresca stress: 1/2*(first principal stress - third principal stress). We also examined the contact pressure distribution and peak contact pressure on the medial and lateral tibial cartilage and the medial meniscus. Peak stress and contact pressure were defined as the average of the 99^{th} percentile to omit numerical outliers introduced by the FEM. We also examined the contact pressure distribution and peak contact pressure on the medial and lateral tibial cartilage and the medial meniscus. Peak stress and contact pressure were defined as the average of the 99^{th} percentile to omit numerical outliers introduced by the FEM.

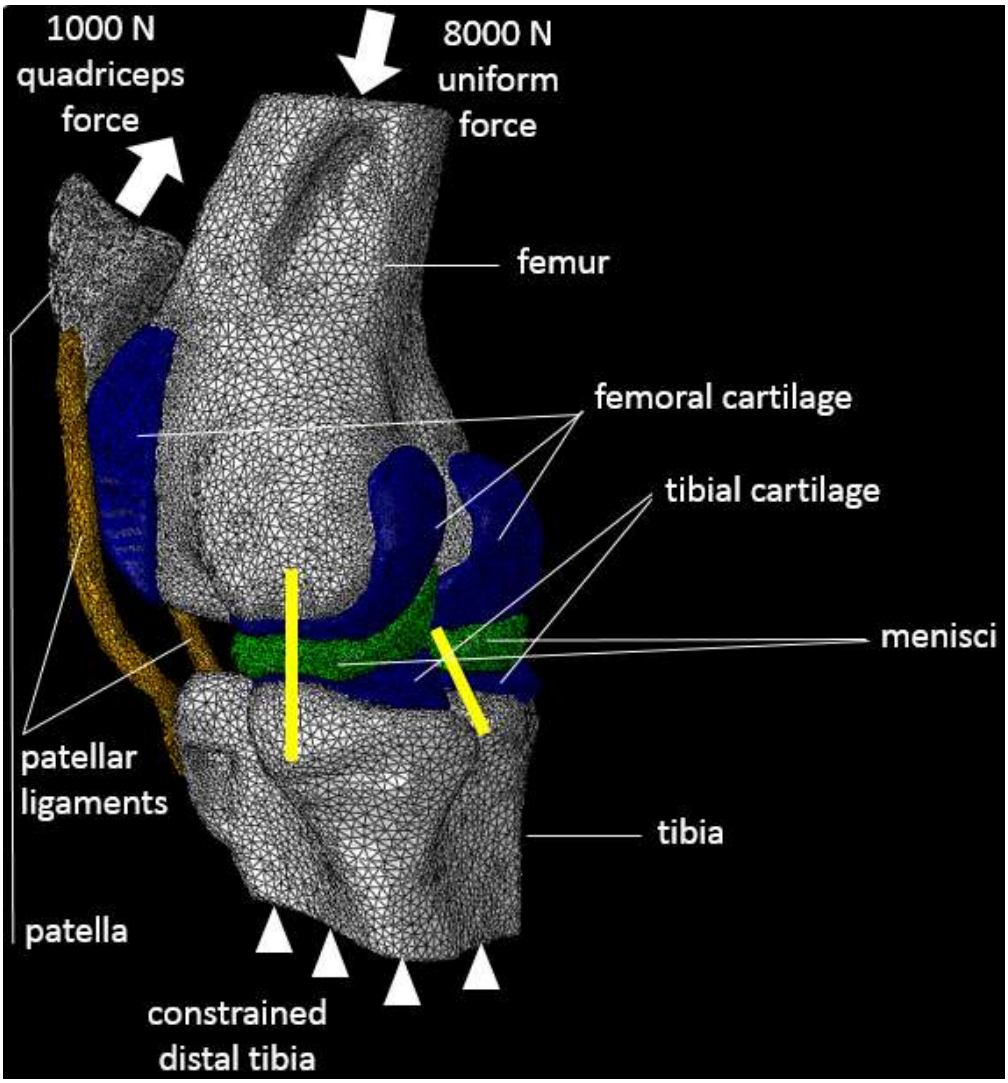

Figure 2.4. Caudolateral 3D view of the finite element mesh and boundary conditions. A normal compressive force of 8000 N was uniformly distributed across the proximal aspect of the femur, and a normal tensile force of 1000 N parallel to the direction of force from the quadriceps muscle on the patella was uniformly placed across the proximal patella. The distal tibia was fully constrained. Patellar ligaments (orange) are visible in the left of the image. Cartilage is dark blue and the menisci are green. Also visible is the LCL and the PCL in yellow, modeled as one-dimensional, nonlinear springs.

2.4 Results

2.4.1 Effect of a Subchondral MFC Void

2.4.1.1 Bone stresses

In the loaded intact MFC model the major bone stress was compression. Peak stress occurred at the articulation between the MFC and tibia, and smoothly decreased radially outwards from the central point of contact (Figure 2.5). Tensile stress in the intact MFC was low and uniformly distributed (Figure 2.6), but substantial shear stress was present in the intact MFC over a small area in the contact region with the tibia (Figure 2.7). Adding a 2 cm^3 void in the central aspect of the distal MFC increased all MFC peak bone stresses measured (tension, compression and shear; Table 2.2). Peak compressive stress increased the least (about 25%), and peaks occurred at the articulation and decreased proximally (Figure 2.5). Peak shear stress with a void increased about 50% at the site of MFC and tibial articulation (Figure 2.7). Peak tensile stress increased about 200%, and peaks occurred at the proximomedial and distolateral aspects of the void (Figure 2.6). However, all tensile stresses were low.

Table 2.2. Peak bone stresses in the MFC ROI for each rotational condition with and without a 2 cm^3 void. The increase in peak stress with a void is noted parenthetically as a percent change from the intact model for that degree of rotation. All values are in MPa. IRF=internal rotation of the femur (with respect to the tibia). All stresses were increased in the void model, and shear exceeded trabecular bone yield stress in some combinations.

Model/Rotation	Tension (MPa)	Compression (MPa)	Shear (MPa)
Intact/0°IRF	1.2	15.4	11.9
Void/0°IRF	3.6 (200%)	18.9 (23%)	18.6 (57%)
Intact/2.5° IRF	1.4	16.7	13.0
Void/2.5° IRF	3.8 (171%)	20.8 (25%)	20.4 (57%)
Intact/5° IRF	1.4	18.2	14.1
Void/5° IRF	3.9 (179%)	22.9 (26%)	22.4 (59%)

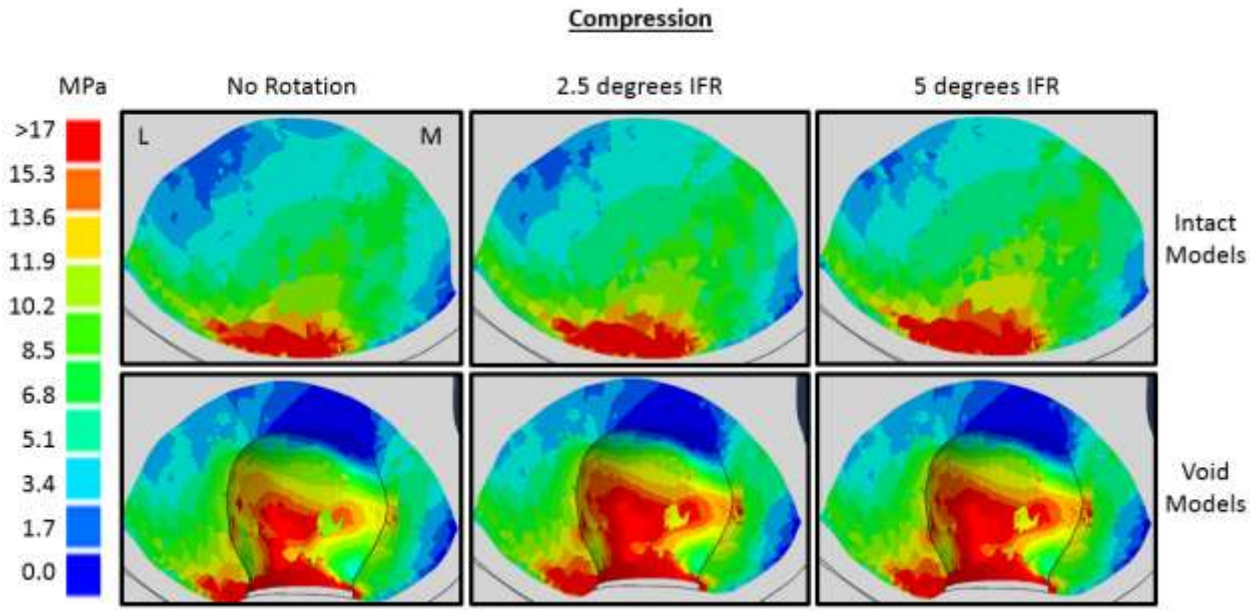

Figure 2.5. Compression map of six tested models/conditions in the medial femoral condyle. Maps are in the frontal plane, centered on the femorotibial extension impact zone, and the view is caudal to cranial. Top row: intact models, bottom row: void models. L=lateral, M=medial, and joint surface is at the bottom of each image. In the intact MFC, peak compression occurred at the central articulation with the tibia. In the MFC with a void, compressive stresses increased (23-26%) cranially on the interior surface of the void, though stresses were still well below compressive yield strength. Internal femoral rotation increased compressive stresses 8-21%.

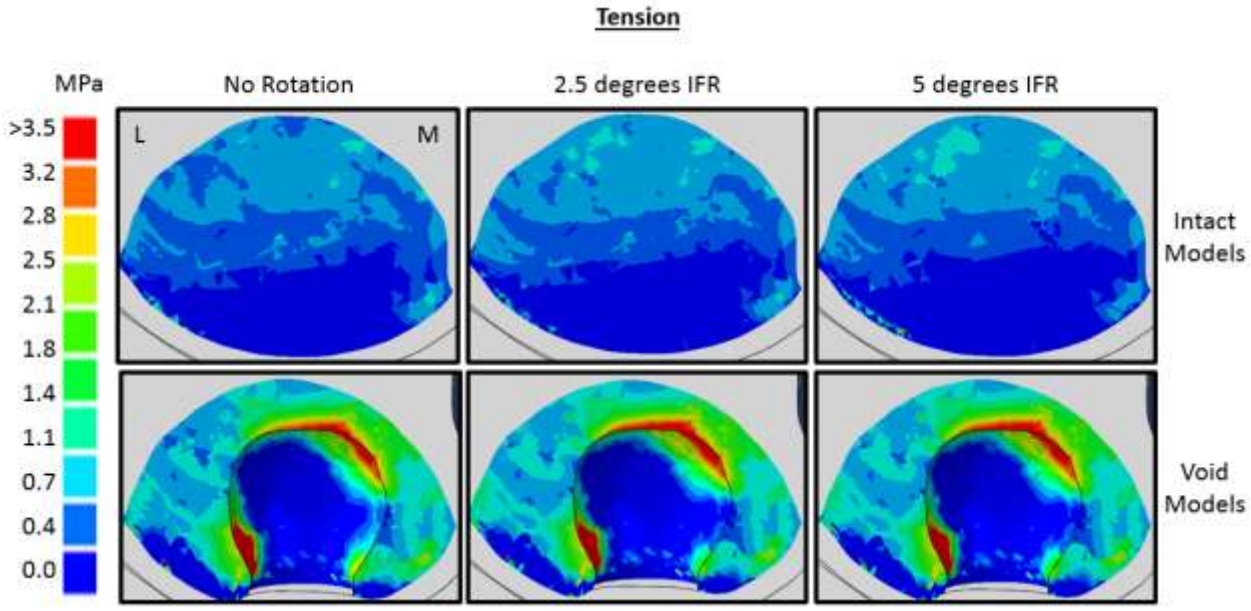

Figure 2.6. Tensile map of six tested models/conditions. Maps are in the frontal plane, centered on the femorotibial extension impact zone, and the view is caudal to cranial. Top row: intact models, bottom row: void models. L=lateral, M=medial, and joint surface is at the bottom of each image. In the intact MFC, very little tension is predicted. In the MFC with a void, tension was focally increased at the proximomedial and distolateral aspects of the void. Internal femoral rotation had a minimal impact on tensile stress.

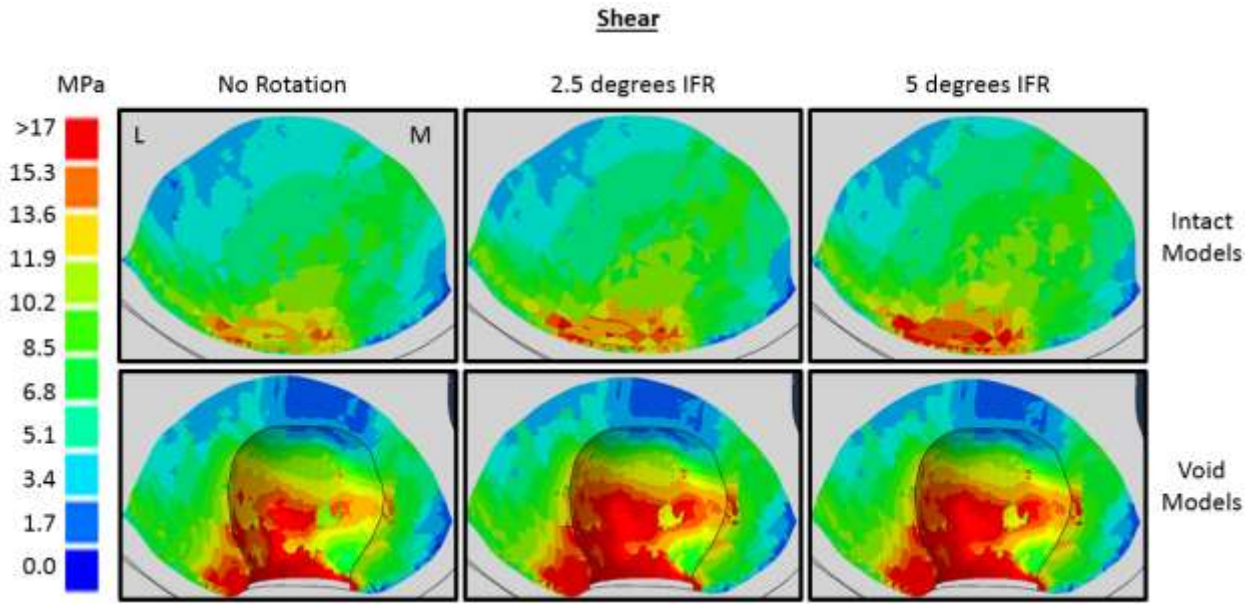

Figure 2.7. Shear stress map of six tested models/conditions. Maps are in the frontal plane, centered on the femorotibial extension impact zone, and the view is caudal to cranial. Top row: intact models, bottom row: void models. L=lateral, M=medial, and joint surface is at the bottom of each image. In the intact MFC, a small focal area of shear stress is present at the articulation. In the MFC with a void, shear stress was increased in size and magnitude (57-59%) at the distal aspect of the void and was elevated on the cranial-lateral interior surface of the void. Increasing internal femoral rotation increased the magnitude (9-20%) and region of high shear stress, and caused peak shear stresses to exceed the shear yield strength.

2.4.1.2 Peak contact pressure and peak meniscal stresses

The MFC void model as compared to the intact model increased peak contact pressures (PCP) on the lateral tibia approximately 10% and decreased PCP approximately 12% on the medial tibia (Table 2.3). PCP in the intact model occurred on the central cartilage of the medial tibia, but in the MFC void the high contact stress region was smaller and more axial toward the medial intercondylar eminence (Figure 2.8). The void in the MFC resulted in 24-31% increase in tension and 23-29% increase in shear in the medial meniscus (Table 2.4), though the pattern of stress in the meniscus was similar with and without a cyst.

Table 2.3. Peak contact pressure (MPa) on tibial cartilage. For each model/condition, the highest peak contact pressure is in bold. IRF= internal rotation (femur). The change in peak stress in the void model with IRF is noted parenthetically as a percent change from the intact model. Note that the void reduced peak medial contact pressure and increased peak lateral contact pressure.

Model/Rotation	Lateral (MPa)	Medial (MPa)
Intact/0°IRF	15.8	**20.0**
Void/0°IRF	**17.4** (10.1%)	17.3 (-13.5%)
Intact/2.5° IRF	15.3	**21.7**
Void/2.5° IRF	16.9 (10.5%)	**18.9** (-12.9%)
Intact/5° IRF	14.8	**23.8**
Void/5° IRF	16.4 (10.8%)	**21.0** (-11.7%)

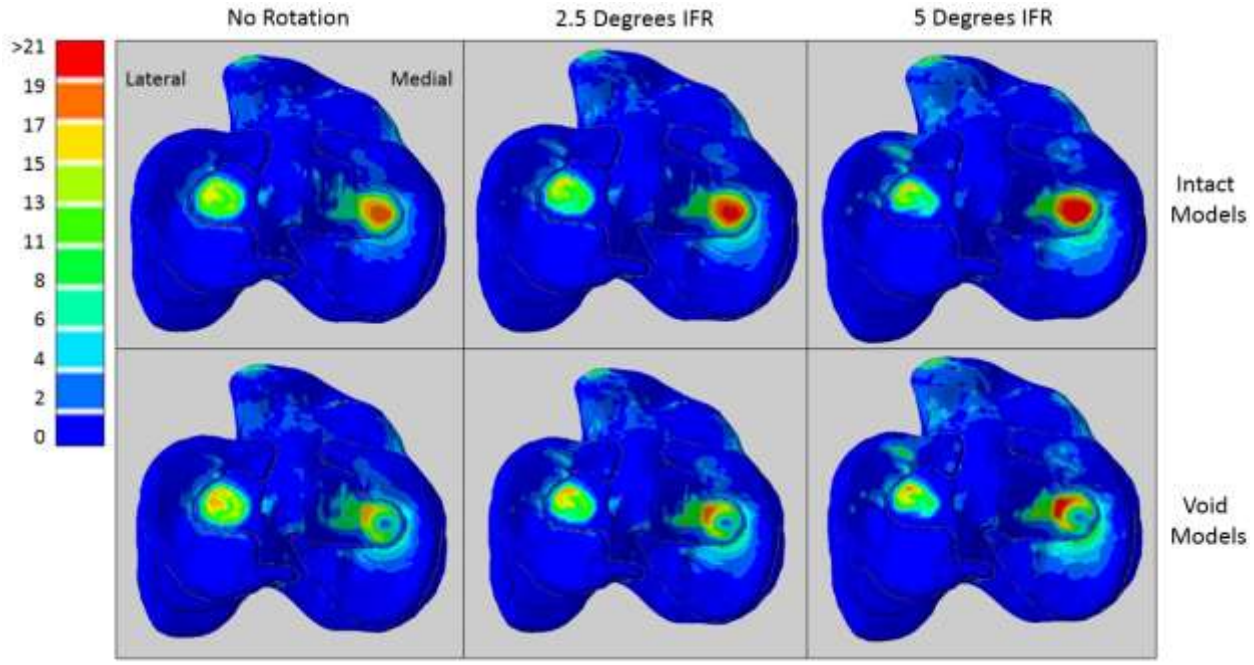

Figure 2.8. Tibial contact pressure maps (MPa) for intact model (top row) and void model (bottom row). In the void model, contact pressure decreased (11-14%) on the medial tibial condyle and increased slightly on the lateral condyle (10-11%). Medial contact pressures increased with IFR.

Table 2.4. Peak tensile and shear stresses in the medial meniscus for the six tested models/conditions. The increase in peak stress in the void model is noted parenthetically as a percent change from the intact model. Both the void and increasing IRF increased tension and shear stress in the medial meniscus.

Model/rotation	Tension (MPa)	Shear (MPa)
Intact/0°IRF	8.2	8.9
Void/0°IRF	10.7 (30%)	11.5 (29%)
Intact/2.5° IRF	9.0	10.4
Void/2.5° IRF	11.8 (31%)	12.9 (24%)
Intact/5° IRF	10.5	12.6
Void/5° IRF	13.1 (24%)	15.5 (23%)

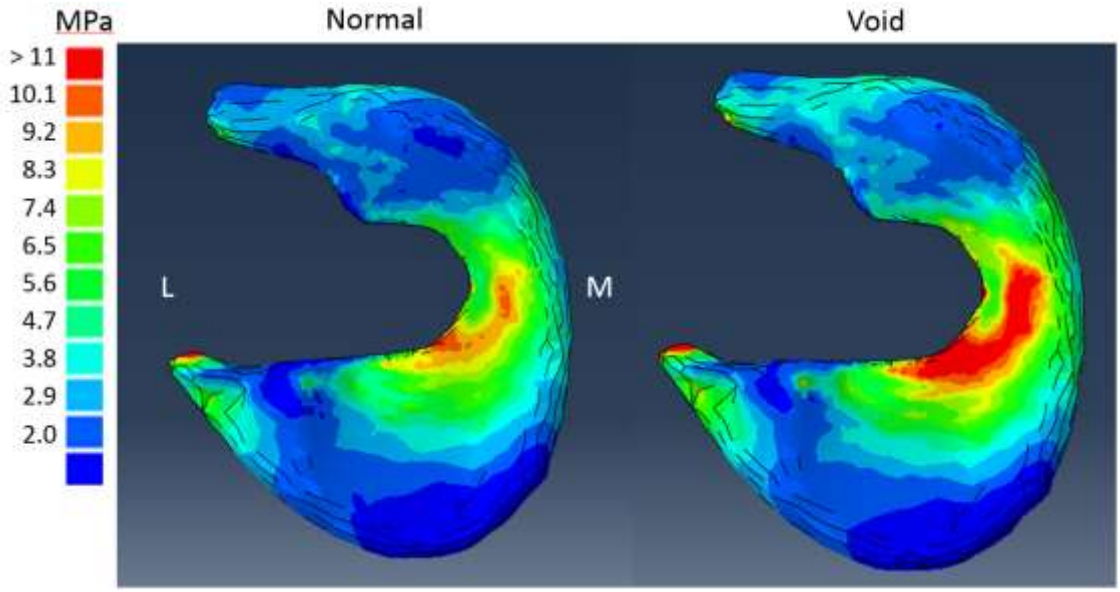

Figure 2.9. Medial meniscus shear stress map for femoral contact surface with 2.5º IFR. Shear stress is increased in area and magnitude (23-29%) in the meniscal body when a void was added to the MFC. L=lateral, M=medial, Cr=cranial, Ca=caudal.

2.4.2 Effect of Internal Femoral Rotation

Complete constraint of long axis femoral internal rotation at 8000 N load required an external rotation reaction torque of 37 N-m. Allowing the femur to freely internally rotate resulted in a maximum of 5° IFR and was restricted by the interaction of the medial tibial eminence with the MFC. The general trend was that increasing IFR increased MFC bone stress (Figures 2.5-2.7) medial tibial cartilage pressure, lowered lateral tibial contact pressure (Figure 2.8), and increased medial meniscus stress (Figure 2.9). The 5° IFR resulted in the highest predicted MFC bone and medial meniscus stress, the highest medial tibial contact pressure, and the lowest lateral tibial contact pressure (Tables 2.2-2.4).

2.4.2.1 Bone stresses and peak contact pressure

Constraining femoral rotation to 2.5° by use of a rotational spring resulted in an 8-16% increase in MFC bone stresses, and allowing free IFR resulted in a 17-18% increase in bone stresses compared to fully constrained (Table 2.2). Allowing 2.5-5° IFR decreased PCP on the lateral tibia by 3-7% and increased PCP on the medial tibia 9-21% in both models and had minimal impact on PCP location (Table 2.3). IFR also resulted in a mild increase in contact pressure on the caudal region of the meniscus (Figure 2.8).

2.4.2.2 Peak meniscal stresses

Allowing femoral rotation of 2.5° by use of a rotational spring resulted in a 10% increase in peak medial meniscus tension and a 12-17% increase in peak shear stress, considering models with and without a void. Allowing free IFR (5°) resulted in increases of 22-28% in peak medial meniscal tension and 35-42% in peak medial meniscal shear stress. Peak meniscal shear and tensile stress occurred in the axial aspect in the central part of the meniscus (Figure 2.9).

2.5 Discussion

This study supports the mechanism proposed by Frazer et al. for cystic development and resistance to treatment.[15] As such, cystic development and treatment resistance may be explained by mechanics in the MFC, especially shear stress. Shear stress can be especially damaging, as trabecular bone is weakest in shear.[34-38] The shear yield stress of equine MFC bone is unknown, but a reasonable estimation can be made using clinical observation and previous human studies. Clinical observations show that the MFC bone is trabecular and its material properties are quite variable depending on anatomic site, bone density, and other factors.[39] In a study of a human

trabecular bone, Sanyal et al. proposed the relationship to quantify yield strength of human trabecular bone in shear:

$$\text{Yield Strength (Shear) (MPa)} = 63\ X^{1.67}$$

where X represents bone volume fraction (BVF).[38] Equine trabecular bone in the MFC has a BVF in the range of 0.4-0.5,[40] resulting in a shear yield strength of 13-20 MPa. The predicted peak shear in the intact MFC (11.9MPa) at the central articulation of the tibia approaches this value and was exceeded at the distal axial aspect of the void (18.6 MPa with IFR and 20.4-22.4 MPa with IFR). This suggests that shear stress may be one of the mechanisms of SBC development and would create a hostile environment for bone healing once a SBC has formed. For periodic, inadvertent higher loads, the bone in the intact femur may be damaged, initiating a cyst. The elevated stresses around the cyst, may lead to cyst persistence and/or growth.

Meniscal injury has been associated with equine medial femorotibial disease including MFC SBCs both before and after treatment.[41,42] This is the first report examining the mechanical impact of a MFC void on the equine meniscus. We believe that the changes in the meniscus stress that occur with an MFC SBC may explain some meniscal injuries, as our model predicts about a 30% increase in peak tension and shear on the meniscus when an MFC void was present. This increase in stress occurs in the meniscal body, a common location of injury[42] (Figure 2.9), and may be exacerbated when the loaded stifle is flexed.[2] Two previous studies have measured contact pressure ex vivo on the proximal tibia under the equine medial meniscus,[3,4] but do not agree on the shape of the pressure maps. The present results are most similar to Bonilla et al, predicting substantial abaxial pressure in the middle of the meniscus that is increased when an MFC void is present. If the increase in stress is magnified when joint flexion is allowed as was

demonstrated ex vivo,[3] this may provide a mechanism for meniscal damage in horses with MFC SBCs.

This study also examined long-axis internal femoral rotation. Sagittal rotation (joint flexion) was constrained to consider outcomes in stifle extension, a likely position when MFC damage occurs. Preliminary finite element results allowing frontal plane rotation (varus/valgus angulation) produced increased pressure in the lateral femoro-tibial joint and were at odds with clinical stifle lameness[33,42] and anatomic observations, and so varus/valgus rotation was constrained. This decision is supported by a kinematic analysis of an unloaded, nearly complete equine stifle that suggest that frontal plane rotation is limited in terminal extension.[7] The valgus rotation in our preliminary test could be the result of uniform femoral loading (versus a higher medial load). Also, there is not any pre-tension present in the collateral ligaments, and they do not provide substantial resistance to varus/valgus rotation. However, long axis rotation, specifically automatic (passive) internal femoral rotation (IFR) during terminal extension, has been well-described in man,[16,31] has been noted in canines,[17] and was noted passively ex vivo in the equine stifle.[7] Internal femoral rotation is the result of anatomy, specifically of the curve of the femoral condyle and the attachments and fiber orientation of the cruciate ligaments. It appears that IFR may exist in the horse, but the magnitude of rotation is unknown, so models were tested at 0° IFR (constrained), 2.5° IFR, and 5° IFR (unconstrained).

Even though the amount of IFR in terminal extension in the equine stifle joint is unknown, a reasonable estimation can be made using our model, clinical evidence, and data from human studies. The reaction torque needed to completely constrain IFR was 37 N-m. This high reaction torque would have to be provided by soft tissues (ligaments, muscles, fascia, etc.) not included in the model. Allowing IFR reduces this burden supporting the conclusion that IFR is

present in terminal extension for the horse as is present in human knees.[16] Our model predictions of increases in medial compartment stress and decreases in lateral compartment stress with increasing IFR is are consistent with clinical observation that medial compartment injuries are more common. Thus, clinical observation in combination with our model supports the conclusion that IFR exists in the stifle joint. The magnitude of IFR is not known, but 5° appears to be the upper boundary based on predicted bone-on-bone contact. A lower rotation angle closer to 2.5° seems to be a more reasonable estimate.

The authors acknowledge the limitations associated with this study. The CT was obtained in an unloaded specimen, and only one stifle joint was used to construct the model, and results could be dependent on specific stifle geometry. The lack of in vivo equine kinematic information reduced our focus to the MFC ROI bone stress, meniscal stress and proximal tibial pressure maps. To attempt to simulate stifle kinematics, we substituted some structures with linear springs to mimic their mechanics and eliminated most muscle action, except an estimation of the proximal tension on the patella. Additionally, assumptions have been made about material properties and equine kinematics, and data from human and animal studies have been used to fill in the gaps. Future work in obtaining kinematic data of the stifle joint and equine soft tissue properties would be very beneficial to further refine/validate this model. However, we believe the assumptions made in this study are reasonable to develop a preliminary understanding of stifle joint mechanics and the mechanical impact of MFC SBCs. Furthermore, due to the comparative nature of the study, our results are still useful for drawing conclusions as to how joint mechanics are altered with a SBC.

2.6 Conclusion

In the equine stifle finite element model, the intact MFC loaded to 8000 N largely experienced compressive stress with shear stress present at the distal aspect. Removing long-axis rotation constraints resulted in internal femoral rotation and increases bone and meniscal stress in the medial femorotibial joint. Adding a 2 cm^3 MFC void substantially increased shear stress in the periphery that can exceed the yield strength of trabecular bone (13-20 MPa).[37] The void also increased tension and shear in the medial meniscus. The changes in tissue stresses and joint contact pressures predicted in the medial femorotibial joint with a MFC void suggest that under continued strenuous activity joint mechanics promote void persistence and meniscal injury. Future work will evaluate treatment strategies building on the present finite element model.

2.7 Acknowledgment

This work was supported by a Madison and Lila Self Graduate Fellowship at the University of Kansas.

2.8 Disclosure

The authors declare no conflict of interest related to this report.

2.9 References

1. O'Brien EJO: What is the best treatment for medial femoral condylar subchondral bone cysts? *Equine Veterinary Education*. 2018; doi: 10.1111/eve.12927.
2. Santschi EM, Williams JM, Morgan JW, et al: Preliminary investigation of the treatment of equine medial femoral condylar subchondral cystic lesions with a transcondylar screw. *Vet Surg*. 2015; 44:281-288.
3. Bonilla AG, Williams JM, Litsky AS, et al: Ex vivo equine medial tibial plateau contact pressure with an intact medial femoral condyle, with a medial femoral condylar defect, and after placement of a transcondylar screw through the condylar defect. *Vet Surg*. 2015; 44:289-296.
4. Fowlie J, Arnoczky S, Lavagnino M, et al: Resection of Grade III cranial horn tears of the equine medial meniscus alter the contact forces on medial tibial condyle at full extension: an in-vitro cadaveric study. *Vet Surg*. 2011; 40:957-965.
5. Walker WT SJ, Kawcak CE, Nelson BB, Fortier LA: Morphological characteristics of subchondral bone cysts in medial femoral condyles of adult horses as determined by computed tomography. *Am J Vet Res.* 2016; 77:265-274.
6. Fowlie JG, Arnoczky SP, Lavagnino M, et al: Stifle extension results in differential tensile forces developing between abaxial and axial components of the cranial meniscotibial ligament of the equine medial meniscus: a mechanistic explanation for meniscal tear patterns. *Equine Vet J.* 2012; 44:554-558.
7. Halley SE, Bey MJ, Haladik JA, et al: Three dimensional, radiosteriometric analysis (RSA) of equine stifle kinematics and articular surface contact: A cadaveric study. *Equine veterinary journal.* 2014; 46:364-369.

8. Parashar SK, Sharma JK: A review on application of finite element modelling in bone biomechanics. *Perspectives in Science.* 2016; 8:696-698.

9. Belytschko T, Kulak RF, Schultz AB, et al: Finite element stress analysis of an intervertebral disc. *Journal of Biomechanics.* 1974; 7:277-285.

10. Rybicki EF, Simonen FA: Mechanics of oblique fracture fixation using a finite-element model. Journal of Biomechanics 10:141-148, 1977.

11. O'Hare LM, Cox PG, Jeffery N, et al: Finite element analysis of stress in the equine proximal phalanx. *Equine Veterinary Journal*. 2013; 45:273-277.

12. Schrock P, Lüpke M, Seifert H, et al: Finite element analysis of equine incisor teeth. Part 2: Investigation of stresses and strain energy densities in the periodontal ligament and surrounding bone during tooth movement. *The Veterinary Journal.* 2013; 198:590-598.

13. Harrison SM, Chris Whitton R, Kawcak CE, et al: Evaluation of a subject-specific finite-element model of the equine metacarpophalangeal joint under physiological load. *Journal of Biomechanics.* 2014; 47:65-73.

14. Hinterhofer C, Stanek C, Haider H: The effect of flat horseshoes, raised heels and lowered heels on the biomechanics of the equine hoof assessed by finite element analysis (FEA). *Journal of Veterinary Medicine Series.* 2000; 47:73-82.

15. Frazer LL, Santschi EM, Fischer KJ: The impact of subchondral bone cysts on local bone stresses in the medial femoral condyle of the equine stifle joint. *Med Eng Phys.* 2017; 48:158-167.

16. Kim HY, Kim KJ, Yang DS, et al: Screw-Home Movement of the Tibiofemoral Joint during Normal Gait: Three-Dimensional Analysis. *Clinics in Orthopedic Surgery.* 2015; 7:303-309.

17. Anderst WJ, Tashman S: Using relative velocity vectors to reveal axial rotation about the medial and lateral compartment of the knee. *J Biomech.* 2010; 43:994-997.
18. Roland ES, Hull ML, Stover SM: Design and demonstration of a dynamometric horseshoe for measuring ground reaction loads of horses during racing conditions. *J Biomech.* 2005; 38:2102-2112.
19. Robin D, Chateau H, Falala S, et al: Ground reaction forces in the horse at the walk, trot and gallop measured with an instrumented shoe. *Computer Methods in Biomechanics and Biomedical Engineering*. 2008; 11:195-196.
20. Donzelli PS, Spilker RL, Ateshian GA, et al: Contact analysis of biphasic transversely isotropic cartilage layers and correlations with tissue failure. *J Biomech.* 1999; 32:1037-1047.
21. Armstrong CG, Lai WM, Mow VC: An analysis of the unconfined compression of articular cartilage. *J Biomech Eng.* 1984; 106:165-173.
22. Kiapour A, Kiapour AM, Kaul V, et al: Finite element model of the knee for investigation of injury mechanisms: development and validation. *J Biomech Eng.* 2014; 136:011002.
23. Donahue TL, Hull ML, Rashid MM, et al: A finite element model of the human knee joint for the study of tibio-femoral contact. *J Biomech Eng.* 2002; 124:273-280.
24. Lewis CWW, A K; Chen, A C; Bae, W C; Temple, M M; Wong, V W; Nugent, G E; Harmel J L; Walker J E; James, S P; Wheeler, D L; Sah, R L; Kawcak C E: Relationship between functional demand, subchondral bone mineral density, and articular cartilage structure and integrity. *Proceedings, ORS, Washington, D.C.* 2005.

25. Butler DL, Kay MD, Stouffer DC: Comparison of material properties in fascicle-bone units from human patellar tendon and knee ligaments. Journal of Biomechanics 19:425-432, 1986.

26. Aldrich ED, Goodrich LR, Monahan MK, et al: Radiographic localisation of the entheses of the equine stifle. *Equine Veterinary Journal.* 2017; 49:493-500.

27. Li G, Gil J, Kanamori A, et al: A Validated Three-Dimensional Computational Model of a Human Knee Joint. *Journal of Biomechanical Engineering.* 1999; 121:657-662.

28. Rich FR, Glisson RR: In vitro mechanical properties and failure mode of the equine (pony) cranial cruciate ligament. *Vet Surg.* 1994; 23:257-265.

29. Mootanah R, Imhauser CW, Reisse F, et al: Development and validation of a computational model of the knee joint for the evaluation of surgical treatments for osteoarthritis. *Comput Methods Biomech Biomed Engin*. 2014; 17:1502-1517.

30. Malekipour F, Whitton C, Oetomo D, et al: Shock absorbing ability of articular cartilage and subchondral bone under impact compression. *J Mech Behav Biomed Mater.* 2013; 26:127-135.

31. Fuss FK: Anatomy of the cruciate ligaments and their function in extension and flexion of the human knee joint. *American Journal of Anatomy.* 1989; 184:165-176.

32. Freeman MAR, Pinskerova V: The Movement of the Knee Studied by Magnetic Resonance Imaging. *Clinical Orthopaedics and Related Research.* 2003; 410:35-43.

33. Nelson BB, Kawcak CE, Goodrich LR, et al: Comparison between computed tomographic arthrography, radiography, ultrasonography, and arthroscopy for the diagnosis of femorotibial joint disease in western performance horses. *Vet Radiol Ultrasound.* 2016; 57:387-402.

34. Ford CM, Keaveny TM: The dependence of shear failure properties of trabecular bone on apparent density and trabecular orientation. *J Biomech.* 1996; 29:1309-1317.

35. Kopperdahl DL, Keaveny TM: Yield strain behavior of trabecular bone. *Journal of Biomechanics.* 1998; 31:601-608.

36. Keaveny TM, Wachtel EF, Kopperdahl DL: Mechanical behavior of human trabecular bone after overloading. *J Orthop Res.* 1999; 17:346-353.

37. Bayraktar HH, Morgan EF, Niebur GL, et al: Comparison of the elastic and yield properties of human femoral trabecular and cortical bone tissue. *Journal of Biomechanics.* 2004; 37:27-35.

38. Sanyal A, Gupta A, Bayraktar HH, et al: Shear strength behavior of human trabecular bone. *J Biomech.* 2012; 45:2513-2519.

39. Hodgskinson R, Currey JD: Young's modulus, density and material properties in cancellous bone over a large density range. Journal of Materials Science: *Materials in Medicine.* 1992; 3:377-381.

40. Chevrier A, Kouao ASM, Picard G, et al: Interspecies comparison of subchondral bone properties important for cartilage repair. *Journal of Orthopaedic Research.* 2015; 33:63-70.

41. Hendrix SM, Baxter GM, Mc Ilwraith CW, et al: Concurrent or sequential development of medial meniscal and subchondral cystic lesions within the medial femorotibial joint in horses (1996–2006). *Equine Veterinary Journal.* 2010; 42:5-9.

42. Dubuc J, Girard C, Richard H, et al: Equine meniscal degeneration is associated with medial femorotibial osteoarthritis. *Equine Veterinary Journal.* 2018; 50:133-140.

3. How a Transcondylar Screw Affects Bone Formation in an Equine Subchondral Bone Cyst

Manuscript submitted to Veterinary Surgery

In Review

Running Head

Bone remodeling stimulus using a transcondylar screw

Title

How a transcondylar screw promotes healing of subchondral bone cysts in the equine medial femoral condyle

Lance L. Frazer[A], MS

Elizabeth M. Santschi[B], DVM, Diplomate ACVS

Kenneth J. Fischer[A], PhD

[A]University of Kansas, Lawrence, KS

[B]Kansas State University, Manhattan, KS

This research is supported by the Madison and Lila Self Graduate Fellowship, University of Kansas

Portions of this data were presented at the World Congress Biomechanics, Dublin, Ireland, July 2018 and The Annual Meeting of the American College of Veterinary Surgeons, Phoenix, AZ 2018.

The corresponding author is Dr. Santschi: Santschi@ksu.edu

Kansas State University

College of Veterinary Medicine

1800 Denison Ave

Manhattan, KS, 66506

3.1 Abstract

Objective: To predict the bone formation stimulus of a transcondylar screw across an equine subchondral bone cyst (SBC) in an equine medial femoral condyle (MFC).

Study design: Finite element modeling (FEM) of an equine MFC with a 2 cm^3 SBC under several transcondylar screw conditions.

Methods: The FEM was constructed using computed tomographic imaging of a yearling Thoroughbred and analyzed using ABAQUS v6.14. The transcondylar screw was modeled as a 4.5mm stainless steel cylinder. The region of interest was the centrodistal MFC and bone stimulus was calculated. The stimulus threshold for bone formation (BFT) was >60 MPa and is presented as the percentage of total bone surface area (BFA) and frontal plane maps. Principal compressive stress vectors were also determined. Tested variables are daily cycles, load, and screw compression and position.

Results: At 750 cycles and 900 N load, <3% of the BFA exceeded the BFT. Increases in BFA >BFT occurred proportionally with load, screw compression and daily cycles (steps). Compressive stress was oriented vertically on the SBC surface without a screw but aligned with the long axis of well-placed lag screws. Screw placement through the void also increased the number and magnitude of compressive vectors.

Conclusions: A lag screw across an SBC increases BFA on the surface and reorients the compression vector to the screw axis. Increasing screw compression, load and steps per day increase the bone formation stimulus.

Clinical significance: This study supports the use of a lag screw thorough a MFC SBC to promote bone formation.

3.2 Introduction

Subchondral bone cysts (SBCs) occur in the growing bones of young horses, most commonly in the medial femoral condyle (MFC).[1-4] SBCs can result in lameness and cause secondary injuries such as meniscal and cartilage damage. Traditional treatments of SBC aim to reduce local inflammation and promote bone healing by use of rest, anti-inflammatory agents, cyst debridement and regenerative substances.[1-8] Reported success rates vary greatly and reflect only reductions in short-term lameness. Radiographic healing rates of SBC after treatment are rarely reported, and when they occur, are described as a reduction in SBC size rather than complete healing.[8]

A finite element model (FEM) of an equine SBC has been developed to investigate stresses and strains in the equine stifle joint. The model predicts shear exceeding yield in the boundary of an MFC SBC at high load.[9] The FEM also predicts increases in stress in the medial meniscus with an SBC due to altered load transfer. This finding is consistent with clinical information revealing secondary injuries to the meniscus and proximal tibia which reduce treatment success rates.[10,11] Therefore, incomplete healing or enlargement of the SBC after treatment may impact long-term soundness. It is likely that substantial radiographic healing of an SBC will provide a more durable reduction in lameness. A recent report using a transcondylar lag screw across the void has shown high success rates in both lameness resolution and radiographic healing.[12] Although the transcondylar screw treatment has been in clinical use for several years, its mechanical impact is unknown.

Most of the information available on the mechanics of bone healing describes fracture healing and focuses on dense cortical bone. SBCs are surrounded by porous trabecular bone and while the different fracture environments result in variations in the cellular events during

healing,[13] it appears that the biomechanical principles of healing are similar.[14] Because the architecture of trabecular bone is largely dictated by the applied mechanical forces,[15] the biomechanical environment of an MFC SBC must be insufficient to promote trabecular bone formation. The transcondylar screw is believed to promote healing by altering that environment.

Characteristics of the transcondylar screw such as neutral versus lag placement and screw position can vary between surgeons, so testing several screw conditions in the FEM should provide a better understanding of how the screw may influence healing. The prediction of BFA can be calculated and includes several variables including load and daily cycles (steps)[16,17] and was added to the FEM. Because trabecular bone realigns itself to the peak loading direction,[18] the direction of the principal stress was determined to determine if the screw altered the principal stress to predict the orientation of trabeculae.

We hypothesize that the FEM will predict that a lag screw placed across the SBC will stimulate bone growth on the surface of the SBC, and that the screw position will affect the area stimulated. Furthermore, we hypothesize that the lag screw will alter the direction of the principal stress on the MFC.

3.3 Materials and Methods

Previous work has developed a finite element model of an equine stifle joint in extension with a 2 cm^3 void in the MFC under gallop ground reaction force loading. [9,19] This initial model served as the baseline model for the present study and details model construction, material properties and loads.[9,19] The present study added a 5 mm radius of sclerotic bone on the periphery of the SBC with a density of 1.0 g/cc and was given a corresponding modulus of 3770 MPa using the density-modulus relationship,

$$E = 3770 * \rho^3 \qquad \text{(Eq. 1)}^{20}$$

Cartilage material properties were lowered to 8 MPa from the previous model to better represent the tissue response at lower loads and strain rates experienced in a post-operative environment. All model testing and calculations were performed in ABAQUS v6.14-2 (SIMULIA, Providence, Rhode Island).

3.3.1 Criteria for Effectiveness

In order to evaluate the efficacy of various surgical treatment strategies, Beaupre, Carter, and Orr's theory of bone remodeling was adopted.[16,17] In this theory, a tissue stimulus (Ψ) is calculated that predicts bone resorption, bone apposition, or no net bone change. Ψ is calculated using the following equation:

$$\Psi = \left(\sum_{day} n_i * \sigma_{b_i}^m \right)^{\frac{1}{m}} \qquad \text{(Eq. 2)}$$

where n_i is the number of cycles per day (for given load, i), σ_{b_i} is a true bone tissue-level effective stress for load i, and m is an empirical constant assumed in these simulations to be 6[21]. Tissue level effective stress, σ_{b_i}, is defined as:

$$\sigma_{b_i} = \frac{\rho_c^2 \sqrt{2 * E * U}}{\rho_a^2} \qquad \text{(Eq. 3)}$$

where ρ_c is the tissue density of cortical bone (assumed to be 1.92 g/cc), ρ_a is the local apparent density of the tissue, E is the local elastic modulus, and U is the local strain energy density. The theory is based on the idea of an "error" between the tissue stimulus and an attractor state, a theoretical equilibrium value that bone is trying to achieve. Using previous studies of bone's response to loading, Beaupre et al. determined that the attractor state was 50 MPa. The error term is then Ψ – 50 MPa. If this error is positive, bone apposition occurs. If the error is negative, bone resorption occurs. Furthermore, they defined a "dead zone". The dead zone is a range of Ψ in which there is neither bone resorption nor apposition. They determined this dead zone to be ± 20% of the attractor stimulus. Therefore, the dead zone lies between 40-60 MPa. Thus, values of Ψ greater than 60 MPa predict bone apposition, and values of Ψ less than 40 MPa predict bone resorption.

As a complement to using Beaupre, Carter, and Orr's theory of bone remodeling, third principal stress (compression), σ_{III}, directions were calculated by ABAQUS for various screw conditions Third principal stresses are important for understanding the direction of trabecular remodeling. As such, the bone remodeling theory predicts the answer to the question, "will bone form?", and the third principal stress vectors can answer the question, "in which direction?"

3.3.2 Screw Construction

For all model variations that included a transcondylar lag screw, a simplified screw was made in ScanIP v7.0 (Simpleware, United Kingdom) that did not possess any microstructure, such as threading. A 40 mm in length, 4.5 mm diameter cylinder was constructed and smoothed into a cone-like tip at the axial end. The head of the screw was 6 mm in diameter and constructed by dilating the abaxial end of the screw. The axial portion (tip) of the screw was tied to the bone, and the abaxial portion (head) was in frictionless contact with the bone. This choice of constraint was used to simulate the thread engagement of a lag screw on the far side of the cyst. The screw was given a modulus of 200 GPa to represent stainless-steel.

3.3.3 Effect of Compression

Compression was applied axially along the screw. This was performed by running a pre-step analysis prior to applying a joint load. In this pre-step, the elements in the middle aspects of the screw (inside of the SBC) were removed (Figure 3.1). Six connector elements were then inserted to connect the exposed surfaces of the screw. The connector elements were given a pre-tension and ABAQUS solved this initial configuration. Upon completion of the compression, the elements were put back into place. Previous pilot experiments using artificial bone (Sawbones, Vashon, WA) of 30 pcf solid polyurethane foam (E = 400 MPa) of 15 mm thickness revealed that a lag screw would generate a peak compression at 1.5-2 Nm torque of 700 N. However, the compression generated across the lag screw diminished rapidly and plateaued around 60% of the peak compression. As such, a conservative estimate of post-surgery compression of 300 N was chosen for the stainless-steel lag screw treatment.

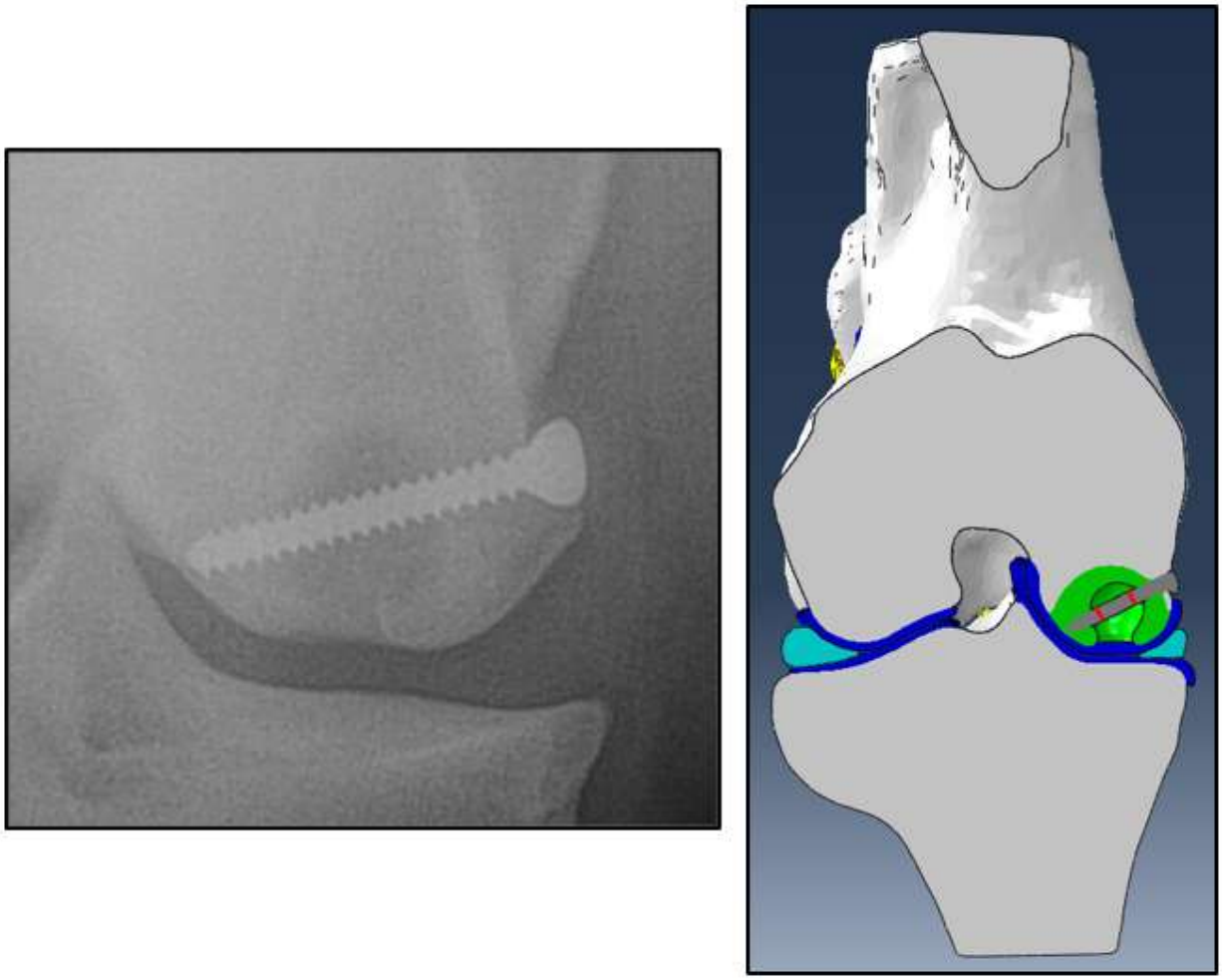

Figure 3.1. Left) Caudocranial radiographic projection of a yearling Thoroughbred with a proximodistal oblique transcondylar lag screw. Right) Caudal frontal planar view of the finite element stifle model. Bone is white, cartilage is blue, the region of interest is green, and the menisci are light blue. The screw is grey, and the red lines indicating the section removed to apply the axial compression. The axial end of the screw was tied to the bone and the screw head was in frictionless contact on the abaxial aspect.

3.3.4 Effect of Daily Cycles (steps)

Furthermore, this study investigated the effects of increasing the cycles per day (cpd) by adjusting n_i in Equation 2. Three n_i values were chosen as 750, 3000, and 6000 cycles per day. Preliminary results from a pedometer placed on 2 stall-confined Thoroughbred yearlings after screw placement reveals less than 1000 steps (cycles) daily, and that 10 minutes of hand-walking adds about 1000 more steps (unpublished data).

3.3.5 Effect of Load

Three different magnitudes of load were placed on the proximal femur to simulate different activities. Stall confinement was estimated to be 900 N by taking the average weight of a yearling (368 kg) and dividing by 4. The second magnitude was 1800 N, to estimate hand-walking or confinement in a small area such as a round pen, and the third magnitude was 3000 N to estimate light exercise in a paddock. These three joint loads estimate primary loads in the first two months of a typical post-surgery protocol.

3.3.6 Effect of Screw Placement

All screws were placed from abaxial to axial in the MFC. Three screw placements were tested: a proximodistal oblique transcondylar (PDO) screw that passed through the central void (Figure 1), a horizontal screw that intersected the proximal aspect of the void, denoted as proximal horizontal (PH), and lastly, a horizontal screw that passed through the central cavity of the void, denoted as distal horizontal (DH). Although the distal horizontal placement is not feasible in an MFC as it would contact articular cartilage and meniscus, it can be used in other joints such as the equine cubital joint.[22]

3.3.7 Boundary Conditions and Analysis

The compressive load on the proximal femur was applied evenly and varied from 0-3000 N. A tensile force at the quadriceps attachment on the proximal patella was applied to prevent unrealistic femoral anterior translation and was scaled from the previous study to 100 N.[9] The proximal aspect of the femur was constrained in varus-valgus (0°) and flexion/extension rotation (155°). The tibia was fully constrained, and femoral translation was allowed, and internal rotation was allowed and did not exceed 2.5°. Frictionless contact was defined between all articulating surfaces using general contact in ABAQUS. On the interior surface elements of the SBC, stress stimulus was predicted and the percentage of the available surface area exceeding 60 MPa was calculated (BFA). Peak strain values were also calculated to determine whether yield strains were exceeded in any of the tested surgical interventions.

3.4 Results

For all models tested, maximum strains did not exceed yield (2%).

3.4.1 Impact of screw compression and daily cycles (steps)

At 900 N model load and varying screw compression and CPD, BFA with Ψ above threshold (>60 MPa), did not exceed 1% until 300 N of screw compression was provided and only exceeded 10% at 6000 cpd (Table 3.1). BFA mapping (900 N load and 750 cpd) reveals that the greatest increases in BFA were located around the screw outside the void (Figure 3.2). At 900 N load, 300 N screw compression, and varied cpd, BFA mapping reveal Ψ above threshold at the void articular surface at 3000 cpd which enlarged at 6000 cpd (Figure 3.3).

Table 3.1: Percentage of bone formation area (BFA) on the inner surface of the void at 900N load predicted to experience Ψ above the apposition threshold (60 MPa) with only the void, with a proximodistal oblique (PDO) hole through the void and with a stainless steel screw (SSS) in the PDO position with varying compression and cycles (steps).

900 N load			
Model	BFA% 750 cycles	BFA% 3000 cycles	BFA% 6000 cycles
Void only	0	0	0
Void/PDO hole	0	0	0
Void/ SSS 0 N	0	0	0
Void/SSS 75 N	0	0	1
Void/SSS 150 N	0	1	1
Void/SSS 300 N	2	7	11

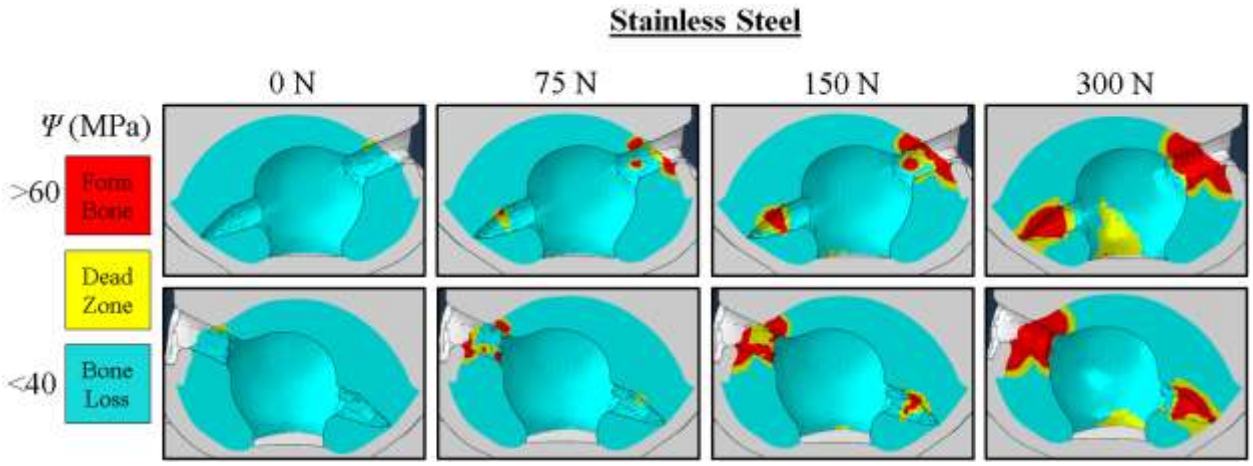

Figure 3.2. Bone formation stimulus (Ψ) maps in the MFC region of interest with varying screw compression. Conditions for all trials were 750 cycles per day and 900 N load to estimate stall confinement. Top row: caudal to cranial view, bottom row: cranial to caudal. The screw point is axial. The void surface area exceeding the bone formation threshold (60 MPa) is negligible for all screw compressions tested.

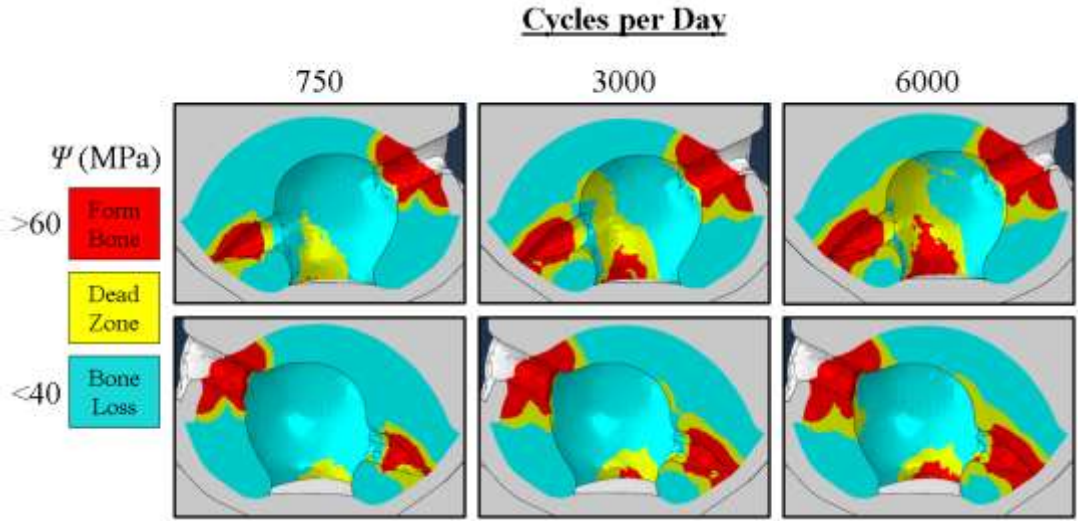

Figure 3.3. Bone formation stimulus (Ψ) maps in the MFC region of interest with varying cycles per day. Conditions for all trials were 300 N compression on the screw and 900 N load to estimate handwalking. Top row: caudal to cranial view, bottom row: cranial to caudal. Cycles per day (cpd) >750 has a proportional increase in surface stimulation and exceeds the bone formation threshold (60 MPa) at the articular surface and extends proximally at 6000 cpd.

3.4.2 Impact of load

At 1800 N model load without screw compression, BFA with Ψ above threshold was <10% for all cpd tested (Table 3.2). BFA increased with increasing screw compression and cpd but only exceeded 10% at the highest cpd and screw compression. Increasing model load to 3000 N predicted BFA >10% for most trials (Table 3.3) indicating larger areas of bone formation stimulus. However, computation of the third principal stress vector ($\sigma_{III,}$ compression) at 3000 N without a lag screw reveals a proximal to distal alignment with the direction of compression (Figure 3.4). Adding a lag screw with 300 N compression alters σ_{III} to align with the screw axis (medial to lateral), increases the magnitude of stress, and multiplies the vectors, most notably at the joint margin.

Table 3.2: Percentage of bone formation area (BFA) on the inner surface of the void at 1800 N load predicted to experience Ψ above the apposition threshold (60 MPa) with only the void, with a proximodistal oblique (PDO) hole through the void and with a stainless steel screw (SSS) in the PDO position with varying compression and numbers of daily cycles (steps).

1800 N load			
Model	BFA% 750 cycles	BFA% 3000 cycles	BFA% 6000 cycles
Void only	0	1	4
Void/PDO hole	1	2	7
Void/ SSS 0 N	1	3	9
Void/SSS 75 N	1	5	12
Void/SSS 150 N	2	9	20
Void/SSS 300 N	9	25	39

Table 3.3: Percentage of bone formation area (BFA) on the inner surface of the void at 3000 N load predicted to experience Ψ above the apposition threshold (60 MPa) with only the void, with a proximodistal oblique (PDO) hole through the void and with a stainless steel screw (SSS) in the PDO position with varying compression and numbers of daily cycles (steps).

3000 N load			
Model	BFA% 750 cycles	BFA% 3000 cycles	BFA% 6000 cycles
Void only	5	19	31
Void/PDO hole	20	53	66
Void/ SSS 0 N	24	59	72
Void/SSS 75 N	30	63	75
Void/SSS 150 N	37	68	78
Void/SSS 300 N	50	76	84

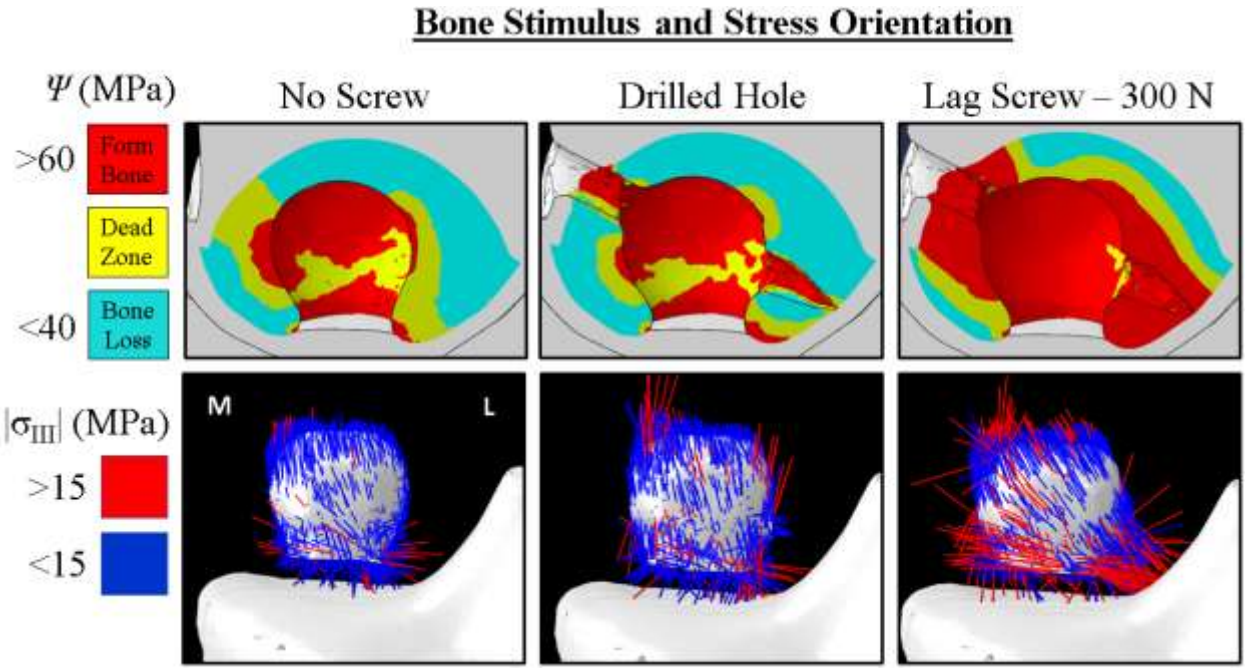

Figure 3.4. Top row: Bone formation stimulus (Ψ) maps (cranial to caudal view) in the MFC region of interest at 3000 N model load and 6000 cpd with no screw, proximodistal oblique (PDO) hole, and PDO lag screw (300 N screw compression). Bottom row: Third principal stress vectors (σ_{III}) on the surface of the void at same load and screw conditions. Without screw compression, σ_{III} is mostly <15 MPa and primarily oriented vertically. With screw compression, σ_{III} exceeds 15 MPa in multiple sites, aligns with the screw, and crosses the void. L=lateral, M=medial.

3.4.3 Impact of screw position

Three screw positions were tested: PDO, proximal horizontal (PH) and distal horizontal (DH). All models had 1800N load and screws had 300N compression. The BFA at 750 cpd was < 10% for all screw positions (Table 3.4), but increased with increasing cpd. The BFA for the PDO screw was 25-30% higher than PH or DH screws at 3000-6000 cpd. Analysis of σ_{III} for the 3 screw positions shows alignment with the PDO and DH screws, especially at the joint margin.

Use of a PH screw does not change σ_{III} except at the most proximal portions of the cyst near the screw (Figure 3.5).

Table 3.4. Percentage of bone formation area (BFA) on the inner surface of the void at 1800 N load predicted to experience Ψ above the apposition threshold (60 MPa) using a proximodistal oblique (PDO), a proximal horizontal screw (PH), and a distal horizontal (DH) screw with varying daily cycles (steps). The screws were modeled as 4.5 mm cylinders of stainless steel with a 6 mm head and a tapered point.

1800 N load			
Model	BFA% 750 cycles	BFA% 3000 cycles	BFA% 6000 cycles
PDO	9	25	39
PH	8	20	29
DH	7	19	31

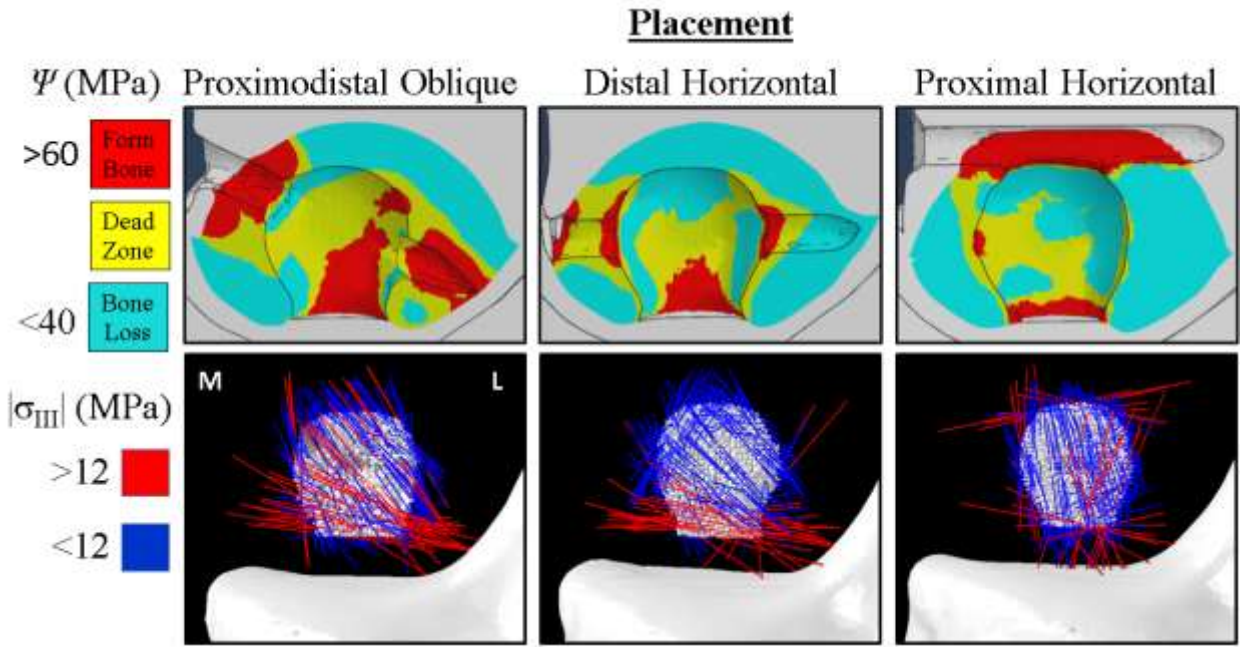

Figure 3.5. Top row: Bone formation stimulus (Ψ) maps (cranial to caudal view) in the MFC region of interest at 1800 N model load and 3000 cpd with a proximodistal oblique(PDO) screw, a distal horizontal (DH) screw, and a proximal horizontal (PH) screw with 300 N compression. Bottom row: third principal stress vectors (σ_{III}) on the surface of the void at same load and screw conditions. All screw placements stimulate bone formation, but only the PDO and DH screws alter the principal stresses to align with the screw across the void. In the PH placement, principal stresses primarily have a proximal to distal orientation, except for a few vectors at the proximal and distal aspect of the cyst. L=lateral, M=medial.

3.5 Discussion

Traditional surgical treatments for equine SBC are directed primarily towards reducing inflammation within the SBC and secondarily to promote bone formation through the use of bone substitutes or biologic substances and do not address SBC biomechanics. Radiographic healing of SBC after these traditional treatments is not often described but was less than 20% in a study that filled the debrided void with bone graft or bone substitutes.[8] Higher rates of an unspecified reduction in cyst size are reported, but cyst enlargement occurred in about 30% of patients.[8] We believe a major goal of treatment should be bone healing in the SBC at the joint to provide a foundation for attachment of remaining hyaline cartilage, prevention of contact of joint fluid with damaged bone, and load transfer. The transcondylar screw treatment of MFC SBC focuses on altering the biomechanical environment of the SBC to promote bone healing.[12]

Trabecular bone healing begins with the arrival of mesenchymal cells, followed by the formation of primary woven bone on the surface of a fracture with a random orientation, which subsequently assumes a more organized structure and forms new trabeculae.[23] When the injury is an osteochondral defect, new bone forms from the circumference during healing.[24] Biomechanical analysis of trabecular bone healing is in early stages, but appears to be similar to diaphyseal healing, and is optimized within a range of bone strain.[15] The elevated bone strains predicted by the FEM[9,19] are likely a factor in the poor bone healing of SBC observed clinically. The changes in bone strain caused by the transcondylar screw in this model suggest that the screw helps to change the stress and strain environment to promote healing.

Increasing PDO screw compression at all loads and cycles per day resulted in increases in BFA, suggesting that drilling a forage hole or placing a screw without compression are less effective in stimulating bone formation. Similarly, increasing joint load and cycles per day

increased BFA. The 900 N load was selected to model 25% of the bodyweight of a yearling and 750 cycles per day estimated activity when stall confined. The small increases in BFA without a screw even at the highest cycles per day (unlikely to be achieved in stall confinement) is in accordance with clinical experience that rest is not often successful in healing MFC SBC.[1] The presence of a small area experiencing tissue stimulus above the BFT at the joint surface may explain the incomplete bone formation frequently seen at the joint surface of SBC over time (Figure 3.6A). However, BFA above BFT for >20% of the SBC area were predicted at 1800 N load (infrequently) and frequently at 3000 N. Clinical experience indicates that SBC in these horses do not heal with regularity, indicating that tissue stimulus alone may be insufficient to predict SBC healing.

To further characterize the mechanical impact of the lag screw, the compression stress vector was calculated at 3000 N and 6000 cycles per day and was determined to be parallel to the compression on the long axis of the bone without a screw and found to align with the lag screw with screw compression. Without a screw the bone formation stimulus is vertical on the periphery of the SBC and is likely the mechanism for SBC marginal sclerosis (Figures 3.5A and 3.6A). This vector corresponds to the main trabecular orientation which is already adapted to sustain compressive loads. As such, although the model predicts bone formation, the bone formation that occurs is peripheral sclerosis around the cyst. However, with a screw, the stimulus is multiplied and directed across the MFC. Providing compression across a fracture has been advocated for decades as a method to promote fracture healing by increasing interfragmentary forces and adding stability to a fixation, but compression across a void to promote healing is a new strategy. The transverse compression combined with the general stress stimulus appears to promote bone formation across the void (Figure 3.6B). The ability of trabecular bone to adjust

and realign to the peak loading direction has been reported.[18] Further support for this mechanism is provided by the increased number and magnitude of horizontal vectors at the joint surface which is where the earliest bone healing occurs after screw placement (Figure 3.6B).

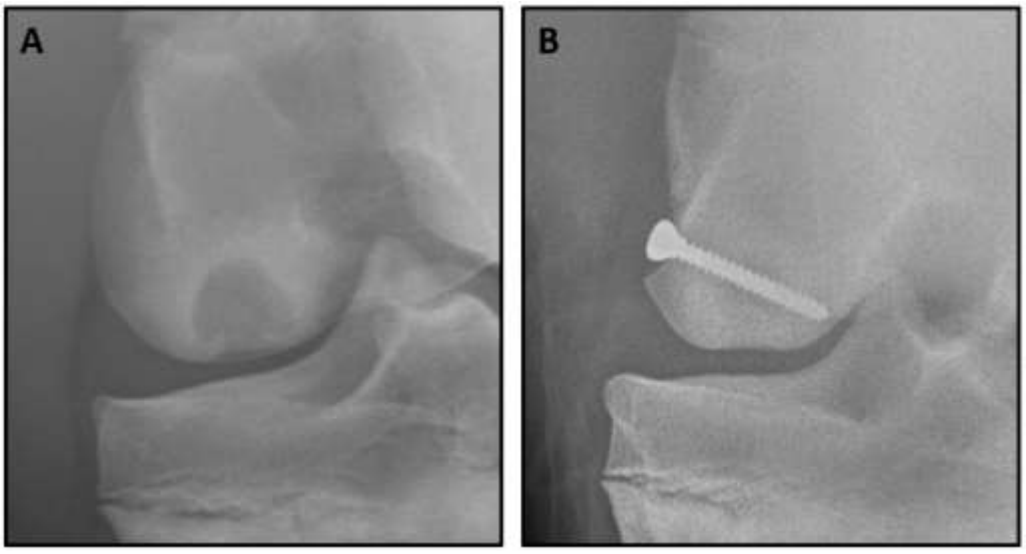

Figure 3.6. Caudal to cranial radiographs of an equine MFC before placement of proximodistal lag screw (A) and 60 days post-surgery (B). Before surgery, the incomplete healing of the SBC at the joint resulting in an apparent stoma is apparent followed after screw placement by more substantial healing at the joint and circumferential healing toward the center of the void.

Our experience with the transcondylar screw for the treatment of SBC and evaluation of scores of radiographs from other surgeons indicated that screw position is associated with clinical success. Specifically, it appeared that if the screw position was horizontal and proximal, SBC healing was less likely than with PDO screw placement (Figure 3.7). This model predicts that some additional bone remodeling stimulus is present with a proximal horizontal screw, but the principal stresses remain vertical (Figure 3.5). This reinforces the use of the PDO screw to orient the principal stress across the SBC. The distal horizontal screw configuration also orients

the principal stress across the SBC but cannot be used with a standard screw in a MFC SBC due to interference of the screw head with the meniscus and abaxial cartilage surface. A headless dual-pitch screw could be used but may not provide sufficient compression across the SBC. However, horizontal screw placement is effective in the treatment of SBC in other joints such as the equine cubital joint,[22] and these results suggest that a screw close and parallel to the joint surface will provide the necessary bone formulation stimulus for healing.

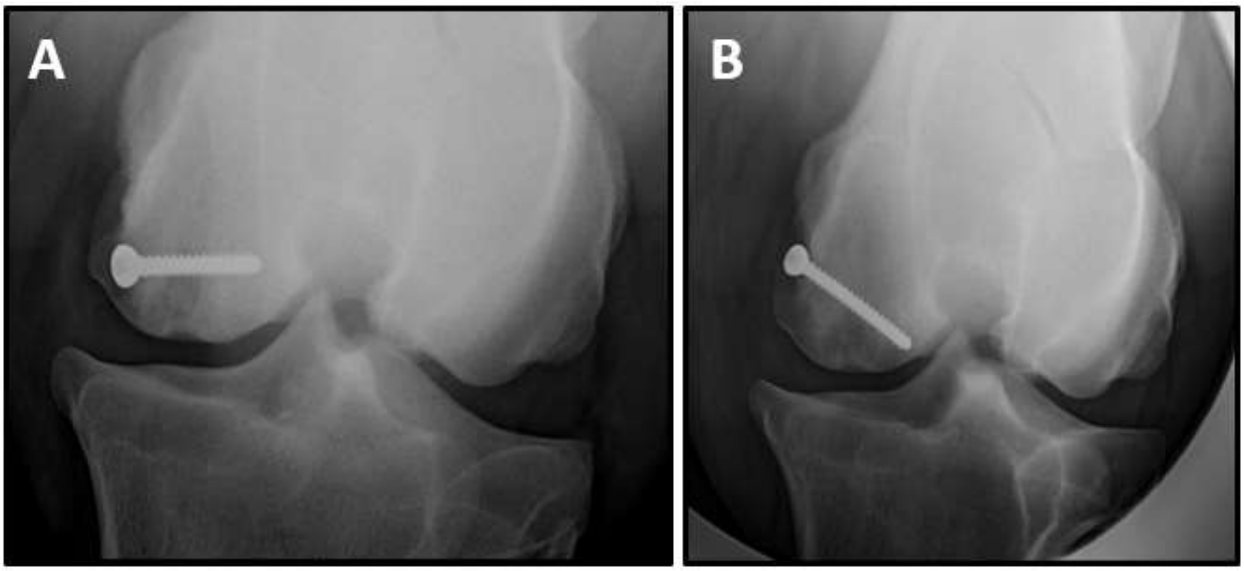

Figure 3.7. Caudo-cranial radiographs of an equine stifle at A) 365 days after placing a proximal horizontal transcondylar screw, and B) 180 days after removing the first screw and placing a proximodistal oblique (PDO) screw. The horizontal screw did not result in loss of sclerosis on the SBC periphery nor formation of trabecular bone, and the lameness was still present. Six months after placing the PDO screw the sclerosis has reduced, a trabecular bone pattern is present in the void and the stifle lameness was eliminated.

For all screw conditions, bone remodeling stimulus increases with increasing steps per day. This finding is consistent with anecdotal evidence early in the clinical use of the screw that horses allowed early exercise appeared to heal sooner than stall confined horses. The number of

CPD used in this study estimated stall confinement (750 cpd), light exercise such as handwalking or round pen turn out (3000 cpd) or pasture exercise (6000 cpd). Our present postoperative recommendations for horses < Grade 3 lame are stall confinement for 2 weeks after screw placement followed by handwalking for two weeks, followed by 4 weeks turnout in a small paddock or round pen. In the early stages of SBC healing, controlled exercise appears to be superior to at liberty exercise as a small number of horses have reinjured their MFC if heavy exercise commences before sufficient articular bone formation.

There are several limitations of this study. All the tested configurations were manipulations of a single finite element model of a healthy stifle joint. The SBC and the sclerotic region surrounding the void were assumed from clinical averages but are idealized. Stifle boundary conditions are estimated due to the lack of equine stifle kinetic data. The screw does not include threads or the micro-interactions between the threading and the bone, however, tie constraints are believed to provide a reasonable estimation of screw mechanics.[25] Finally, the bone remodeling theory was based on non-equine data and are therefore approximations. However, the comparative trends found in this study should remain consistent with parameter changes.

In conclusion, the results from this computational study support the use of a proximodistal oblique transcondylar lag screw to treat SBCs in the equine MFC and illustrate the likely mechanisms promoting bone formation and healing. Providing controlled exercise after surgery appears to improve the biomechanical environment for bone formation in the MFC.

3.6 Acknowledgements

Thanks to Drs. Casille Batten and James Morehead for the collection of the postoperative daily cycle data on Thoroughbred yearlings. Also thanks to Matthew Dickinson for the help with scripting.

3.7 Disclosure

The authors declare no conflict of interest related to this report.

3.8 References

1. Jeffcott LB, Kold SE. Clinical and radiological aspects of stifle bone cysts in the horse. *Equine Vet J*. 1982;14:40-46.
2. Stewart B, Reid CF. Osseous cyst-like lesions of the medial femoral condyle in the horse. *J Am Vet Med Assoc*. 1982;180:254-257.
3. McIlwraith CW. Subchondral Cystic Lesions (Osteochondrosis) in the Horse, *Compend Contin Educ Pract Vet*. 1982;4:282-294.
4. Baxter GM. Subchondral cystic lesions in horses, in Joint disease in the horse, Philadelphia, *WB Saunders*. 1996;384-397.
5. Lewis R. A retrospective study of diagnostic and surgical arthroscopy of the equine femorotibial joint. In: *Proceedings from the Am Assoc of Equine Pract*. 1987.
6. Howard RD, McIlwraith CW, Trotter GW. Arthroscopic surgery for subchondral cystic lesions of the medial femoral condyle in horses: 41 cases (1988-1991). *J Am Vet Med Assoc*. 1995;206:842-850.
7. Smith MA, Walmsley JP, Phillips TJ, Pinchbeck GL, Booth TM, Greet TRC, Richardson DW, Ross MW, Schramme MC, Singer ER, Smith RK, Clegg PD. Effect of age at presentation on outcome following arthroscopic debridement of subchondral cystic lesions of the medial femoral condyle: 85 horses (1993--2003). *Equine Vet J*. 2005;37:175-180.
8. Ortved KF, Nixon AJ, Mohammed HO, Fortier LA. Treatment of subchondral cystic lesions of the medial femoral condyle of mature horses with growth factor enhanced chondrocyte grafts: a retrospective study of 49 cases. *Equine Vet J*. 2012;44:606-613.
9. Frazer LL, Santschi EM, Fischer KJ. Impact of a void in the equine medial femoral condyle on bone stresses and peak contact pressures in a finite element model. *Vet Surg*. 2018.

10. Hendrix SM, Baxter GM, Mc Ilwraith CW, Henrickson DA, Goodrich LR, Frisbie DD, Trotter GW. Concurrent or sequential development of medial meniscal and subchondral cystic lesions within the medial femorotibial joint in horses (1996–2006). *Equine Vet J*. 2010;42:5-9.
11. Bonilla AG, Bertone AL, Brokken MT, Santschi EM. Concurrent or sequential tibial subchondral cystic lesions in 4 horses with medial femoral condyle subchondral cystic lesions. *J Am Vet Med Assoc*. 2016;249:1313-1318.
12. Santschi EM, Williams JM, Morgan JW, Johnson CR, Bertone AL, Juzwiak JS. Preliminary investigation of the treatment of equine medial femoral condylar subchondral cystic lesions with a transcondylar screw. *Vet Surg*. 2015;44:281-288.
13. Bernhardsson M, Aspenberg P. Osteoblast precursors and inflammatory cells arrive simultaneously to sites of a trabecular-bone injury. *Acta orthopaedica*. 2018;89:457-461.
14. Claes L, Reusch M, Göckelmann M, Ohnmacht M, Wehner T, Amling M, Beil FT, Ignatius A. Metaphyseal fracture healing follows similar biomechanical rules as diaphyseal healing. *J Orthop Res*. 2011;29:425-432.
15. Huiskes R, Ruimerman R, van Lenthe GH, Janssen JD. Effects of mechanical forces on maintenance and adaptation of form in trabecular bone. *Nature*. 2000;405:704-706.
16. Beaupre GS, Orr TE, Carter DR. An approach for time-dependent bone modeling and remodeling-application: a preliminary remodeling simulation. *J Orthop Res*. 1990;8:662-670.
17. Beaupre GS, Orr TE, Carter DR. An approach for time-dependent bone modeling and remodeling--theoretical development. *J Orthop Res*. 1990;8:651-661.
18. Barak MM, Lieberman DE, Hublin JJ. A Wolff in sheep's clothing: trabecular bone adaptation in response to changes in joint loading orientation. *Bone*. 2011;49:1141-1151.

19. Frazer LL, Santschi EM, Fischer KJ. The impact of subchondral bone cysts on local bone stresses in the medial femoral condyle of the equine stifle joint. *Med Eng Phys*. 2017;48:158-167.
20. Carter DR, Hayes WC. The compressive behavior of bone as a two-phase porous structure. *J Bone Joint Surg Am*. 1977;59:954-962.
21. Whalen RT, Carter DR, Steele CR. Influence of physical activity on the regulation of bone density. *J Biomech*. 1988;21:825-837.
22. Roquet I, Easter JL, Coomer RPC, Ezquerra LJ, Marsh CA, Trostle SS, Santschi EM. Treatment of subchondral lucencies in the medial proximal radius with a bone screw in 8 horses. *Vet Surg*. 2017;46:478-485.
23. Chen T, Han DC, Zhang PX, et al. A special healing pattern in stable metaphyseal fractures. *Acta orthopaedica*. 2015;86:238-242.
24. Duda GN, Maldonado ZM, Klein P, Heller MO, Burns J, Bail H. On the influence of mechanical conditions in osteochondral defect healing. *J Biomech*. 2005;38:843-851.
25. Inzana JA, Varga P, Windolf M. Implicit modeling of screw threads for efficient finite element analysis of complex bone-implant systems. *J Biomech*. 2016;49:1836-1844.

4. Impact of Cyst Size and Shape on Bone Formation Stimulus Using a Transcondylar Screw

Manuscript prepared for submission to Journal of Biomechanical Engineering

Running Head

Bone formation stimulus in different sized cysts using a transcondylar screw

Title

Impact of size and shape of equine femoral subchondral bone cysts with a transcondylar screw on bone formation area in a finite element model

Lance L. Frazer[A], MS

Elizabeth M. Santschi[B], DVM, Diplomate ACVS

Kenneth J. Fischer[A], PhD

[A]University of Kansas, Lawrence, KS

[B]Kansas State University, Manhattan, KS

This research is supported by the Madison and Lila Self Graduate Fellowship, University of Kansas

The corresponding author is Dr. Fischer: fischer@ku.edu

University of Kansas

Mechanical Engineering

1530 W 15th St.

Lawrence, KS, 66045

4.1 Abstract

Equine subchondral bone cysts (SBCs) develop most often in the medial femoral condyle (MFC) of yearlings intended for performance. A novel treatment strategy using a transcondylar lag screw has shown high rates of lameness reduction and radiographic healing. Using finite element analysis, our lab has determined that the transcondylar screw (TLS) enhances healing by providing mechanical stimulus to the adjacent bone, as well as aligning principal stresses across the void. In this study, we have investigated the effects of different cyst sizes and shapes on bone formation stimulus using a TLS. Using a 3^k factorial analysis, height, width, and depth of the cyst were varied using a published range of cyst parameters. We found that full screw penetration into the cyst creates the highest bone formation stimulus. Additionally, full screw penetration ensures that third principal stresses align transverse to the trabecular orientation around the cyst. Height and depth have the most influence as to whether a screw can fully penetrate or not. As such, larger cysts respond well to the TLS, whereas smaller cysts do not. We recommend the use of the TLS to treat SBCs that allow screw penetration. For smaller cysts, more techniques need to be developed, such as a headless screw surgical technique to address the limitation of the existing TLS surgery.

4.2 Introduction

Equine subchondral bone cysts (SBCs) develop most often in the medial femoral condyle (MFC) of yearlings intended for performance.[1-4] SBCs often cause lameness and can cause secondary injuries to the meniscus and tibial cartilage.[5] Typical SBC treatment strategies involve rest, cyst debridement, and intracystic arthroscopic injection of corticosteroids to reduce inflammation.[6-14] Reported treatment success rates vary from 35-70% and have not improved over the past several decades.[15] Success is most often determined by return to soundness and reduction in lameness, and radiographic evidence of MFC SBC healing is not often reported. Radiographic healing of SBC should achieve long-term lameness reduction and return to function without risk of reinjury or secondary injury.

A novel surgical technique using a transcondylar lag screw (TLS) across an MFC SBC has been described[16] and has shown success in lameness resolution and radiographic healing of MFC SBC. Using finite element modeling (FEM), our lab has investigated the mechanics of MFC SBC[17,18] and the transcondylar lag screw procedure (submitted for review). The FEM predicts that several types of bone stress are elevated in an MFC SBC under normal loading. After placing a TLS, the model indicated that 300 N of screw compression stimulated bone formation on the inner surface of the SBC and altered third principal stress vectors to change the direction of surface compression to align with the screw axis. As third principal stresses influence trabecular alignment and growth,[19,20] we hypothesized that the TLS stimulates bone formation on the inner SBC surface and directs bone formation across the void. However, the previous work used a single idealized SBC with a 2 cm^3 volume, which lacked some characteristics of the clinical condition.

Most equine MFC SBC occur in a similar location but vary in size and shape,[21] and clinical experience has indicated that cyst size and shape can affect the bone healing with a TLS. Developing a FEM from a CT scan of a clinical SBC that includes concurrent MFC changes and subsequently manipulating SBC sizes and shapes may provide information about SBC size and shape and bone formation stimulus after TLS placement. Our objective was to test SBC of several sizes and shapes in a newly developed equine stifle FEM with a TLS to determine how cyst size affects bone formation stimulation. A 3^k factorial analysis was implemented to manipulate the three spatial dimensions of the cyst (height, width and depth) and identify the impact of these parameters on bone formation stimulus. Additionally, several smaller cysts not included in the 3^k factorial analysis were tested to identify a minimum size in which the screw demonstrates efficacy. Finally, the native cystic geometry of the model (from the original CT scan) along with an additional stifle joint model developed using another CT scan of a cystic MFC was used to compare against the 3^k factorial regression results.

4.3 Methods

4.3.1 Image Acquisition

Computed tomographic scans of a femorotibial joints from 2 live horses with an SBC in the MFC that had not been treated surgically were included in the study. These images have been previously published to describe the anatomy of MFC SBC and include details of the CT acquisition and owner permission.[21]

4.3.2 Segmentation and Meshing

The first set of CT images were imported into ScanIP (Simpleware, United Kingdom) for segmentation and meshing (Figure 4.1). Segmentation was performed to include the femur, tibia, patella, articular cartilages, menisci, and the patellar ligaments. The cortical bone was automatically segmented using a threshold filter and subsequent manual filling was performed for the trabecular bone. The femoral and tibial cartilage was assumed to be 2.5 mm thick, so a uniform dilation was performed on the bones for cartilage segmentation. The menisci were segmented by identifying visible tissue boundaries in the CT scan and using best judgement with the aid of available cadaveric menisci and supervision from a professor of equine surgery. The patellar ligaments were visible in the CT images and manually segmented.

The transcondylar lag screw was made by creating a 38 mm length cylinder with a radius of 2.25 mm. The axial end of the screw was smoothed into a conal shape and the abaxial end was dilated outside of the condyle to create a 6mm screw head. The resulting 3-D geometry of the stifle joint and the transcondylar screw was meshed into 4-node tetrahedra and imported into ABAQUS v6.14-2 (SIMULIA, Providence, Rhode Island) for further model development (Figures 4.2-4.3). This model served as the baseline for the 3^k factorial analysis.

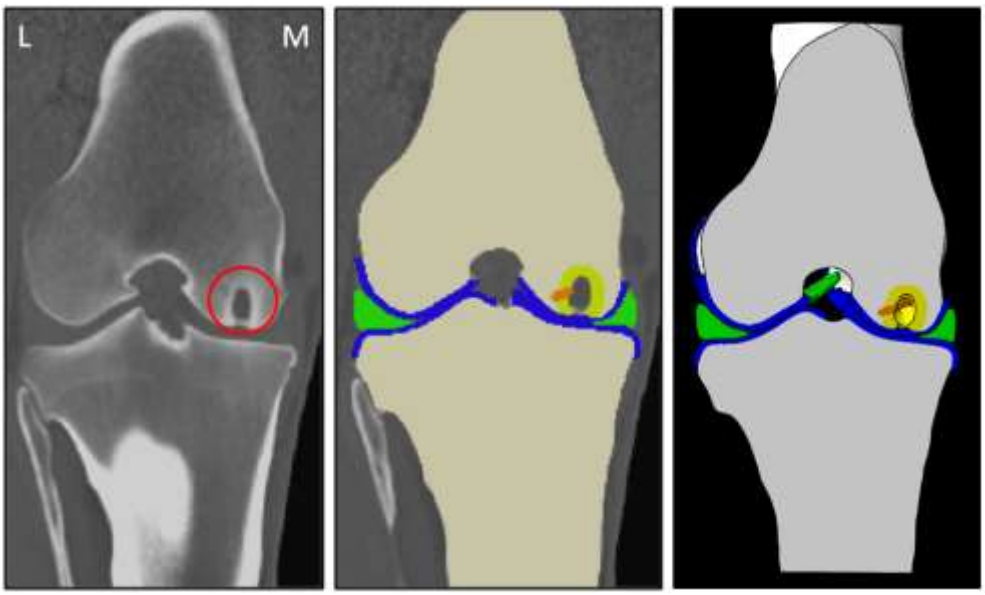

Figure 4.1. Left: image slice from the CT scan used to create the finite element model for the 3^k factorial analysis. SBC circled in red. Middle: Segmented structures using ScanIP. Bone is shown in tan, cartilage is blue, menisci are green, 5 mm of sclerosis is yellow, and the screw is shown in orange. Right: Model imported into ABAQUS for finite element analysis. Note – the SBC geometry was manipulated for the 3^k factorial analysis, and the shown, native SBC size and shape was tested later as a means of comparison to the regression results.

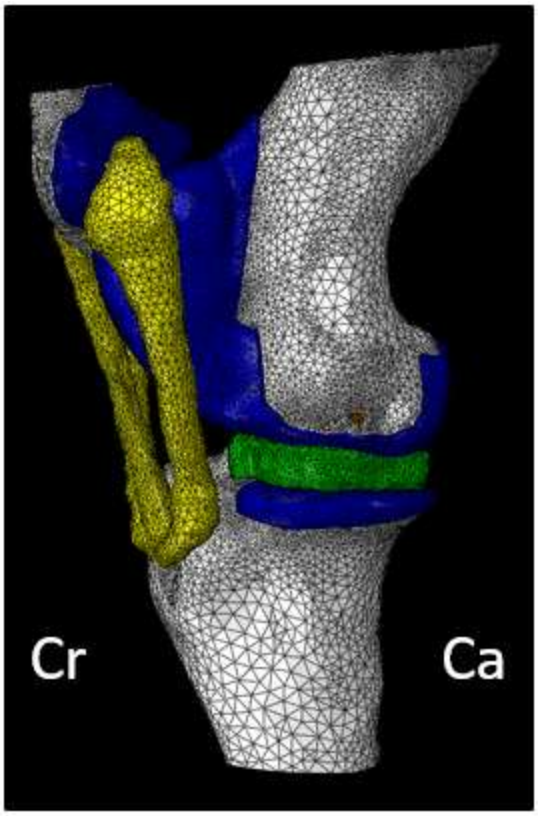

Figure 4.2. Medial view of the finite element model used in this study.

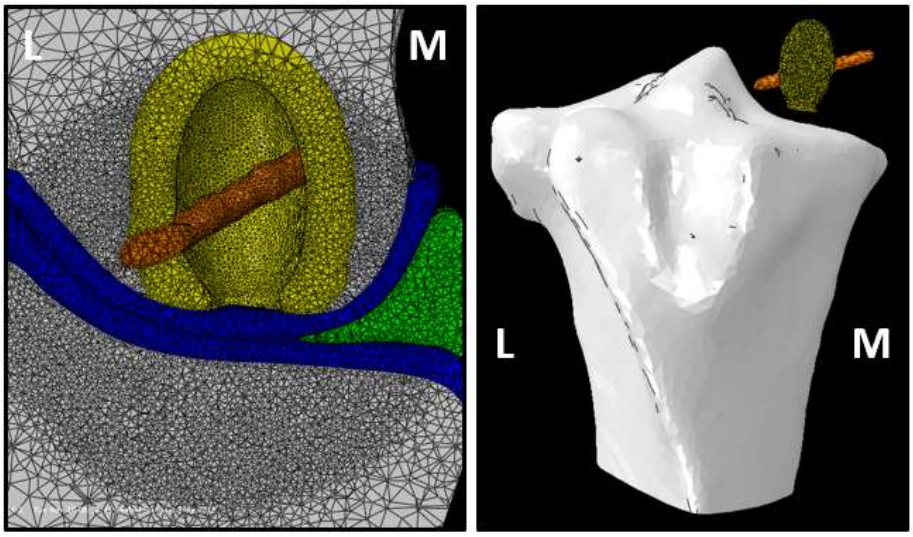

Figure 4.3. Left: Cranial plane showing the mesh refinement in the MFC (including the sclerotic region in yellow), TCS (orange), soft tissues (cartilage, blue; meniscus, green), and proximal tibia. Right: Cranial view of the tibia, sclerotic region around the cyst, and the TCS.

4.3.3 Material Properties

Linear elastic material properties were assigned to all 3-D solid structures used in this study. Bone was modeled as a heterogenous material with 20 unique bone material properties based upon its Hounsfield units (HU). Phantom data from the CT scanner was used to match HU to density. Density was mapped to its modulus using the Equation 1.

$$E = 3770 * \rho^3 \qquad \text{(Eq. 4)}^{22}$$

Soft tissue properties were adapted from earlier studies involving both human and equine data.[17,23-32] With the uncertainty associated with soft tissue properties, sensitivity analyses were performed. It was determined that a reasonable range of material properties does not significantly change the results. Low loading combined with the transcondylar screw only affecting the bone stress both contribute to the non-sensitivity of soft tissue properties.

The ACL, PCL, LCL, and MCL were modeled as 1-D non-linear springs and their insertions were identified from Aldrich et al.[18,28,33-35] Each outer meniscal rim was connected to ground using 10 springs (2 N/mm) to simulate the restraint on excessive meniscal translation from the joint capsule.[36] A summary of material properties can be found in Table 4.1.

Table 4.1. Summary of the material properties used in the study.

Structure	**Type**	**Young's Modulus (MPa)**	**Poisson's Ratio**
Bone	Isotropic	100-18,000	0.3
Menisci	Anisotropic	Radial and Axial = 20 Circumferential = 120	Radial and Axial = 0.3 Circumferential = 0.45
Cartilage	Isotropic	8	0.45
Patellar Ligaments	Isotropic	300	0.3
ACL, PCL, LCL, MCL	Non-linear Springs	-	-

4.3.4 Boundary Conditions

900 N of uniform pressure was applied on the proximal surface of the femoral metaphysis. This pressure was determined by taking the weight of an average weight of a yearling (368 kg) and dividing it by its four limbs. This amount of load approximates the first few weeks of stall-confinement. The quadriceps tensile force on the superior aspect of the patella to prevent unrealistic femoral anterior translation was scaled from our previous study to 100 N. The proximal aspect of the femur was constrained in varus-valgus (0°) and flexion/extension

rotations (155°). The tibia was fully constrained, and femoral translation and internal rotation were allowed (unconstrained). Frictionless contact was defined between all articulating surfaces using general contact in ABAQUS. For each model, 2 analyses were run: 0 N of compression across the transcondylar screw and 300 N of compression across the transcondylar screw. The axial end of the screw was tied to the bone, and the abaxial end was in frictionless contact with the bone. In our previous study (in review), it was found that at 900 N joint load, 0 N of compression (a neutral screw) did not have any effect on BFA compared to no screw at all (baseline). Therefore, for time efficiency, the screw was left in at 0 N of compression as the baseline value. 300 N of compression was chosen after an in-house experiment demonstrated that 300 N of compression was a conservative estimate of how much force is generated during surgical implantation of the screw.

4.3.5 3^k Factorial Study Design

A range of cyst sizes and shapes have been described, characterized by height (proximal/distal in the frontal plane), width (medial/lateral in the frontal plane), and depth (cranial/caudal in the sagittal plane).[21] These dimensions varied between 2-26 mm (height), 2-20 mm (width), and 2-14 mm (depth in the sagittal plane). To model these ranges, a 3^k factorial study with k = 3 was constructed with heights of 2, 14, and 26 mm, widths 2, 8, and 14 mm, and depths of 2, 10, and 20 mm creating a total of 27 cyst sizes. Three of these cysts are shown in Figure 4. For cysts with 14 and 26 mm in height, the cyst was narrowed at the joint margin, as seen clinically (Figure 3). Bone properties were adjusted based on cyst size, and a 5 mm radius of sclerosis was assumed around each cyst, with a density of 1.0 g/cc (Figures 4.1,4.3, and 4.5; yellow). Additionally, in cysts with heights of 2 mm, the cystic region in the scan that was not covered by the artificial sclerosis had to be filled in as a separate part. This was done to ensure

that when bone material properties were mapped to bone elements according to their Hounsfield Unit, the cystic region of the scan was not given a low modulus (Figure 4.5; purple). This artificially created bone region in the cyst space was a given a density of 0.4 g/cc, which was the average density of the trabecular bone in the non-cystic lateral condyle and matched the surrounding density in the MFC. The main objective of this factorial analysis was to determine the spatial dimension that accounts for the most variation in TCS efficacy.

4.3.6 Additional Models

In addition to the 3^k factorial study design, several dome shaped cysts were analyzed with equal dimensions in each spatial direction of 4, 6, 8, 10, and 12 mm. Due to the large range of reported spatial dimensions, more information regarding smaller cysts was warranted. We hypothesized that height would be the most influential characteristic in TCS efficacy, and it was of clinical significance to then determine the height (or another characteristic) in which the TCS begins to be beneficial. Dome-shaped cysts are a common appearance of cysts early in formation.

Finally, an additional model was developed from the other actual cystic CT scan. This model was developed using the same procedures as detailed above. Using the original model with the true cystic geometry and the additional cystic model, comparisons could be made against the factorial study results. These models had cyst height, width, and depth dimensions of 1) 15, 8.5, and 8 mm; 2) 4.5, 4.5, and 5.5 mm.

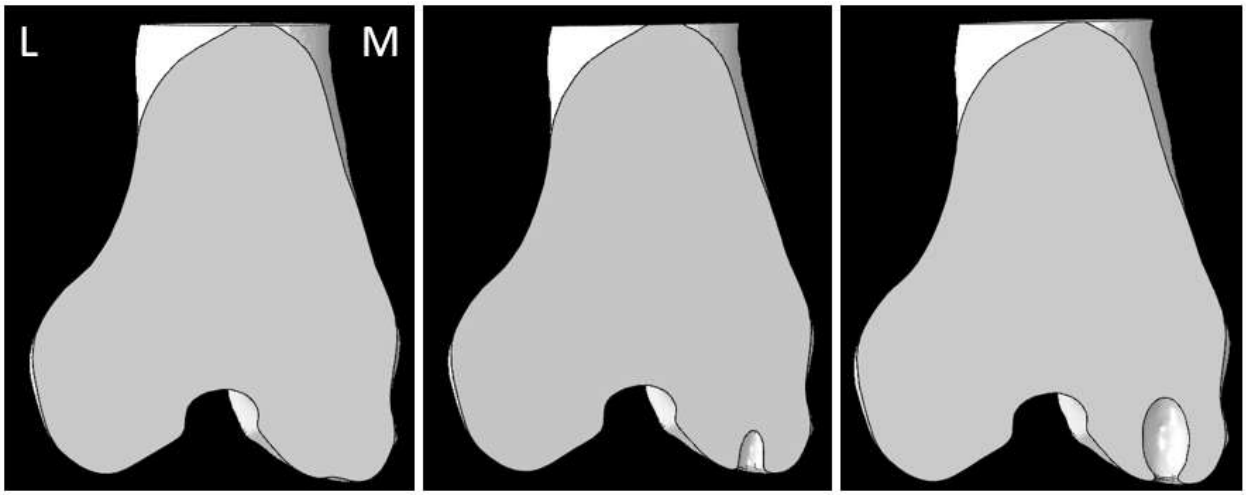

Figure 4.4 Cranial planes revealing 3 different sized cysts used in the study. Left: 2 mm height, 2 mm width, and 2 mm depth. Middle: 14 mm height, 8 mm width, and 10 mm depth. Right: 26 mm height, 14 mm width, and 20 mm depth. These cysts were made by manipulating the cyst shown in Figures 4.1 and 4.3.

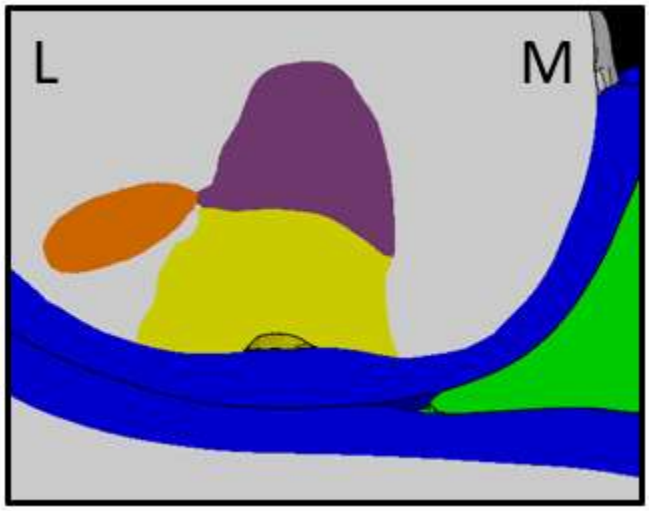

Figure 4.5. Cranial plane showing the artificial bone segmentation that occurred for 2 mm height cysts (purple). The purple region appears radiolucent in the CT scan and had to be filled in with a separate part from bone as to not give it too low of a modulus when properties were mapped using Hounsfield Units.

4.3.7 Bone Formation Area

In our previous study, Beaupre, Carter, and Orr's theory of bone remodeling was utilized to predict SBC healing and will be employed again for this analysis.[37,38] In summary, a tissue stimulus (Ψ) is calculated that predicts bone resorption, bone apposition, or no net bone change. Ψ is calculated using the following equation:

$$\Psi = \left(\sum_{day} n_i * \sigma_{b_i}^m \right)^{\frac{1}{m}} \quad \text{(Eq. 5)}$$

where n_i is the number of cycles per day (for a given load) assumed to be 3000, σ_{b_i} is a true bone tissue-level effective stress, and m is an empirical constant assumed to be 6.[39] σ_{b_i} is defined as:

$$\sigma_{b_i} = \frac{\rho_c^2 \sqrt{2 * E * U}}{\rho_a^2} \quad \text{(Eq. 6)}$$

where ρ_c is the tissue density of cortical bone (assumed to be 1.92 g/cc), ρ_a is the apparent density of the local tissue, E is the local elastic modulus, and U is the local strain energy density. The theory is based on the idea that an "error" between the tissue stimulus,Ψ, and an attractor state, an equilibrium value that bone is trying to achieve, drives bone remodeling. Using previous studies of bone's response to loading, Beaupre et al. determined that the equilibrium state was

between 40 and 60 MPa. If the error between the tissue stimulus and the attractor state is positive, bone apposition is predicted. If the error is negative, bone resorption in predicted. Thus, values of Ψ greater than 60 MPa predict bone apposition, and values of Ψ less than 40 predict bone resorption. Ψ was calculated on the interior surface elements of the SBC, and a percentage of the available surface area exceeding 60 MPa was calculated as the bone formation area (BFA). BFA was calculated at baseline (0 N of compression) and again after 300 N of compression was applied across the screw. The difference between the two analyses was calculated as the final output to quantify the efficacy of the screw. Multivariate regression analysis was performed using the factorial study data to identify the spatial characteristics that best explain the variance in the results.

4.3.8 Third Principal Stress Vectors

In addition to calculating the bone formation area generated from a transcondylar screw at 900 N joint load, third principal stress vectors were plotted for a small (2x2x2 mm, for height, width, and depth), medium (14x4x10mm), and large cyst (26x14x20mm). The goal was to determine if the realignment of the stresses with the screw axis would occur for each SBC size.

4.4 Results

4.4.1 3^k factorial study

In general, using a TLS with 300 N of compression increases BFA in taller and deeper cysts (Table 4.2). Before TLS compression, BFA is <10% in 24/27 (88%) models and was < 20% in the remaining 3. After TLS compression, BFA is <10% in 11/27 (41%) models and >20% in 10/27 models (37%). After TLS compression, BFA on average increased ≤ 3% for SBC 2 mm in height, increased a mean of 16% (range 6-31%) for SBC 14 mm high, and increased a mean of 22% (5-34%) for SBC 26 mm high. Mapping of bone formulation stimulus with TLS by cyst height reveals that the 2 mm high SBC (Figure 4.6A) is not contacted by the TLS and the TLS produces a very small area of bone formation stimulus near the screw, but not near the cyst. At 14 mm high, the screw crosses the top of the cyst (Figure 4.6B) increasing BFA, and at 26 mm in height, (Figure 4.6C) still greater BFA is stimulated. Regression analysis of cyst dimensions revealed that cyst height had the largest effect on BFA stimulated by the TLS. Cyst height accounted for 56% of the variation in BFA ($p < 0.001$), cyst depth accounted for 12% of the variation ($p < 0.005$), and cyst width had negligible effect. The coefficient of multiple determination is 0.68 when accounting for all three variables. Residual plots of height and depth demonstrate that the unaccounted variance is stochastic and cannot be further refined using the spatial predictors. An F-Test shows significance for the regression model ($F < 1.03E-06$).

Table 4.2. Bone formation area (BFA) calculated with 3^k factorial study design ordered by decreasing BFA percent change after 300 N of compression was applied across the transcondylar lag screw (TLS). A neutral screw (0 N of compression) is equivalent to using no screw at all with a small joint load of 900 N.

SBC height	SBC width	SBC Depth	BFA % 0 N TLS Compression	BFA % 300 N TLS Compression	% Increase BFA
26	2	10	0	34	34
26	2	20	0	34	34
14	14	20	17	48	31
26	14	20	1	30	29
26	8	10	0	28	28
14	14	10	1	28	27
26	14	10	1	25	24
26	8	20	1	23	22
14	8	20	6	26	20
14	8	10	1	16	15
26	8	2	0	15	15
14	2	2	0	14	14
14	2	10	0	12	12
14	2	20	0	10	10
14	14	2	0	9	9
26	14	2	0	8	8
14	8	2	0	6	6
26	2	2	0	5	5
2	14	20	19	22	3
2	2	20	6	7	1
2	2	10	4	5	1
2	8	20	4	5	1
2	14	2	1	2	1
2	14	10	12	12	0
2	8	10	3	3	0
2	2	2	0	0	0
2	8	2	0	0	0

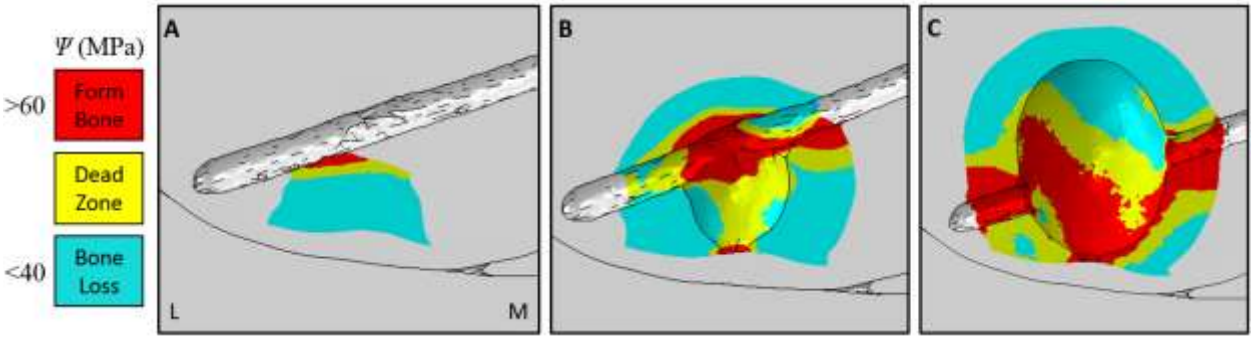

Figure 4.6. Bone remodeling stimulus for three selected cyst sizes. A) 2, 2, 2 mm height, width, and depth. B) 14, 8, 10 mm height, width, and depth. C) 26, 14, 20 mm height, width, and depth. As a larger area of the screw can penetrate the cyst cavity, more appositional stimulus is achieved on the inner surface of the void. L = lateral, M = medial.

4.4.2 Equal dimension dome-shaped cysts

Dome-shaped cysts up to 8 mm parameter lengths demonstrate a 0% increase in BFA using a TLS screw. At 10 mm, the BFA increased by 4% and BFA with 12 mm increased by 5% (Table 4.3). At 10 and 12 mm, the screw is able to partially penetrate the cavity but still does not cleanly cross through the cyst (Figure 4.7). At the typical screw position chosen, the entire screw does not cross through the cyst until the SBC is 14 mm in height, and the factorial study shows larger increases in BFA at this height.

Table 4.3. Equal dimension cyst analyses results listed from least BFA % difference to greatest. At 10 mm height, the compression across the lag screw begins to make a measurable difference.

Height	Width	Depth	BFA % Before	BFA % After	% Difference
4	4	4	0	0	0
6	6	6	2	2	0
8	8	8	1	1	0
10	10	10	2	6	4
12	12	12	2	7	5

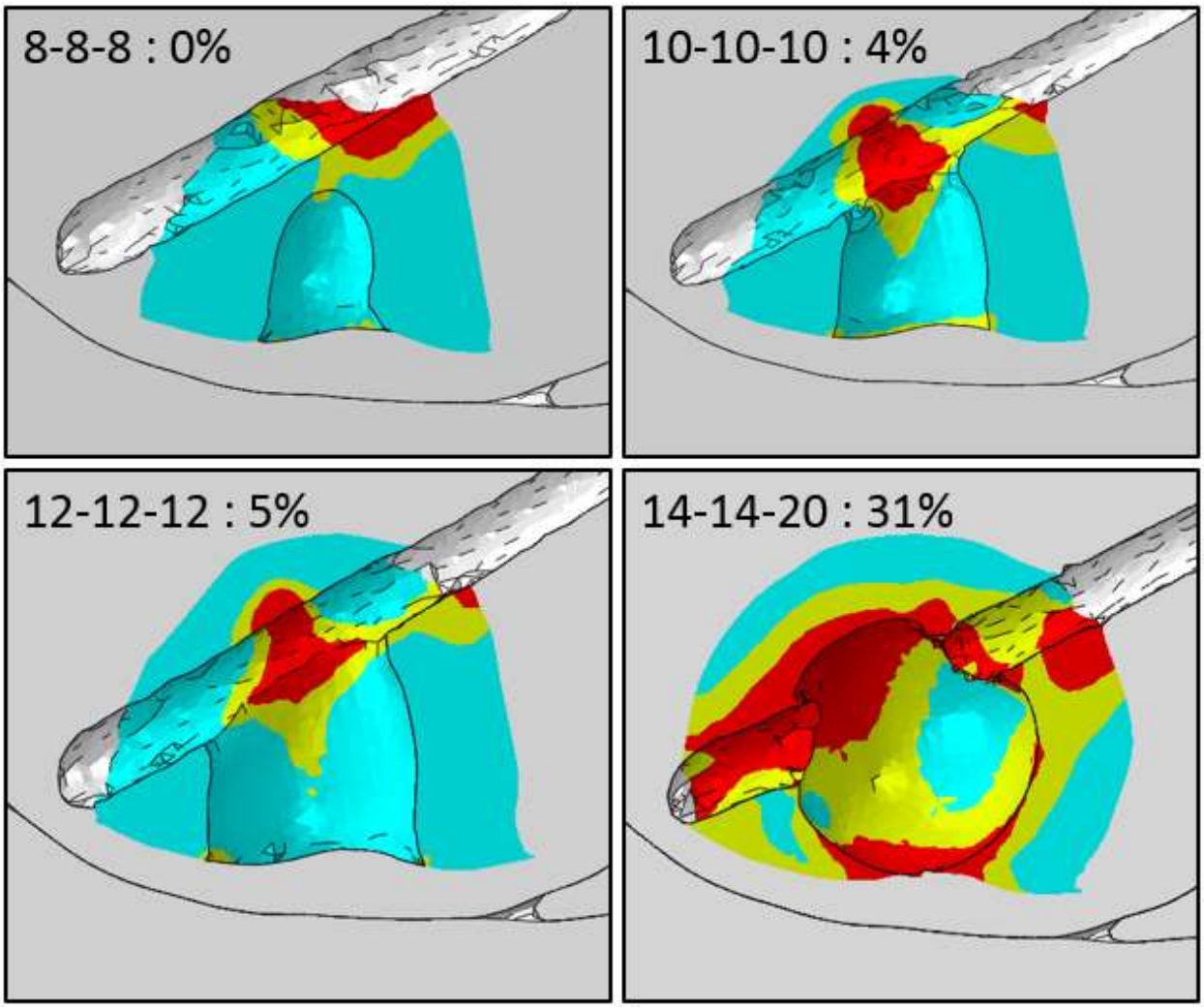

Figure 4.7. Cranial cross-sections showing proximal-distal/oblique screw holes with different sized cysts (shown as height-width-depth : % BFA increase). As more of the screw is able to penetrate into the cavity of the void, % BFA increases. Different planar cuts are used for each cyst to show the screw hole and are not through the centroid of the cyst.

4.4.3 Two comparative cystic CT models

The natural cyst models demonstrated predictable results based on the previous regression analysis (Figure 4.8). For the larger 15.5 mm height cyst, a TLS with 300 N of compression generated a 9% increase in BFA. For the smaller 4.5 mm height cyst, no measurable

BFA was generated. The screw was able to penetrate the cavity of the larger cyst whereas the screw passed over the proximal aspect of the smaller cyst.

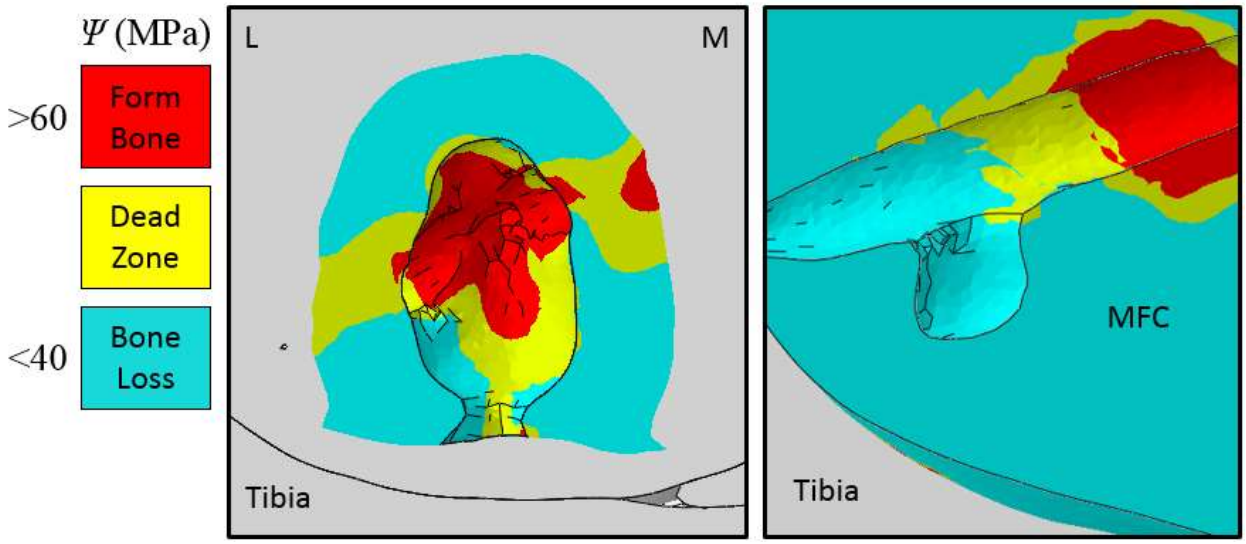

Figure 4.8. Bone-formation stimulus for two natural cysts with 900 N joint load, 300 N of screw compression, and 3000 cycles per day. Left) 15.5 mm height cyst with the cranial planar cut occurring just cranial to the screw to show the cyst's necking at the joint margin. For this cyst, most of the stimulus occurs in the proximal portions of the cyst. Right) 4.5 mm height cyst that does not have any communication with the joint space. The forage hole can be clearly seen for this cranial cross-section. The ROI has been enlarged for this cyst to show the stimulus that occurs in the abaxial portions of the forage hole. L = lateral, M = medial.

4.4.4 Third Principal Stress Vectors

Cyst size influences the screw's ability to realign stresses to be transverse to the MFC. With cystic penetration from the screw, third principal stress vectors are higher in magnitude and are aligned with the screw axis (Figure 4.9). With smaller cysts, there is negligible difference in

third principal stress direction and magnitude before and after 300 N of compression is applied across the screw.

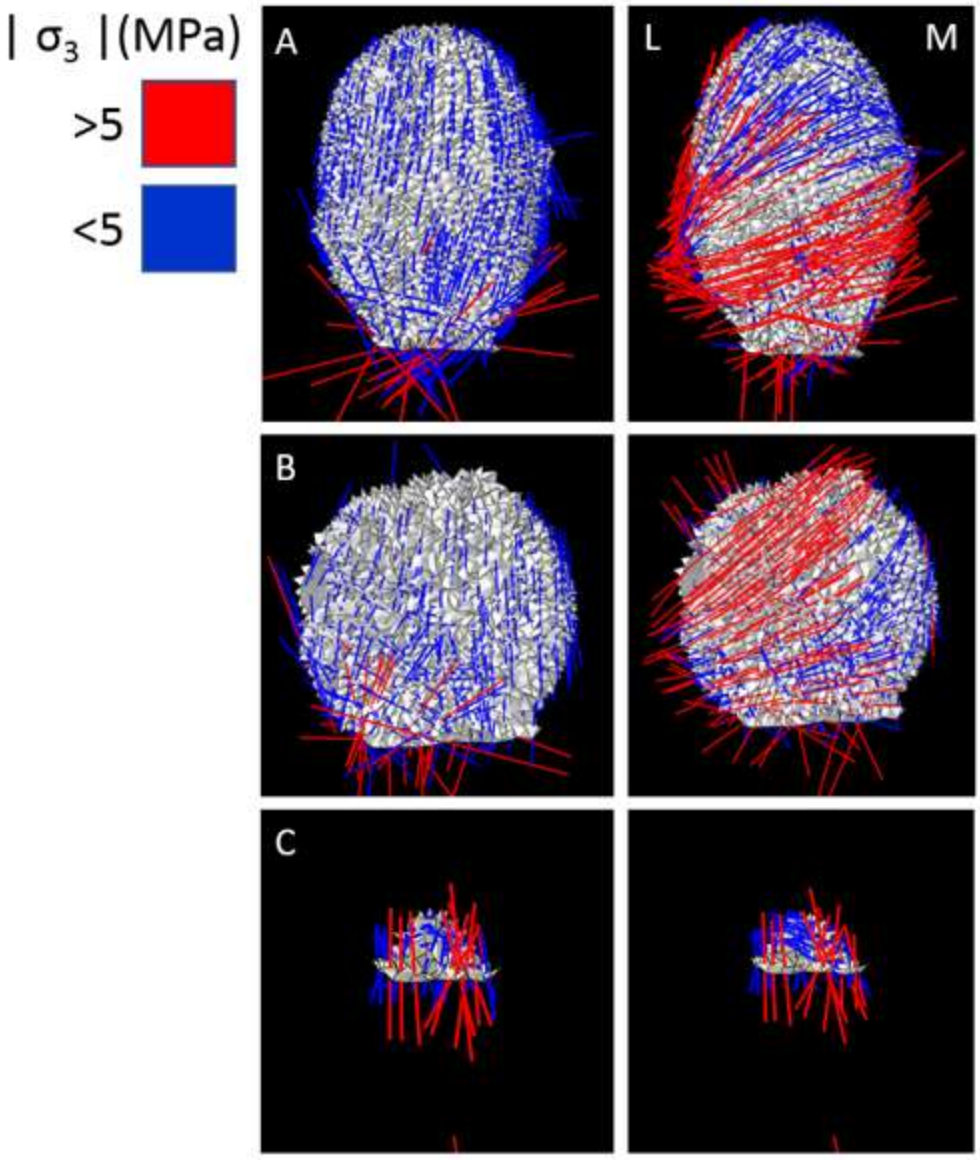

Figure 4.9. Third principal stress vectors without screw compression (left column) and after 300 N of compression across the TLS (right column) for three different sized cysts. The figure shows the 3-D elements with facets that form the inner lining of the cyst.

A) large cyst with 26, 14, 20, height, width, and depth, respectively.

B) medium cyst with 14, 14, 10, height, width, and depth, respectively.

C) small cyst with 4, 4, 4, height, width, and depth, respectively.

L = lateral, M = medial.

4.5 Discussion

In our previous work (in review), a plausible mechanism was identified that enables a TLS to elicit a healing response in a subchondral void. The screw provides mechanical stimulus into the surrounding bone and aligns third principal stress vectors to be transverse to the existing trabecular orientation. In that study, a single cyst was used, and the question of cyst specificity arose. Anecdotal evidence suggests that the transcondylar screw treatment benefits larger cysts more than smaller cysts. As such, this study investigated the issue of cyst specificity and tested the hypothesis that larger (taller) cysts respond more favorably to the TLS.

Compared to existing treatments, the screw is unique in that it substantially alters the biomechanical environment in the trabecular bone surrounding SBCs. It seems reasonable that the screw should penetrate the cavity and have a defined entrance to and exit from the cyst. If the screw achieves this positioning, one would expect larger stresses to be generated in the cyst inner surface upon axial compression of the screw. This would occur because of bending stresses taken on by the surface of the cyst. Also, less stress is in the inner surface of the cyst when the screw is above the cyst because the intact bone carries the load. The results from this study appear to confirm the importance of screw penetration into the cystic cavity.

The two spatial characteristics of the cyst that make full penetration possible are height and depth. Since the PDO screw position is constrained by the regional anatomy, as the screw head cannot contact the cartilage or meniscus, cyst height is especially important. At 14 mm in height, given the screw placement, full penetration of the screw into the cyst is made possible and large increases in BFA are observed. When the screw goes above the cyst, it has little effect on the BFA (Figure 4.6A). Cyst depth (anterio-posterior) had a moderate impact on BFA in this study but may have had a larger effect if the screw position was not held constant. Given a constant

screw position in the MFC, a smaller depth does not ensure that the screw would cross the cavity. As the depth increased, the screw was more likely to penetrate, or able to penetrate to a greater extent, and the BFA increased accordingly. In clinical application, a surgeon would have more control in aiming the screw to account for the depth but less control to accommodate the height. It is important that the screw not damage the subchondral bone or soft tissue.

Cyst width (medial-lateral) does not have a substantial effect on BFA increases when using a TCS. If the cyst is high enough and deep enough, it will pass through a cyst regardless of the medial-lateral width. However, the width at the joint margin appears to have substantial effect on BFA, although not explicitly tested for in this study. In the 3^k factorial study, cysts with heights of 14 mm and 26 mm were narrowed at the joint margin, as observed clinically. This narrowing causes more load to be carried to the central portions of the distal condyle. With less area carrying the load, stress increases. Figure 4.7 illustrates this effect. With the narrowing at the joint margin, large areas of bone formation are predicted at the joint margin compared to the 12-12-12 cystic dimensions. In the 12-12-12 cyst, bone at the joint margin is not present to undergo these large stresses, and there is no extra stimulus generated at the cystic rim.

We hypothesized that smaller cysts (more specifically, lower cysts) would not respond as well to the TCS compared to larger cysts. This was based off poorer clinical outcomes when treating smaller/lower cysts. Our study confirms this hypothesis, and a traditional TCS does not stimulate bone formation in small cysts. The stress generated from axial compression in the screw is not able to affect the bone below the screw. With more joint load, BFA would increase, however, our previous study shows that third principal stress vectors are not across the cyst if the screw is above the void. Not only is the stimulus not present at lower joint loads, but the stress alignment is not preferential for bone growth across the void even if enough load were present to

stimulate formation. Consequently, sclerosis is more likely to form rather than radiographic healing.

In order to reach lower cysts, a lower and more horizontal screw would be required, but the screw head would interfere with the medial meniscus. It may be possible to reach and stimulate bone formation in such cysts with a dual pitch headless screw, if enough compression can be achieved across the cyst. However, 300 N of compression appears to be crucial in order to elicit the high BFA response. Experimental testing would be required before the dual pitch screw could be further considered as a viable clinical option.

There are several limitations to this study. The model was not subject-specific and was not validated using directly measured kinetic data. Equine kinetic data is scarce, and validation is therefore difficult. As such, sensitivity analyses were performed on the material properties and boundary conditions, and the qualitative conclusions of this study were not affected. Also, our previous study addressed the effect of joint loading, and it was found that joint loading has a significant impact on BFA. This study only uses a 900 N load only, which corresponds to the loads expected the first few weeks post-surgery. Higher loads would generate larger BFA. In the factorial study, a single stifle model was used for all 27 cyst configurations. Consequently, the sclerotic region was assumed around all of the cysts, and for the lower cysts, the artificial bone region had to be present. In order to help address this limitation, the two natural cyst models were used to confirm the results from the factorial study. Also, the bone remodeling theory framework is based on limited samples that do not include equine data. While absolute values are not definitive, the relative values of stress stimulus between models clearly indicate the relative effectiveness of the lag screw for various sized cysts.

In conclusion, this study found that a transcondylar screw should be very effective in treating larger cysts. The TLS increases stress stimulus in the bone around the cyst to promote bone apposition and directs compression across the cyst. If full penetration of the screw through the cyst is possible, it is recommended that the transcondylar screw be used to treat subchondral bone cysts. Future work should investigate the use of a dual-pitch headless screw for lower/smaller cysts.

4.6 References

1. Baxter GM: Subchondral cystic lesions in horses, in Joint disease in the horse, Vol. Philadelphia, WB Saunders, 1996, pp 384-397.
2. Jeffcott LB, Kold SE: Clinical and radiological aspects of stifle bone cysts in the horse. Equine Veterinary Journal 14:40-46, 1982.
3. McIlwraith CW: Subchondral Cystic Lesions (Osteochondrosis) in the Horse, in Compend Contin Educ Pract Vet, Vol 4, 1982, pp 282-294.
4. Stewart B, Reid CF: Osseous cyst-like lesions of the medial femoral condyle in the horse. J Am Vet Med Assoc 180:254-257, 1982.
5. Hendrix SM, Baxter GM, Mc Ilwraith CW, et al: Concurrent or sequential development of medial meniscal and subchondral cystic lesions within the medial femorotibial joint in horses (1996–2006). Equine Veterinary Journal 42:5-9, 2010.
6. Jeffcott LB, Kold SE, Melsen F: Aspects of the pathology of stifle bone cysts in the horse. Equine Vet J 15:304-311, 1983.
7. Kold SE, Hickman J, Melsen F: An experimental study of the healing process of equine chondral and osteochondral defects. Equine Vet J 18:18-24, 1986.
8. White NA, McIlwraith CW, Allen D: Curettage of subchondral bone cysts in medial femoral condyles of the horse. Equine Veterinary Journal 20:120-124, 1988.
9. Howard RD, McIlwraith CW, Trotter GW: Arthroscopic surgery for subchondral cystic lesions of the medial femoral condyle in horses: 41 cases (1988-1991). J Am Vet Med Assoc 206:842-850, 1995.
10. Vandekeybus L, Desbrosse F, Perrin R: Intralesional longacting corticosteroids as a treatment for subchondral cystic lesions in horses. A retrospective study of 22 cases. in

Proceedings 8th Annual Scientific Meeting of the European College of Veterinary Surgery 33-35, 1999.

11. Bodo G, Hangody L, Modis L, et al: Autologous osteochondral grafting (mosaic arthroplasty) for treatment of subchondral cystic lesions in the equine stifle and fetlock joints. Vet Surg 33:588-596, 2004.
12. Foerner JJ: Injection of equine subchondral bone cysts with triamcinolone: 73 horses (1999-2005), Proceedings, Vet Clin North Am Equine Pract, 2006 (available from
13. Wallis TW, Goodrich LR, McIlwraith CW, et al: Arthroscopic injection of corticosteroids into the fibrous tissue of subchondral cystic lesions of the medial femoral condyle in horses: a retrospective study of 52 cases (2001-2006). Equine Vet J 40:461-467, 2008.
14. Ortved KF, Nixon AJ, Mohammed HO, et al: Treatment of subchondral cystic lesions of the medial femoral condyle of mature horses with growth factor enhanced chondrocyte grafts: a retrospective study of 49 cases. Equine Vet J 44:606-613, 2012.
15. O'Brien EJO: What is the best treatment for medial femoral condylar subchondral bone cysts? Equine Veterinary Education 0, 2019.
16. Santschi EM, Williams JM, Morgan JW, et al: Preliminary investigation of the treatment of equine medial femoral condylar subchondral cystic lesions with a transcondylar screw. Vet Surg 44:281-288, 2015.
17. Frazer LL, Santschi EM, Fischer KJ: The impact of subchondral bone cysts on local bone stresses in the medial femoral condyle of the equine stifle joint. Med Eng Phys, 2017.
18. Frazer LL, Santschi EM, Fischer KJ: Impact of a void in the equine medial femoral condyle on bone stresses and peak contact pressures in a finite element model. Vet Surg, 2018.

19. Barak MM, Lieberman DE, Hublin JJ: A Wolff in sheep's clothing: trabecular bone adaptation in response to changes in joint loading orientation. Bone 49:1141-1151, 2011.
20. Ruff C, Holt B, Trinkaus E: Who's afraid of the big bad Wolff?: "Wolff's law" and bone functional adaptation. American Journal of Physical Anthropology 129:484-498, 2006.
21. Walker WT SJ, Kawcak CE, Nelson BB, Fortier LA: Morphological characteristics of subchondral bone cysts in medial femoral condyles of adult horses as determined by computed tomography. Am J Vet Res 77:265-274, 2016.
22. Carter DR, Hayes WC: The compressive behavior of bone as a two-phase porous structure. J Bone Joint Surg Am 59:954-962, 1977.
23. Donzelli PS, Spilker RL, Ateshian GA, et al: Contact analysis of biphasic transversely isotropic cartilage layers and correlations with tissue failure. J Biomech 32:1037-1047, 1999.
24. Armstrong CG, Lai WM, Mow VC: An analysis of the unconfined compression of articular cartilage. J Biomech Eng 106:165-173, 1984.
25. Kiapour A, Kiapour AM, Kaul V, et al: Finite element model of the knee for investigation of injury mechanisms: development and validation. J Biomech Eng 136:011002, 2014.
26. Fowlie JG: Functional Anatomy of the Equine Meniscus: Pathogenesis and Pathophysiology of Injury to the Cranial Horn of the Medial Meniscus. Master of Science: Michigan State University, 2011.
27. Haut Donahue TL, Hull ML, Rashid MM, et al: How the stiffness of meniscal attachments and meniscal material properties affect tibio-femoral contact pressure computed using a validated finite element model of the human knee joint. J Biomech 36:19-34, 2003.

28. Donahue TL, Hull ML, Rashid MM, et al: A finite element model of the human knee joint for the study of tibio-femoral contact. J Biomech Eng 124:273-280, 2002.
29. Malekipour F, Whitton C, Oetomo D, et al: Shock absorbing ability of articular cartilage and subchondral bone under impact compression. J Mech Behav Biomed Mater 26:127-135, 2013.
30. Laasanen MS, Toyras J, Korhonen RK, et al: Biomechanical properties of knee articular cartilage. Biorheology 40:133-140, 2003.
31. Lee H, M. Theis K, Jackson R, et al: Equine Articular Cartilage Stiffness Determination Using Indentation, 2014.
32. Oinas J, Ronkainen AP, Rieppo L, et al: Composition, structure and tensile biomechanical properties of equine articular cartilage during growth and maturation. Scientific Reports 8:11357, 2018.
33. Aldrich ED, Goodrich LR, Monahan MK, et al: Radiographic localisation of the entheses of the equine stifle. Equine Veterinary Journal 49:493-500, 2017.
34. Li G, Gil J, Kanamori A, et al: A Validated Three-Dimensional Computational Model of a Human Knee Joint. Journal of Biomechanical Engineering 121:657-662, 1999.
35. Rich FR, Glisson RR: In vitro mechanical properties and failure mode of the equine (pony) cranial cruciate ligament. Vet Surg 23:257-265, 1994.
36. Mootanah R, Imhauser CW, Reisse F, et al: Development and validation of a computational model of the knee joint for the evaluation of surgical treatments for osteoarthritis. Comput Methods Biomech Biomed Engin 17:1502-1517, 2014.
37. Beaupre GS, Orr TE, Carter DR: An approach for time-dependent bone modeling and remodeling--theoretical development. J Orthop Res 8:651-661, 1990.

38. Beaupre GS, Orr TE, Carter DR: An approach for time-dependent bone modeling and remodeling-application: a preliminary remodeling simulation. J Orthop Res 8:662-670, 1990.

39. Whalen RT, Carter DR, Steele CR: Influence of physical activity on the regulation of bone density. J Biomech 21:825-837, 1988.

5. Conclusion

5.1 Summary

In this study, finite element analysis provided a detailed look at the mechanics of subchondral bone cysts (SBCs). Specifically, intra-osseous stresses were analyzed in the medial femoral condyle (MFC) of a healthy stifle joint to predict whether or not an SBC could form from daily loading. Furthermore, these stresses were analyzed once a defect was already in place in the MFC to predict further damage and SBC progression. Finally, the mechanics of the transcondylar screw (TCS) treatment were examined. Evidence has been provided to support the TCS as a uniquely effective surgical technique for equine SBC treatment.

5.2 Major Findings and Conclusions

5.2.1 Mechanics Associated with an Equine Subchondral Bone Cyst

Chapter 2 addressed mechanics in the equine stifle joint with and without a SBC. The initial findings from the study were that intra-osseous stresses in a healthy MFC during high-impact (ground reaction force during gallop) could initiate an SBC. Shear stresses above yield strength were found on the surface of the MFC where SBCs most often develop, and these high stresses extended several millimeters into the subchondral bone. The study continued by creating a void in the MFC to create a simulated SBC. With high-impact loading, shear stresses increased substantially above yield, and the potential for further SBC progression was made evident. These findings support the trauma hypothesis and SBCs forming with mechanical overload in the absence of cartilage degeneration.

In addition to the increased intra-osseous stresses that occur with an SBC, increased shear stresses in the medial meniscus were found. These increased stresses occur along the inner rim of

the meniscus, an area prone to secondary injury with a MFC SBC. This finding highlights the altered load path that occurs when load cannot properly transfer through the condyle into the articulation with the tibial plateau. Instead of load passing through the void, the load must be transferred around the cyst, creating higher stresses in the cystic boundary and into the medial meniscus. Therefore, a major conclusion from this study confirms that treatment strategies addressing SBCs in the medial femoral condyle should seek to improve radiographic healing in order to restore proper load transfer. Return to soundness as a metric for surgical success does not protect against future reinjury or secondary injury in the soft tissues of the joint.

5.2.2 How a Transcondylar Screw Affects Bone Formation in an Equine Subchondral Bone Cyst

Chapter 3 investigated the hypothesis that the transcondylar screw treatment achieves radiographic healing by providing bone formation stimulus to the adjacent bone of a SBC. Bone stimulus was quantified using an existing theory of bone remodeling, and the hypothesis was confirmed. The axial compression provided by the screw through the applied torque of implantation creates increased, non-damaging stresses in the adjacent bone. Perhaps, equally as important, the compression across the SBC aligns third principal stresses to be transverse to the trabecular orientation, which encourages growth across the void as opposed to trabecular densification (sclerosis). This ability to reorient stresses explains why the TCS achieves radiographic healing, while regular post-surgery rehabilitation does not. Further, if the screw is placed above the cyst, likelihood of healing is decreased. The TCS is the only available treatment for equine SBC that provides this effect. Therefore, the major conclusion from this study supports the use of a TCS as the most rational surgical option to veterinarians treating SBCs.

5.2.3 Impact of Cyst Size and Shape on Bone Formation Stimulus Using a Transcondylar Screw

Chapter 4 extended the work of chapter 3 by further examining the TCS. Chapter 3 confirmed the effectiveness of the TCS but only for a specific SBC size and shape. Chapter 4 investigated 30+ additional cyst sizes and shapes and identified the cysts that best respond to the TCS treatment. The major finding from this study was that the screw must penetrate the cystic cavity to achieve a high bone-formation stimulus, as well as realigning stresses to be transverse to trabecular orientation. Therefore, smaller cysts are not as responsive to the current standard of TCS implantation. However, at the onset of lameness, cysts are generally large enough to achieve screw penetration through the cyst.

5.3 Future Work

While this study has provided substantial findings and conclusions, there is a tremendous amount of opportunity for additional research. Based off of the findings from this study, three proposed studies could provide further impact in properly treating bone lesions:

1) Patient-specific modeling of an equine SBC with monitored progress after TCS implantation.
2) Identify other surgical techniques (TCS variations) to address smaller SBCs.
3) Translate the findings for human applications.

5.3.1 Patient-Specific Modeling

Chapter 3 provided substantial evidence that the mechanism of healing using the TCS has been identified. With clinical results and the finite element modeling predictions in good agreement, initial healing of SBCs using a TCS has been demonstrated. The finite element model predicts that the strongest stimulus for bone apposition occurs at the joint margin. Clinical observations support this finding with SBCs usually healing by closing at the joint margin first. Beyond the initial healing, it is unknown how the TCS influences SBC mechanics, nor is it

known if the screw is even able to maintain consistent compression after several weeks. By carefully tracking the healing progress of an SBC after TCS implantation, more information can be gathered to compare against future model predictions.

For example, after 4 weeks of TCS implantation, a newer CT scan can be taken of the stifle joint to gain a 3-D understanding of the bone growth that has occurred. The model can then be updated to put bone back into the void where bone has grown in the live animal. Using this updated configuration, the finite element model can then be used to predict the mechanics of the SBC after initial healing has already occurred. Due to the deposition of woven bone with little trabecular alignment, the healing response may not be as sensitive to direction of loading. Therefore, future healing may depend on joint load more so than the TCS. Perhaps, the TCS is not even able to generate compression anymore as trabecular creep and remodeling occur. Nonetheless, different scenarios can be tested in the model, bone healing response can be predicted, and these results can then be compared against updated CT scans of the horse as time progresses to better understand how bone and joint mechanics affect healing.

The woven bone that initially occurs may cause a cascading effect of more healing for a few reasons. 1) it is not as sensitive to the direction of loading, 2) the newly formed bone at the joint margin will see a high local mechanical stimulus as the joint loading can now affect this part of the MFC and stimulate further apposition, and 3) cellular and chemical agents necessary for growth would already be present at the joint margin. With these three factors occurring, the model may show that the TCS is no longer providing the primary influence for bone formation. Currently, there is clinical support for this hypothesis with anecdotal evidence that removing the screw from a partially healed SBC does not inhibit further healing. In addition, more sophisticated screw materials could be considered that are resorbed into the body. This would

eliminate the need for screw removal (an additional surgery), and the degradation products may even be beneficial to bone growth. Immediate future work should investigate the use of novel screw materials, such as resorbable magnesium alloys, to treat SBCs.

Using time-updated model progressions (simulations) would allow for a much deeper understanding in how SBCs continue to heal after the initial healing at the joint margin. With a deeper understanding would come further refinements in treatment strategies, further improving success rates.

5.3.2 Small Subchondral Bone Cysts

With more and more frequent radiography performed on horses intended for performance, the likelihood of identifying early, smaller SBCs increase. The currently administered TCS placement does not appear to provide sufficient healing stimulus for these smaller defects. While rest and conservative treatment has historically been more successful with smaller cysts than larger cysts, the need for improvement still warrants novel treatment options. As a preliminary investigation, using the finite element models from chapters 2-4, a theoretical, headless screw (e.g. Herbert screw) was placed lower in the MFC in horizontal fashion. This configuration showed a substantial increase in bone formation stimulus not exhibited with the traditional proximoblique TCS (currently unpublished data).

While the early findings are encouraging, too many assumptions were made to validate this as a possible treatment option, and more information is needed before this option is recommended. For one, the model assumed 300 N of compression could be generated across the headless screw. The importance of compression was demonstrated in chapter 3, and the amount of compression from a headless screw is unknown. A recent study produced ~100 N of compression using a headless screw, much lower than the assumed 300 N.[1] Second, the

positioning possible for the clinical application has not been determined, and a low, distal position was assumed. More work is needed experimentally, computationally, and clinically to assess headless screws as a treatment for small SBCs.

If more work is spent to develop techniques for smaller and/or difficult to access bone lesions, the benefits could be enormous. Clearly, developing variations of the trans-cyst screw treatment for use in smaller, lower cysts could reduce the incidence of equine SBC lameness substantially. With radiography becoming more frequent in developing horses, the chances to discover a small, asymptomatic cyst is higher. Stopping these cysts from further developing and jumpstarting the healing process early could have a monumental impact in the equine performance industry. Furthermore, smaller and/or difficult to access cysts exist in areas outside the equine stifle joint. Bone defects can occur in all equine extremity bones. This would provide additional research needed for the eventual translation into human application.

5.3.3 Human Application

This work detailed the mechanical advantage that a trans-cyst screw gives to promote bone formation. Its utility and efficacy were clearly described in chapters 3 and 4 for equine SBCs. However, the trans-cyst screw treatment's utility may benefit not only equine SBCs but human bone lesions, as well. Described in chapter 1, humans suffer from a wide variety of bone lesions that exhibit similar characteristics to equine SBCs. There is no consensus on how best to treat these defects, and there is plenty of room for improvement. The trans-cyst screw's ability to stimulate bone formation could be a simple, low-cost, and very effective solution to human bone lesion problems worldwide.

The same finite element modeling approach could be used with human anatomy to determine if enough stimulus from a trans-cyst screw could theoretically be generated to promote

bone formation. Considering differences in bone density, expected loading from activity, geometry, cyst location, etc., the trans-cyst treatment could be tailored to benefit the wide spectrum of human bone lesions. Millions of patients suffering from bone lesions could benefit from an effective treatment that promotes bone formation. It is envisioned that the low-cost, low-risk surgery could readily be applied to human patients.

5.4 References

1. Grewal R, Assini J, Sauder D, et al: A comparison of two headless compression screws for operative treatment of scaphoid fractures. Journal of orthopaedic surgery and research 6:27-27, 2011.

6. Appendix

Sensitivity analysis was performed for several of the models used in Aim 2. These models were tested with 1800 N joint load and 3000 cycles per day. For the meniscal values, half represents a half-value modulus for the 6 anisotropic moduli, while double represents double-value moduli. The reported stresses and strain energy densities (SED) are peak values obtained as the 95% percentile. Also reported is the available surface area of the cyst stimulated for bone formation (% BFA). Varying various soft tissue parameters, as well as loading conditions did not substantially change the reported result. The most influential change was raising the loading angle to 10 degrees. This loading angle doesn't appear to be physiological as the line of loading would extend significantly anterior to the femoral shaft and condyles at the distal end of the bone.

Table 6.1. Sensitivity analysis for the baseline model in Aim 2 – Void only.

1800 N Load - 2 cm^3 void - No Screw - Model Used in Aim 2					
	Tension (MPa)	**Compression (MPa)**	**Shear (MPa)**	**SED**	**% BFA**
Low Cartilage (4 MPa)	0.67	3.27	3.20	7.58E-04	1
High Cartilage (16 MPa)	0.90	3.78	3.83	1.10E-03	3
Low Meniscus (Half)	0.88	3.67	3.72	1.00E-03	2
High Meniscus (Double)	0.70	3.35	3.30	8.02E-04	1
Low Load Angle (0)	0.75	3.60	3.49	9.32E-04	1
High Load Angle (10)	0.96	4.11	4.12	1.20E-03	7
Low Patellar Load (50 N)	0.74	3.60	3.49	9.32E-04	1
High Patellar Load (200N)	0.76	3.61	3.52	9.34E-04	1
				Reported Value	**1**

Table 6.2. Sensitivity analysis for the Drilled Hole model used in Aim 2.

1800 N Load – 2 cm^3 void – Drilled Hole – Model Used in Aim 2					
	Tension (MPa)	**Compression (MPa)**	**Shear (MPa)**	**SED**	**% BFA**
Low Cartilage (4 MPa)	0.82	3.62	3.62	9.44E-04	1
High Cartilage (16 MPa)	1.09	4.14	4.24	1.30E-03	1
Low Meniscus (Half)	1.06	4.04	4.11	1.20E-03	3
High Meniscus (Double)	0.85	3.71	3.72	9.95-04	1
Low Load Angle (0)	0.96	3.76	3.84	1.00E-03	2
High Load Angle (10)	1.23	4.55	4.66	1.50E-03	9
Low Patellar Load (50 N)	1.01	3.94	4.00	1.10E-03	2
High Patellar Load (200N)	0.80	3.67	3.64	9.69E-04	1
				Reported Value	**2**

Table 6.3. Sensitivity analysis for the proximoblique screw model with 300 N of compression used in Aim 2.

1800 N Load - 2 cm^3 void - Lag Screw 300 - Model Used in Aim 2					
	Tension (MPa)	**Compression (MPa)**	**Shear (MPa)**	**SED**	**% BFA**
Low Cartilage (4 MPa)	2.66	5.62	6.97	3.10E-03	21
High Cartilage (16 MPa)	2.75	6.05	7.52	3.50E-03	31
Low Meniscus (Half)	2.73	6.00	7.42	3.50E-03	31
High Meniscus (Double)	2.67	5.66	7.02	3.10E-03	22
Low Load Angle (0)	2.69	5.81	7.18	3.20E-03	25
High Load Angle (10)	2.80	5.92	7.40	3.40E-03	30
Low Patellar Load (50 N)	2.75	5.87	7.28	3.30E-03	28
High Patellar Load (200N)	2.59	5.62	6.92	3.00E-03	20
				Reported Value	**25**